2015-11-01

Low-Shield Volcanism: A Comparison of Volcanoes on Syria Planum, Mars and Snake River Plain, Idaho

Amanda Olivia Henderson
Brigham Young University

Low-Shield Volcanism: A Comparison of Volcanoes on Syria Planum, Mars and Snake River Plain, Idaho

Amanda Olivia Henderson

A thesis submitted to the faculty of
Brigham Young University
in partial fulfillment of the requirements for the degree of

Master of Science

Eric H. Christiansen, Chair
Jani Radebaugh
Michael Dorais

Department of Geological Sciences

Brigham Young University

November 2015

ABSTRACT

Low-Shield Volcanism: A Comparison of Volcanoes on Syria Planum, Mars and Snake River Plain, Idaho

Amanda Olivia Henderson
Department of Geological Sciences, BYU
Master of Science

Volcanoes are key indicators of a planet's internal structure, mechanics, and evolutionary history. Consequently, understanding the types and ages of volcanoes on a planet's surface is an important endeavor. In an attempt to better understand the relationship between morphometry and volcanic processes, we compared low-shield volcanoes on Syria Planum, Mars, with basaltic shields of the eastern Snake River Plain. We used 133 volcanoes on Syria Planum that are covered by Mars Orbiting Laser Altimeter (MOLA) and High Resolution Stereo Camera (HRSC) elevation data and 246 eSRP shields covered by the National Elevation Dataset (NED) for this comparison. Shields on Syria Planum average 191 +/- 88 m tall, 12 +/- 6 km in diameter, 16 +/- 28 km^3 in volume, and have 1.7° +/- 0.8 flank slopes. eSRP shields average 83 +/- 44 m tall, 4 +/- 3 km in diameter, 0.8 +/- 2 km^3 in volume, and have 2.5° +/- 1 flank slopes.

Bivariate plots of morphometric characteristics show that Syria Planum and Snake River Plain low shields form the extremes of the same morphospace shared with some Icelandic olivine tholeiite shields, but are generally distinct from other terrestrial volcanoes. Cluster analysis of Syria Planum and Snake River Plain shields with other terrestrial volcanoes separates these volcanoes into one cluster and the majority of them into the same sub-cluster that is distinct from other terrestrial volcanoes. Principal component and cluster analysis of Syria Planum and Snake River Plain shields using height, area, volume, slope, and eccentricity shows that Syria Planum and Snake River Plain low-shields are similar in shape (slope and eccentricity). Apparently, these low shields formed by similar processes involving Hawaiian-type eruptions of low viscosity (mafic) lavas with fissure controlled eruptions, narrowing to central vents. Initially high eruption rates and long, tube-fed lava flows shifted to the development of small lava lakes that repeatedly overflowed, and on some with late fountaining to form steeper spatter ramparts. However, Syria Planum shields are systematically larger than those on the eastern Snake River Plain. The larger size of Syria Planum shields is likely due to the smaller gravity of Mars, requiring larger magma batches to generate sufficient buoyant force to overcome the strength of rocks in the lithosphere and rise to the surface. Thus, Syria Planum lavas erupt in larger volumes and at higher rates generating larger volcanoes with slightly smaller slopes.

Keywords: Volcanism, Mars, Idaho

ACKNOWLEDGEMENTS

I thank my family for their unfailing support and generosity; I could not have done this without them. I thank Kathryn Tucker for always making sure I had the right paperwork turned in, and Kris and Randy for always giving me a job. I acknowledge and thank my committee for their guidance, direction, and instruction, and most of all their patience. I would also like to acknowledge the assistance of Dr. Ames from the Engineering department and his assistance with ArcGIS, and Dr. Eggert of the Statistics department.

Table of Contents

Low-Shield Volcanism: A Comparison of Volcanoes on Syria Planum, Mars and Snake River Plain, Idaho i
Abstract ii
Acknowledgements iii
Table of Contents iv
List of Figures v
List of Tables vi
1. Introduction 1
1.1. Regional Geologic Settings 6
1.1.1. Snake River Plain 6
1.1.2. Syria Planum 7
1.2. Statement of the Problem 7
2. Methods 10
3. Analysis 13
3.1. Shield Volcanoes on the eastern Snake River Plain 13
3.2. Shield Volcanoes on Syria Planum 15
3.3. Statistical Analysis 17
3.3.1. Principal component and cluster analysis of various terrestrial and martian volcanoes 18
3.3.2. Principal component and cluster analysis of Snake River Plain low-shields 21
3.3.3. Principal component and cluster analysis of Syria Planum low-shields 23
3.3.4. Morphometric comparison with regression analysis 26
3.4. Morphometric comparison with regression analysis 26
3.4.1. Orientations of shields and craters 30
3.4.2. Vent structures 32
4. Discussion 34
5. Conclusions 40
References 41

List of Figures

Figure 1: Shield Types and Cross Section 46
Figure 2: Syria Planum Regional Map 47
Figure 3: eastern Snake River Plain Regional Map 48
Figure 4: eastern Snake River Plain Shield Profiles 49
Figure 5: Histograms of Morphometric Properties 50
Figure 6: Elevation Dataset and Measurement Method Comparison 51
Figure 7: Syria Planum Shield Profiles 52
Figure 8: Syria Planum Crater Types 53
Figure 9: Principal Component Analysis of all Volcano Types 54
Figure 10a: Cluster Analysis of all Volcano Types 55
Figure 10b: Cluster Analysis of Snake River Plain Shield Volcanoes 56
Figure 10c: Cluster Analysis of Syria Planum Shield Volcanoes 57
Figure 10d: Cluster Analysis of Snake River Plain and Syria Planum Shield Volcanoes 58
Figure 11: Map of Snake River Plain Cluster Analysis and Two-Point Azimuth Analysis 59
Figure 12: Map of Syria Planum Cluster Analysis and Two-Point Azimuth Analysis 60
Figure 13: Shield Profiles for Snake River Plain and Syria Planum Cluster Analysis 61
Figure 14: Morphometric Characteristic Plot Height v. Diameter 62
Figure 15: Morphometric Characteristic Plot Volume v. Diameter 63
Figure 16: Morphometric Characteristic Plot Volume v. Height 64
Figure 17: Morphometric Characteristic Plot Slope v. Diameter 65
Figure 18: Morphometric Characteristic Plot Slope v. Height 66
Figure 19: Rose Diagrams 67
Figure 20a: Crater Analysis, Crater Diameter v. Depth 68
Figure 20b: Crater Analysis, Volcano Diameter v. Ratio of Volcano and Crater Diameters 69
Figure 20c: Crater Analysis, Volcano Diameter v. Crater Diameter 70
Figure 21: Possible Magma Source 71
Figure 22: Buoyancy Cross Section 72

List of Tables

Table 1: Shield Morphometric Characteristics Statistical Summary 73
Table 2: Crater Morphometric Characteristics Statistical Summary 74
Table 3: Statistical Summary of Morphometric Characteristics for eSRP by Bury Category 75
Table 4: Volcano Type Index, Pike & Clow (1981) 76
Table 5: eSRP and SP Morphometric Characteristic Statistical Summary by Cluster 78
Table 6: Principal Component Analysis 80
Table 7: Regression Analysis..... 81

1. Introduction

Volcanoes are common on all terrestrial planets and the morphology of a volcano is influenced by the eruption mechanism, composition and temperature of magma, which in turn is influenced by the tectonic setting in which the volcano is formed. Thus, detailed morphologic studies of volcanic landforms are enlightening on multiple levels. In this study we make a detailed morphologic comparison of the low-shield volcanoes on the eastern Snake River Plain, Idaho and Syria Planum, Mars.

Both the eastern Snake River Plain and Syria Planum are areas where the distinctive plains-style volcanism is observed. Both areas are bounded by distinct extensional tectonic features, possibly influenced by uplift related to mantle plumes, thermal contraction, and volcanic loading. Although high resolution images are now available for the study of the martian surface, it is still not possible to do human-led field studies. Therefore, comparing the two areas can yield a more comprehensive understanding of the volcanic evolution of Mars. If a detailed morphologic study shows sufficient similarity between the two regions of volcanic activity, then it is likely that they have the same, or at least very similar, eruptive histories and mechanisms. The Snake River Plain is easily accessible for field study, and much has already been done on the geochemistry and physical volcanology of the region, so its structure, lava rheology, and eruptive mechanisms are better understood; thus allowing us to better understand the volcanism of Syria Planum by comparison.

Over half of the volcanoes on Earth and many volcanoes on other planets in the solar system are basaltic in composition (Spera, 2000). Basaltic magma erupts at temperatures between 1,000-1,300°C and has a typical chemical composition of SiO_2 (50 wt%), Al_2O_3 (15%), CaO (12%), and approximately equal amounts of FeO and MgO (10%). Magmas of this

composition are made through incongruent partial melting of the mantle at relatively shallow depths. The geometry of the structures produced from the eruption of basaltic magma is influenced by a multitude of factors including: composition, viscosity, yield strength, lithospheric structure, and the rate and volume of magma supply as well as the tectonic setting. Small amounts of volatile compounds are commonly found in basalt, which also influences the explosivity of the eruptions as well as the rates of eruption and ascent (Walker, 1993).

The morphologic structures resulting from basaltic eruptions are classified and described by Bemis (1995), the Basaltic Volcanism Study Project (BVSP) (1981), Cas and Wright (1988), and Wilson and Head (1994) as cinder cones, maars, domes, stratovolcanoes, table mountains, and shield volcanoes.

Cinder cones are formed through strombolian eruptions followed by ballistic deposition of highly vesicular scoria which eventually becomes gravitationally unstable and gives way and slides or avalanches to form relatively steep flanks (>20°) at the angle of repose. Other identifying characteristics for cinder cones are bowl-shaped summit craters and nearly circular bases (Bemis, 1995). The break in slope at the base is generally sharp and well defined. Maars form in phreatic and phreatomagmatic eruptions (Cas and Wright, 1988). Maars have larger or deeper craters which are generally below the pre-eruption ground surface. They typically are made of finer-grained scoria than cinder cones and in general have much shallower flank slopes than cinder cones. Bemis (1995) included tuff rings and tuff cones in the same hydrovolcanic category as maars, distinguishing them as having large amounts of juvenile material, steeper flank slopes and greater heights.

Shield volcanoes, as defined by Walker (1993), consist of lava flows that have low flank slopes typically between 4°-15°. He makes the distinction that shield volcanoes range widely in

size. The largest are polygenetic and typified by Hawaii basaltic shield volcanoes and the smallest are a few kilometers across and monogenetic. The latter are the low profile shield volcanoes that Noe-Nygaard (1968) termed *shield volcanoes of scutulum type*, which he defined as having volumes of 0.1-15 km^3. Greeley (1982) proposed the terms *low-shield volcanoes* and *plains-style volcanism* for these low profile shield volcanoes to avoid confusion with the larger shield volcanoes and awkward phrasing. Shields, small and large, can have rifts or central vents; however, the rifts are typically narrow and grade into radial vent systems on the large polygenetic shields. Shield volcanoes also typically have small spatter ramparts or small cinder cones at or near the eruptive fissure or vent (Figure 1).

Bemis (1995) described shields in general as piles of wedge-shaped lava flows of varying length resulting from Hawaiian style eruptions of lava that eventually become circular to elliptical in plan view, convex-up, and gently sloped morphologic structures. Ideal shields are described as those created from 100% effusive activity whereas composite volcanoes have over 50% pyroclastic deposits (Cas and Wright, 1988, Pike and Clow, 1981a). She further subdivided shield volcanoes into three categories; Hawaiian, Galapagos, and Icelandic. Hawaiian style shields are large polygenetic edifices with summit calderas, major rift zones, and complex eruptive histories, and Galapagos shields as similar to Hawaiian shields but smaller with more complex shapes. Icelandic shields are described as small and symmetric with small central craters. Her analysis of four different volcanic populations (Guatemala, northern and west-central Iceland, South Pacific submarine, and Snake River Plain) shows small differences in morphometry between the same type of volcano in different locations, suggesting that tectonic setting may have more impact on the morphology of a volcano than the eruptive style. Bemis

(1995) concludes that the most notable difference between shields and other volcanic structures is the rarity of a discernible break in slope near the summit region.

Walker (1993) organized these morphometric structure into five main types of basaltic volcano systems: shield volcanoes, stratovolcanoes, monogenetic volcano fields, flood-basalt fields, and central volcanoes. In general, the magma that feeds these basaltic volcano systems originates in the mantle and then rises as a result of density differences, sometimes aided by tectonics, to a level of neutral buoyancy or to a strength barrier. Cinder cones, maars and tuff rings, structures that result from the addition of liquid water to magma, are included in monogenetic volcano fields and flood-basalt fields. Though Walker (1993) assigns specific volcanic morphologic structures as typical of each of these systems, it is not unusual to find more than one within a single volcanic province.

Even though terrestrial domes and stratovolcanoes (also called composite volcanoes) are generally associated with more silicic eruptions, they are discussed here to contrast with shield volcanoes. Stratovolcanoes are generally a stratified succession of lava flows interbedded with pyroclastic deposits (Walker, 1993). Large pyroclastic eruptions deposit loose ash on slopes that are close to the angle of repose around 33-36° (Walker, 1993, Bemis, 1995). The lower slopes are influenced by mass wasting of loosely deposited ash, where the upper cone is primarily lava flows and welded pyroclastics from smaller eruptions (Bemis, 1995). Pyroclastic deposits are the main difference between stratovolcanoes and shields. Lava domes generally result from the eruption of highly viscous magma with minor pyroclast composition, talus slopes on their flanks and broad flat top with steep flanks and viscous flow features (Bemis, 1995).

Of the several types of volcanoes on Mars, shield volcanoes are the most prominent (Baptista et al., 2008). Within the Tharsis bulge region, the largest volcanic province on Mars

(Figure 2), polygenetic shield volcanoes, cinder cones, and low shields have been identified (Hauber et al., 2009, Richardson et al., 2013). Low shields formed near the larger shields in the Tharsis bulge, but in greater numbers in Syria Planum (Figure 2). Low-shield volcanism is found in only a few locations on Earth: Hawaii, Iceland, Guatemala, Jordan, Saudi Arabia and the Snake River Plain of southern Idaho. The Snake River Plain is the most prominent type location and has the most numerous low shields that have been cited as being similar to those in Syria Planum (Greeley, 1982, Baptista et al., 2008, Hauber et al., 2009, Richardson et al., 2013).

The Snake River Plain may be the most appropriate area for an analog study of volcanism on Syria Planum. Both have swarms of low-shield volcanoes (Figure 2, Figure 3) that may have been influenced by large mantle upwellings and regional upwelling and extensional tectonics (Shervais and Hanan, 2008, Hauber et al., 2009, Richardson et al., 2013). While both Hawaii and Iceland have low-shield volcanoes, they are not the dominant type of volcano, and the geologic settings are not as comparable to that of Syria Planum. While Iceland is influenced by a mantle plume, it is located on a divergent plate boundary; this unique interaction as well as the presence of numerous glaciers heavily influences the volcanism there. This type of plate boundary has yet to be found on Mars. Hawaii is the result of an intraplate hotspot, but it is surrounded by copious amounts of water that is currently absent on Mars, and the initial stages of volcano development are subaqueous, thus making a comparison between the areas challenging.

1.1. Regional Geologic Settings

1.1.1. Snake River Plain

The Snake River Plain is a northeast-trending topographic depression created by the Yellowstone plume that is bounded on the north and south by the extensional Basin and Range province (Figure 3). The axis of the Snake River Plain runs nearly perpendicular to the structural

trends of the Basin and Range (Smith, 1994, Anders et al., 1989, Rodgers et al., 1990, 2002b, Pierce and Morgan, 1992) and the eastern part parallels the direction of plate motion. It extends approximately 650 km in a NE direction, and is 80 to 200 km wide, covering an area approximately 30,000 km^2. The plain rises to the east, possibly due to the heat from the Yellowstone hot-spot, with an average elevation of 1500 m and a total relief of 900 m. This study is focused on the plains-style volcanism of the eastern portion of the Snake River Plain. This section consists of Pleistocene and Holocene basaltic lavas (Greeley, 1982, DeNosaquo et al., 2009) erupted as monogenetic shields and fissure-fed lava flows, as well as rhyolitic lava domes; the basalt flows bury silicic ignimbrites that are as old as Miocene.). The low shields are an average of 4 +/- 3 km across, 83 +/- 44 m high, and many have two prominent slopes, the main part of the shield having a slope less than 1/2° with a steeper, asymmetric summit region up to about 5° (Greeley, 1982). Many of the shields are aligned in distinctive rift zones.

The volcanism of the Snake River Plain was bimodal during the Pliocene through Pleistocene (Hackett and Smith, 1992, Kuntz et al., 1992, Hackett et al., 2004, Christiansen and McCurry, 2008). Shervais and Hanan (2008) proposed that the plume tail hotspot track that contains the plains-style volcanism may be controlled by a preexisting structural boundary in a thinner lithosphere. Christiansen and McCury (2008) propose that decompression melting from the rising plume creates low fO_2, low fH_2O olivine tholeiite magmas that stagnate in the middle crust where it could differentiate to a denser Fe-rich magma. The injection of newer magma batches rising from the plume may trigger the eruption of these differentiated magma packets.

1.1.2. Syria Planum

Syria Planum lies on the southeastern margin of the Tharsis province of Mars (Figure 2). It is bordered by Noctis Labyrinthus to the north, Claritas Fossae to the west and Solis Planum to

the southeast. This area forms a regional plateau with a maximum elevation of 8000 m above the geoid based on the analysis of Mars Orbiter Laser Altimeter (MOLA) (Smith et al., 2003). A total relief of 4000 m exists between this point and the southeastern portion of the planum. The area, as defined by Scott and Tanaka (1986), is roughly 900,000 km^2 with abundant volcanic vents focused in an area roughly 420,000 km^2 (Richardson et al, 2010, 2012). The volcanoes concentrate in the eastern portion of the planum and range in age from early Hesperian to early Amazonian, apparently spanning nearly 900 million years of martian history (Baptista et al., 2008, Richardson et al., 2013) in strong contrast to the eastern Snake River Plain where volcanism is restricted to a 10 million year span. On the geologic map of Tanaka et al. (2013), Syria Planum consists of the Late Hesperian volcanic unit (lHv) and where the shields are concentrated it is mapped as Late Hesperian volcanic field unit (lHvf).

1.2. Statement of the Problem

Greeley (1977) was the first to state that the plains style volcanism of the Snake River Plain was an appropriate analog for areas of the Moon and Mars that exhibited similar features. Greeley and Spudis (1981) were the first to specifically compare Syria Planum with the Snake River Plain. Recently, with higher resolution imagery available, several more studies of Syria Planum have been conducted. Baptista et al. (2008) used images taken by the high resolution stereo camera (HRSC) on the Mars Global Surveyor (MGS). Due to the availability of the images at the time, their study was limited to a portion of Syria Planum approximately 65,000 km^2 (Figure 2) where they made detailed morphologic studies of 30 small shield volcanoes and lava flows and compared them to shields in Iceland. They also discussed the possibility that the low-shields could signify late-stage activity that began with the emplacement of a large shield volcano now called Syria Mons, about 60 km in diameter, and suggested that crustal thickening

may be linked to the cessation of volcanic activity. Though mentioning a similarity between Syria Planum and the Snake River Plain, no formal comparison was made.

Hauber et al. (2009) conducted a survey of martian low-shields in the Tharsis region using topographic data from MOLA elevation dataset combined with a slightly larger image set from HRSC than used by Baptista et al. (2008), as well as Mars Orbiter Narrow-Angle Camera (MOC). They determined that the only difference between terrestrial low-shield volcanoes and those of Mars is the flank slope; those on Mars having a shallower slope (< 0.5° for martian shields and < 11° for terrestrial shields), and the only volcanoes on Earth with comparable flank slopes being on the Snake River Plain. They cite Greeley (1982) and Walker (2000) but make no numerical comparisons. Hauber et al. (2009) suggested high eruption temperatures and high iron content as well as near surface magma chambers could explain the low flank slopes. If high morphologic similarity is proven to exist between the volcanoes of Syria Planum and the Snake River Plain, then this hypothesis can be tested by examining the iron content and eruption temperatures of lavas from Snake River Plain shields (e.g., Leeman, 1978, Putirka et al., 2007, Bradshaw, 2013) with low and high flank slopes. Hauber et al. (2009) also concluded that the low-shield volcanism in Syria Planum is not related to a deep mantle plume, but to a shallow zone of partial melting in a persistently warm mantle under thickened crust.

By examining the volcano distribution, Richardson et al. (2013) concluded that each volcano on Syria Planum was formed by a separate magma body that was not part of a large, common, shallow magma reservoir. They determined that Syria Planum volcanism was influenced by changing stress fields in the three major tectonic centers (Noctis Labyrinthus, Claritas Fossae, and Solis Planum) that surround it (Figure 2); the changes forced an evolution from a single central vent volcano (Syria Mons) to the dispersed volcanism of the low shields.

Their impact crater retention ages support the proposed evolution of the region. This hypothesis can also be tested to see if changing stress fields resulted in dispersed volcanism on the Snake River Plain.

Although each of these papers mention similarities between Syria Planum and the Snake River Plain, none made formal comparisons. The purpose of this study is to complete a detailed analysis of the morphometry and distribution of volcanoes in both Syria Planum and the Snake River Plain to determine the extent of similarity in these two factors between the volcanoes of the two areas. If there is a high degree of similarity, then field studies of the Snake River Plain will have important and direct implications for understanding volcanism on Syria Planum.

Thus, the major questions to be addressed are: (1) How similar are the morphologies and sizes of the volcanoes of Syria Planum and the Snake River Plain? (2) Does distribution of volcanic vents on the Snake River Plain reveal a tectonic control by regional extension and, if so, is it comparable to what is observed in Syria Planum? What do tectonic controls on the volcanism in both regions imply about the structure and character of the lithosphere? (3) Using an understanding of the compositions, eruptive histories, and mechanisms of the Snake River Plain low-shield volcanoes, what do the similarities or dissimilarities of the volcanoes in the two regions imply about the Syria Planum volcanoes?

2. Methods

To answer these questions, the morphometry and distribution of the low-shield volcanoes on Syria Planum and the eastern Snake River Plain were analyzed using images, digital elevation models, several tools in ArcGIS 10 software by ESRI, and JMP statistical software from SAS Institute Inc. In order to maintain consistency, the same methods for identifying and processing low-shields were used on both the Snake River Plain and Syria Planum.

Using nine quadrangles from the National Elevation Dataset produced by the U.S. Geological Survey (USGS), a 10 m resolution DEM (digital elevation model) was mosaicked together for coverage of the Snake River Plain. These quadrangles were obtained through the USGS National Map Viewer and Download web page. Orthorectified 1 m resolution photographs from World Imagery downloaded from ArcGIS online, as well as geologic maps developed by LaPoint (1977), Kuntz et al. (2007), Lewis et al. (2012) and others were used to assist in the identification and measurements of topographic shields and summit craters if present.

Digital elevation models from MOLA (Mars Orbiter Laser Altimeter, Smith et al., 2003) with an approximate ground resolution of 462 m per pixel, and from HRSC (High Resolution Stereo Camera, Neukum et al., 2004, Jaumann et al., 2006) with an approximate resolution of 75 m per pixel were used for morphometric measurements on Syria Planum. MOLA calculated elevations using the time to reflect laser pulses from the surface giving a vertical resolution of approximately 13 m (mola.gsfc.nasa.gov/topography.html), and HRSC gives a vertical resolution of approximately 10 m using stereo imaging (Jaumann et al. 2006). We carefully evaluated the usefulness of the two types of elevation data on Mars. The HRSC DEM gave better correlations between Syria Planum and Snake River Plain volcanoes.

The Mars Odyssey THEMIS (Thermal Emission Imaging System, Christensen et al., 2004) day and night images with an approximate resolution of 100 m per pixel, as well as CTX (Context Camera, Malin et al., 2007) images with an approximate resolution of 8 m per pixel were used to aid in the identification and measurements of topographic shields and summit craters. JMARS (Java Mission-planning and Analysis for Remote Sensing, Christensen et al.,

2009) was used to identify the correct orbit and image tracts with sufficient coverage of the area for download and processing.

Morphometric characteristics considered for each topographic shield were area, diameter, height, slope, volume, the orientation and length of major and minor axes, and eccentricity of the shape in plan view. Crater diameter, depth, and orientation were also measured. Spatial distribution parameters considered were orientation angle of the major axis, number of overlapping shields, number and alignment of vents, nearest neighbor and two point azimuth distributions. Using tools in ArcGIS, shields were defined by draping a color stretched DEM on a vertically exaggerated shaded relief image of the area. Images were carefully evaluated for vent and/or radial flow patterns where "bull's eye" patterns were seen in the colorized DEM or in the shape of calculated contour lines. The edge of each shield was identified as a break in slope and disappearance of simple concentric contour lines. The resulting outline was then used to clip the surfaces of the shields from the DEM for further analysis. Only the topographic shield was measured; the surrounding flow field was excluded. This facilitates comparison between the two planets because the extents of flow fields around many of the martian shields are unknown and flow contacts are completely obliterated.

This "shape file" was used to define the base of the shield and summit craters, and the area was found by using the "calculate geometry tool" in ArcGIS. Shield and crater diameter were defined as the diameter of a circle with the same area as the topographic shield or crater. Shield volumes were measured using the "Surface Volume tool" in ArcGIS. Heights were defined as the difference between the highest and lowest points of the shield's clipped DEM. Flank slopes were measured using two methods. The first method was consistent with current convention and uses the height of the shield and radius of a circle with the same area as the

shield base to calculate the slope of a cone using the equation $\theta = tan^{-1}\left(\frac{h}{r}\right)$, where **θ** is the angle of the flank slope in degrees. The second method uses the "Slope tool" in ArcGIS to create a slope map of the shield. Each cell value on this slope map is the average slope from that cell to its eight immediate neighbor cells. The slope of the shield is then taken to be the average of all cell values in the slope map. The standard deviation of the slope angle calculated in this way is a measure of surface roughness. A statistical summary of these morphometric measurements is listed in Tables 1and 2, and all morphometric measurements for shields and craters are listed in Appendix A.

The "Zone geometry tool" in ArcGIS was used to find a best fit ellipse to shield and crater outlines. The tool gives the length and orientation of the major axis as the first eigen-vectors and the minor axis perpendicular to it; these axes were then used to determine the eccentricity of each shield and crater. Eccentricity is defined as E = $\sqrt{1-\frac{b^2}{a^2}}$ where **a** is the length of the semi-major axis and **b** is the length of the semi-minor axis (when a = 0 the object is circular and when a = 1 it is linear). A statistical summary of eccentricity is listed in Tables 1 and 2; all ellipse information is listed in Appendix A.

Spatial distribution and structural indicators were analyzed using nearest neighbor, two point azimuth analysis, and the orientation of the major axis of each shield and crater. The nearest neighbor and two point azimuth analysis were similar to methods used by Richardson et al. (2013) and Cebriá et al. (2011), but adapted for use in ArcGIS; using the "Generate near table" and "Bearing distance to line" tools. The minimum significant distance used to find alignments possibly influenced by structural regimens is defined by Cebriá et al. (2011) as $d \leq \frac{(\bar{x}-1\sigma)}{3}$ where $\bar{x}$ is the mean distance and σ is the standard deviation.

We used a Ward Hierarchical clustering analysis in JMP (2007) to explore and define relationships among the shields within each area, and between the areas. Height, slope, volume, area, and eccentricity of the shields were used as the clustering variables and for principal component analysis, also conducted in JMP. A one way analysis of variance test was employed to fit regression lines to pairs of morphometric characteristic variables to evaluate the correlation between variables and determine any predictive relationships.

3. Analysis

3.1. Shield Volcanoes on the eastern Snake River Plain

Analysis of the eastern Snake River Plain reveals a variety of volcanic structures including rhyolite domes, cinder cones, maars, and 246 low-shield volcanoes. As seen in Figure 3, the distribution of these shields appears to be more random to the west and becomes more tightly clustered in the east and on the axis of the plain. This tight spatial clustering appears to be related to north/south trending normal faults and to the central axis of the plain, and possibly to ring faults of silicic calderas that underlie the plain (Figure 3).

The basic morphometric characteristics for Snake River Plain low shields and craters are listed in Tables 1, 2, and 3. A complete listing of all morphometric measurements is found in Appendix A. Profiles of representative Snake River Plain low shields are shown in Figure 4.

The shields have heights between 26 m and 244 m with 90% of heights less than 150 m, and flank slopes between 1° and 8° with 79% of slopes less than 3° (Table 1; Figure 4). These slope measurements fit within Walker's (1993) definition of shield volcano slopes of less than 15°. Diameters of these shields are between 0.5 km and 14 km with 90% of diameters less than 8 km and volumes between 0.001 km^3 and 13 km^3 with 93% of volumes less than 3 km^3 (Table 1;

Figure 5). These volumes also fit within Walker's (1993) definition of low-shield volumes of less than 15 km^3. However, these volumes may be a low estimate as over half the Snake River Plain shields have more than 75% of their flanks buried by adjacent flow fields and further 10% of shields with 50 to 75% of their flanks buried by adjacent flow fields (Table 3). Category 0 shields (n=20) are shields with 0% of their topographic shield flanks buried by adjacent flow fields. These are on average 3 times larger in volume, 1.5 times taller, and have diameters almost 2 times larger than the average of the category 4 shields (n=167) which have 75 – 100% of their flanks buried by adjacent flow fields.

The eruptions that formed these shields likely started as fissure eruptions that condensed to a central point vent. This, along with the regional slope and original topography would likely influence the eccentricity of the shields. The eccentricity of the craters is likely influenced by the location, orientation and shape of the feeder dikes. Eccentricity, especially on the Snake River Plain, is also influenced by the spatial density of the volcanoes.

All topographic shields have identifiable vent structures. These vent structures are divided into two categories, pit crater or point vent. We define a pit crater as a recognizable depression at the volcanic vent and a point vent as the highest topographic point where recognizable radial flow textures can be identified and no pit crater is present. We delineated 186 pit craters (76% of the shields), and 159 point vents (65% of the shields). About 23% of the shields have multiple vents: half of these are multiple point vents and half are multiple pit craters, only 5 shields have both multiple point vents and pit craters. Although these vents do show alignment, they do not form chains of spatially overlapping pit craters or fissure like collapse features like the multiple vent structures on Syria Planum.

3.2. Shield Volcanoes on Syria Planum

A catalog of 258 low-shield volcanoes was constructed for Syria Planum; 133 of these are covered by both the MOLA and HRSC elevation datasets (Fig. 2). The distribution of these shields is sparse in the northwest part of the plain; volcanoes are concentrated in a triangular area on the topographically higher, eastern part of the planum (Fig. 2).

We used both MOLA and HRSC datasets to make measurements on the shields in Syria Planum. We compared corresponding measurements for 133 shields covered by both elevation datasets and found that when HRSC data is used, shields are higher, steeper, and have greater volumes than when measured with MOLA data (Figure 6). We found an average height difference for volcanoes measured using both DEMs of 88 m +/- 51, and volume difference of 6 km^3 +/- 8 km^3.According to Jaumann et al. (2007) there is a height difference between HRSC and MOLA datasets that is distributed around 0 with a standard deviation of 98 m; they attribute this difference to interpolation artifacts in lower latitudes. Because the HRSC elevation dataset is developed using stereo images, image quality is a factor; high dust concentration and atmospheric effects may cause lower quality images and those images could degrade the accuracy of the elevation dataset. However, a careful inspection of the images available for the study area shows that sufficient high quality images were available that the DEMs produced form the stereo images should not have been negatively affected. As explained below, we prefer the elevations from the HRSC DEM for volcano measurements.

A statistical summary of the basic morphometric characteristics for low-shields and craters are listed in Tables 1 and 2. A complete listing of all morphometric measurements is found in Appendix A, using both MOLA and HRSC elevations. Topographic profiles of representative low shields on Syria Planum, organized by cluster, are shown in Figure 7.Using HRSC elevation

information (Fig. 5), the shields on Syria Planum have heights between 60 m and 550 m with 90% less than 320 m, and flank slopes between 0.5° and 7° with 94% less than 3°. These slope measurements fit within Walker's (1993) definition of shield volcano slopes of less than 15°. Diameters of these shields are between 3 and 40 km with 90% less than 20 km and volumes between 0.5 km^3 and 250 km^3 with 93% less than 45 km^3. Approximately 70% of the Syria Planum low-shields fit within Walker's (1993) volumetric definition for low-shields of < 15 km^3.

Previous studies have reported volumes and flank slopes by assuming the shields had the shape of a right cone using measured heights and diameters (e.g. Greeley, 1981, Baptista et al., 2008, Hauber et al., 2009). Although this is an appropriate first order approximation for the volume and slope of a shield, it is not the most accurate method of measuring the volume or slope. For example, volumetric measurements using the complete surface shape in ArcGIS are circa 17% larger than those calculated using a simple cone estimation, as would be predicted because of the concave-down shapes of most shield volcanoes (Figure 7).

All shields have identifiable vents, with 131 point vents (approximately 50% of the shields) and 134 pit craters (approximately 50% of the shields). Whereas a significant number of Snake River Plain shields have multiple vents, only 27 (about 10%) of Syria Planum shields have multiple vents at the resolution of the THEMIS imagery used. All but one of these multiple vents are pit craters, with 78% forming linear chains with an average of 3 pit craters in a chain (Figure 8). Instead of pit craters, many of Syria Planum's volcanoes have highly elongate fissure-like vents (Figure 8); these are rare on the eastern Snake River Plain. The lack of scalloping on the rims of the long edges suggests that these are not spatially overlapped pit craters. These structures comprise approximately 30% of the identified vent structures on Syria Planum. They

have eccentricities greater than 0.9, making them nearly linear and they are included in the total pit crater count.

3.3. Statistical Analysis

A statistical analysis of the morphometry of volcanoes gives a quantitative breakdown of the similarities and differences between volcanic types. In statistical analysis, principal component analysis groups variables (measured attributes of the shields) that appear to explain the same variance in the data. These groups are then ranked such that the first group defines the greatest variance, the second is the greatest variance orthogonal to the first, and so on, each of them being principal components. Cluster analysis groups data points (i.e., shields) based on their response to specified variables. We completed both cluster analysis and principal component analysis on Snake River Plain low shields as well as Syria Planum low shields and as a combined dataset. To broaden the analysis and see if low-shield morphometry is distinctive from other terrestrial volcano morphometry, we also did cluster and principal component analyses of terrestrial volcanoes measured by Pike and Clow (1981) and Rossi (1995). For both cluster analysis and principal component analysis we used height, slope, volume, area, and eccentricity as the variables for Snake River Plain and Syria Planum low-shields. However, Pike and Clow (1981) reported eccentricities for calderas and craters, but not for the shield or cone and Rossi (1995) did not report any eccentricities. For this reason we excluded eccentricity as a variable in all analyses that include data from Pike and Clow (1981) and Rossi (1995). We excluded Pike and Clow's (1981) pseudocraters, maars, and tuff ring/tuff cones from principal component and clustering analyses due to the overpowering dimensions of their craters creating "negative" volumes. We calculated volumes for terrestrial volcanoes measured by Pike and Clow

(1981) by assuming the shape of a truncated cone and subtracting the cylindrical volume of the crater.

Principal component analysis is useful in reducing the number of variables to orthogonal linear combinations of the original variables. These analyses produced two principal components that combined usually explain over 75% of the variance in the datasets. Principal component one is always a linear combination of height, area, and volume, and we call this the "size" component. Principal component two is either a linear combination of slope and eccentricity or just slope when eccentricity is excluded; we call this the "shape" component.

3.3.1. Principal component and cluster analysis of various terrestrial and martian volcanoes

According to principal component analysis (PCA) of Snake River Plain and Syria Planum low-shields in combination with the terrestrial volcanoes, the size component accounts for 58% of the variances in morphometry, whereas the shape component (which consists solely of slope, as eccentricity is excluded in this analysis) accounts for 26% of the variances in morphometry. Although there is overlap, a plot (Figure 9) of the size component and shape component shows distinctive patterns for several categories of terrestrial volcanoes. The analysis shows cinder cones (C), cinder-spatter cones (Cs), lava domes with summit depressions (D), and cratered table mountains all fall in the same very narrow size range; for this reason we group them together and refer to them as *terrestrial cones*. These terrestrial cones form a continuous spectrum of slopes and the different classes form overlapping segments of this continuum.

Stratocones, both with summit craters (SCr) and with summit calderas (KCa), have a wider size range, with the majority being much larger, and a similar range in slope when compared with terrestrial cones. Shields include large shields (LS), Icelandic shields (SI), small

steep shields (SS), olivine tholeiite shields (OT) (Rossi, 1995), and picrite basalt shields (P) (Rossi, 1995). Table 4 list the abbreviations for volcano classifications used in this study and by Pike and Clow (1981). Like the terrestrial cones, the shields appear to form a continuous spectrum but in the size component instead of the slope component with the Icelandic, small steep, olivine tholeiite, and picrite basalt shields occupying a vary narrow range on the small end of the size spectrum and the large shields occupying the remainder of the spread. It appears that all shields have a well-defined range in shape (Figure 9). Ash-flow calderas appear to have the same extensive size range as lava shields, but half the shape range. Snake River Plain and Syria Planum low-shields plot virtually on top of one another in the principal component analysis (Figure 9). They have the same very narrow range in size as terrestrial cones, but little to no overlap with the terrestrial cones on the slope axis. Showing that though the Snake River Plain and Syria Planum low-shields are comparable in size, their slopes are distinctly smaller than terrestrial cones. The analysis shows that the slopes of the ash-flow calderas reported by Pike and Clow (1981) are comparable to Snake River Plain and Syria Planum low-shields, however, the ash-flow calderas are much larger in the size component and there is little to no overlap in size.

The smallest of the stratocones reported by Pike and Clow (1981) have comparable slopes to Snake River Plain and Syria Planum low-shields, but there is no overlap in size with the Snake River Plain shields and only the largest of the Syria planum shields overlap in size with the stratocones. The principal component analysis shows that some of the smaller shields reported by Pike and Clow (1981) have comparable slopes to those of the Snake River Plain and Syria Planum low-shields, but the majority are larger in both size and slope. However, the olivine tholeiite and picritic basalt shields measured by Rossi (1995) overlap completely in both size and slope with the Snake River Plain low-shields. The very little to no overlap in either

component of the Snake River Plain and Syria Planum low-shields with all other terrestrial volcanoes, with the exception of the olivine tholeiite and picrite basalt shields (Rossi, 1995), shows that the Snake River Plain and Syria Planum shields together form their own category.

Cluster analysis compliments the principal component analysis of this combined dataset (Figure 10a). Height, area, volume, and slope were used as clustering criteria, we used the scree plot to identify a natural break in grouping resulting in six characteristic groups. *Cluster 1* (n = 560) contains volcanoes that are short (h < 1 km), have low volume and base area (v < 3,000 km^3, a < 10,000 km^2), and low to moderate slopes (s < 16°). All Snake River Plain and Syria Planum low-shields are part of this cluster and account for 68% of the volcanoes in the cluster. Sub-cluster 1a (Figure 10a) consists almost entirely of shields from these two volcanic fields. Small stratocones with summit calderas (KCa) and ash-flows calderas (AF) are the next most abundant type of volcano included in cluster 1, and account for 9% and 5% respectively of the volcanoes in the cluster. However, most are in a clearly defined sub-cluster (1b on Figure 10a). Sub-clusters (1c and 1d) contain all of Rossi's (1995) Icelandic olivine tholeiite and picrite basalt shields and Pike and Clow's (1981) small steep shields (SS) as well as several volcanoes from Syria Planum. Small stratocones with summit craters (SCr) and a few large shields account for about 2% of cluster 1 and are concentrated in sub-clusters 1b, 1c, and 1d.

Cluster 2 (n = 109) contains volcanoes that have slightly larger sizes and flank slopes than cluster 1 volcanoes. The inter-variable relationships of this cluster are slightly more exaggerated than those of cluster 1. This cluster is dominated by stratocones; Stratocones with summit craters (SCr) account for 41% and Stratocones with summit calderas (KCa) account for 48%. The remaining 9% are 8 large shields (LS) and 2 Icelandic shields (SI). *Cluster 3* (n = 59) is composed of tall volcanoes (1.7 < h < 3 km) that have moderate volumes, base areas, and

slopes ($v < 7{,}000$ km^3, $a < 6{,}000$ km^2, $3° < s < 16°$). This cluster is also dominated by stratocones (SCr 32%, KCa 52%) and large shields (15%). *Cluster 4* (n = 22) is similar to cluster 3, but with much larger heights ($2.5 < h < 5$ km). Volume, base area, and slope ranges for this cluster are comparable to cluster 3. Over 90% of the volcanoes in *Cluster 5* (n = 85) are terrestrial cones with the remainder accounted for by stratocones. This cluster is characterized by low ($h < 1$ km), exceptionally small volume and base area ($v < 10$ km^3, $a < 20$ km^2), very steep ($16° < s < 55°$) volcanoes. *Cluster 6* (n = 8) is composed of 7 large shields and 1 ash-flow caldera. These are all very tall ($h > 1.8$ km), large volume and base area ($v > 15{,}000$ km^3, $a > 6{,}000$ km^2) and low slope ($s < 7°$). The ash flow is distinguishable from the large shields by having a greater base area for the height and volume.

In summary, principal component analysis reveals, as expected, that size (height, basal area, and volume) and shape (flank slope) are important variables for volcano morphometry. Cluster analysis shows that Snake River Plain and Syria Planum low shields are more similar to each other than any other type of volcano considered here (cluster 1a in Figure 10a).

3.3.2. Principal component and cluster analysis of Snake River Plain low-shields

The principal component analysis of only Snake River Plain low-shields using height, area, volume, slope and eccentricity as variables yields two significant principal components that are very similar to those identified for the combined dataset. The first component is a linear combination of height, area, and volume that accounts for 50% of the variance in the dataset, which we again term the size component. The second component is a linear combination of slope and eccentricity, the shape component, which accounts for 20% of the variance in the dataset.

Based on the natural breaks in the scree plot of the cluster analysis, six clusters adequately describe the main morphometric groups of the plain. Figure 4 shows profiles of an

exemplary volcano in each cluster and Figure 10b the results of the cluster analysis and the morphometric character profiles. Two-point azimuth analysis of Snake River Plain shields reveals possible structural controls on the emplacement of the shields on the plain (Figure 11).

Cluster 1(n = 45), exemplified by Little Wildhorse Butte, contains shields that are low to moderate (as compared to all other shields in the plain) in height (h < 96 m), have moderate base areas but small volumes (a < 40 km^2, v < 1 km^3). The slopes of these volcanoes widely varies from very low to moderate (1° < s < 5°), and all have relatively moderate eccentricities (e < 0.6). These shields are spread through the whole plane (Figure 4, 11) with 58% buried by younger or adjacent flows on more than 75% of their flanks. Two-point azimuth analysis of this cluster does not reveal any obvious alignments or structural influence. *Cluster 2* (n = 113) includes shields that are similar in size and slope to cluster 1 shields, but have greater eccentricities (0.5 – 1). These shields are also fairly evenly distributed through the plain (Fig 4, 11) with 58% of the shields buried by younger or adjacent flows on more than 75% of their flanks. Two-point azimuth analysis of this cluster reveals two areas where strong structural influence is possible (Figure 11) including the Spencer-High Point rift zone west of Island Park. *Cluster 3* (n = 27), e.g. Cottrells Blowout, contains shields that are moderate in height (h < 132 m) with very small volumes and base areas (v < 0.5 km^3, a < 10 km^2). These shields are relatively steep (compared to the remainder of Snake River Plain low-shields) with slopes between 3° and 8° as well as highly eccentric (0.5-0.9) (Figure 4, 11). These shields are also found throughout the plain with a small tight group of them along the Spencer-High Point rift near the Island Park caldera, which is the only place that two-point azimuth analysis of this cluster suggests a strong structural influence. Over 85% of these shields are buried by younger or adjacent flows on more than 75% of their flanks. *Cluster 4* (n = 42) is characterized by shields similar to Dietrich Butte; tall (81 m

– 257 m) with mid-range volume (v < 3km^3), base area (a < 62 km^2), and slope (1° – 4°). These shields vary widely in eccentricity (0.2 - 0.8) and 52% of them are buried by younger or adjacent flows on more than 75% of their flanks. In the western half of the plain they are evenly spread north to south as well as east to west. However, in the eastern part of the plain, these shields are concentrated around the central axis of the plain. *Cluster 5* (n = 17), characterized by Kimama Butte, are relatively tall (79 m – 240 m) shields with large base areas (a < 155 km^2) but moderate volumes (v < 7 km^3) and moderate to low slopes (s < 3°). These shields vary in eccentricity and 47% of the shields are buried by younger or adjacent flows on less than 25% of their flanks; the remaining half are buried on more than 75% of their flanks. Two-point azimuth analysis of this cluster does not show any significant structural controls for this small group. However, the majority of these shields are located in the western half of the eastern Snake River Plain where there are fewer shields, and those that are located in the eastern half of the plain are also in areas of low vent density. *Cluster 6* (n = 2) contains the largest of the shields, exemplified by Rocky Butte. These shields are tall (157 m, 209 m) with large base areas (144 km^2, 152 km^2) and volumes (13 km^3) but low slopes (< 2°) and moderate eccentricity (0.4, 0.6). These shields are also located in the western half of the field where vent density is relatively low. Table 5 is a statistical summary of Snake River Plain and Syria Planum clusters.

3.3.3. Principal component and cluster analysis of Syria Planum low-shields

Principal component analysis of Syria Planum low-shields gives three components that explain a significant amount of the variance in the dataset without repeating combinations of the variables. Principal component 1 is size, as found for the other comparisons, and accounts for 49% of the variance. However, principal component 2 consists only of slope (27 % of variance)

and component 3 has only eccentricity (19% of variance) as the sole variable, showing that eccentricity is more influential on Syria Planum (Table 6).

Using the scree plot from the cluster analysis six clusters are identified that adequately describe the main morphometric groups of the planum (Figure 10c). Figure 7 shows profiles of examples of each cluster. Two-point azimuth analysis of Syria Planum shields reveals possible structural controls on the emplacement of the shields on the planum (Figure 12).

Cluster analysis was performed on shields in the HRSC elevation dataset. *Cluster 1* (n = 15) are relatively small shields that have low to moderate values for height (< 260 m), base area (< 290 km^2), volume (< 26 km^3), slope (< 2°), and eccentricity (< 0.4), as compared to all other shields in the planum (Figure 7). These shields are concentrated in near the central portion of the area covered by the HRSC elevation dataset (Figure 12). *Cluster 2* (n = 74) are also relatively small in size, but have a wider range of slopes (0.6° – 3°) and larger eccentricities (0.5 -0.9). These shields are fairly evenly dispersed within the HRSC elevation dataset area. *Cluster 3* (n = 10) are tall (260 m – 470 m), steep (2° – 6°) shields with moderate base area and volumes (a < 275 km^2, v < 50 km^3) with a wide range of eccentricities (0.3 – 0.8). This small group of shields is concentrated in the central portion of the area covered by HRSC elevation model. *Cluster 4* (n = 23) volcanoes are moderately sized shields with low slopes (< 2°) that are highly eccentric (0.5-0.8). These shields are very evenly distributed throughout the area. *Cluster 5* (n = 9) are medium sized shields with low slopes (< 2°) and lower eccentricities (0.3 – 0.6). These shields are also evenly dispersed through the area. *Cluster 6* (n = 2) contains the two largest shields in the HRSC dataset (Shield 47 and Shield 151); they are tall with large base areas and volumes, low slopes and moderate eccentricities and are located in the center and north of the area.

Cluster analysis was also conducted on the dataset combining Snake River Plain and Syria Planum shields (Figure 10d). The scree plot was used to determine that six clusters were sufficient to describe the main morphometric groupings. Profiles of example shields from each cluster are shown in Figure 13. Snake River Plain shields are distributed in four clusters where Syria Planum shields are distributed throughout all six clusters. *Cluster 1* (n = 45: n_{eSRP} = 43, n_{SP} = 2). This cluster contains small base area and volume (a < 13 km^2, v < 3 km^3) shields that have relatively steep slopes for their size (3° - 8°) which consists of the majority of the steepest sloped shields in the two areas. The Snake River Plain shields in this cluster are average heights for the plain (h < 140 m) and the two Syria Planum shields are taller than the average for the planum. This cluster exhibits a wide variety of eccentricities. *Cluster 2* (n = 130: n_{eSRP} = 113, n_{SP} = 17) is characterized by shields that are of average height for the Snake River Plain, but smaller in height for Syria Planum, slightly larger base areas and volumes than cluster 1 (a < 72 km^2, v < 3.5 km^3) and highly eccentric (0.6 -1). These shields have average slopes for the two areas (~2°). *Cluster 3* (n = 60: n_{eSRP} = 56, n_{SP} = 4) shields have the same height, area, volume and slope characteristics as cluster 2 shields do, but are less eccentric (0.1 – 0.6). Over half of the Syria Planum shields are grouped into *Cluster 4* (n = 114: n_{eSRP} = 34, n_{SP} = 80) which also contains about 14% of the Snake River Plain shields. This cluster contains relatively tall Snake River Plain shields with average height Syria Planum shields (h < 385 m) that have larger base areas and volumes than clusters 1, 2, and 3 (a < 288 km^2, v< 26 km^3). These shields have average slopes (~2°) and a wide range of eccentricities (0.2 – 0.8). *Cluster 5* contains only Syria Planum shields (n = 28: n_{eSRP} = 0, n_{SP} = 28) that are average to large in height, base area, and volume (h < 480 m, a < 645 km2, v < 88 km3). These shields are slightly smaller in slope than clusters 1, 2, 3, and 4 (~ 1.6°) and have a range of eccentricities (0.3 – 0.8). *Cluster 6* contains the largest 2

shields in the HRSC dataset and no Snake River Plain shields. That Snake River Plain and Syria Planum shields are not separated into individual clusters with no overlap shows that the shields do have similar morphometries. However, the majority of the Syria planum shields are found in clusters that are characterized by comparatively larger measurements.

Principal component analysis of a combination of both Snake River Plain and Syria Planum low-shields again produces the first principal component as a linear combination of height, area, and volume that accounts for 52% of the variance within the dataset. A second component as a linear combination of slope and eccentricity accounts for 20% of the variance in the dataset. The score plot of these components shows that separation between the two groups of shields lies in the first principal component, which we have termed size. Snake River Plain and Syria Planum shields do form separate groups along the size axis with Snake River Plain shields appearing smaller than Syria Planum shields, but there is also considerable overlap in the two groups. From this, we conclude that slope and eccentricity are not significantly different between Snake River Plain and Syria Planum low shields; and that the morphometric difference between the volcanoes in the two areas lies in the overall size of the shields. This confirms the results of the cluster analysis.

3.3.4. Morphometric comparison with regression analysis

We compare pairs of morphometric characteristics using bivariate plots and regression line analysis to further demonstrate similarities and dissimilarities of Snake River Plain and Syria Planum low-shields with other terrestrial shields. The regression analysis gives a quantitative expression of the functional relationship between morphometric characteristics. The r^2 value we report represents how well the regression line represents the variation in the data, thus how well the regression line expresses how one variable is likely to be affected by a change in another

variable. An r^2 value close to 1 suggests that the regression line is a good fit and all points lie along the line, making the regression line equation a good predictor of the effect one variable has on another. In statistical analysis the p-value is a measure of the probability of rejecting the null hypothesis. The null hypothesis in this study is that the coefficient is equal to zero. A low p-value ($p < 0.05$) indicates that the null hypothesis can be rejected and the coefficient is likely statistically meaningful. We consider measurements from this study, as well as for other terrestrial volcanoes measured by Pike and Clow (1981) and Rossi (1995) as well as for Syria Planum low-shields measured by Baptista et al. (2008). (Although Richardson et al. (2013) and Hauber et al. (2009) measure low-shields from Syria Planum, the measurements of morphometric characteristics used in this study were not published and therefore the shields included in their studies are not included in this comparison.) For simplicity we have combined several of Pike and Clow's (1981) terrestrial volcano classifications. We also exclude Pike and Clow's (1981) tuff ring/tuff cones, pseudocraters, and maars from volumetric analyses.

Because the range of measurements is so large and the use of different units of measure, we use a log scale for the axes of each bivariate plot. Regression analysis was performed on natural log transforms of the data to accommodate for the skewed distributions of the data. The line resulting from a regression analysis is a power law of the form $y = (e^b)x^m$, where y is the y-axis variable, b is the y-intercept, x is the x-axis variable and m is the slope of the line. Results of regression line analysis for all volcanic groups are given in Table 7.

Though forming a distinct group, heights and diameters of both Snake River Plain and Syria Planum low-shields are comparable to other small terrestrial basaltic shields and some terrestrial cones (Figure 14) but their trends are not the same. When diameter and height are plotted (Figure 14), Snake River Plain and Syria Planum shields lie at opposite extremes of the

same trend that has a slope of 0.63 ($p < 0.0001$, $r^2 = 0.66$). On the other hand, regression analysis of the shields measured by Baptista et al. (2008) using MOLA elevations are consistently low for a given diameter and form a trend with a slope of 1.32 ($p < 0.0001$, $R^2 = 0.46$). This slope is more than 2 times steeper than the line for Snake River Plain and Syria Planum low-shields using HRSC elevations for Syria Planum shields. We suggest that this is because the HRSC DEM is more accurate. The sizes of the Icelandic olivine tholeiite and picritic shields (Rossi (1995) overlap with the Snake River Plain and Syria Planum (Figure 14b). With regard to diameter and height ratios, regression analysis shows that Snake River Plain and Syria Planum low-shields are more closely similar to the large shields than to various types of stratocones, although the slope of the best fit line for these large shields is 0.81 ($p < 0.0001$, $r^2 = 0.58$) is 1.2 times steeper. Moreover, the large shields are systematically higher and larger in diameter (Figure 14). Unexpectedly, as seen in Figure 14c, the D/H relationship for Snake River Plain and Syria Planum low-shields is similar to that of ash-flow calderas (Pike and Clow, 1981) with a slope of 0.63 ($p < 0.0001$, $r^2 = 0.46$) which is within 15% of the slope of the Snake River Plain and Syria Planum line. These similar trends may be due to how the ash-flow calderas are defined and measured.

Regression analysis of diameter and volume produce very well fitted lines showing a very close functional relationship between diameter and volume. Snake River Plain and Syria Planum low-shields maintain a distinctive group that overlaps with small steep shields (Pike and Clow, 1981) and olivine tholeiite shields (Rossi, 1995) but has a smaller variance in height for any given diameter (Figure 15). The combined Snake River Plain-Syria Planum line has a slope of 2.69 ($p < 0.0001$. $r^2 = 0.97$). The regression line for the 30 martian shields studied by Baptista et al. (2008) has a slope of 3.77 ($p < 0.0001$. $r^2 = 0.76$), which is 1.4 times steeper than the line

for our measurements (Figure 15b). As seen in Figure 15, the volumes of Syria Planum volcanoes are similar to the larger Snake River Plain and Icelandic shields, but smaller for a given diameter than stratocones because of their lower heights, as evidenced by their nearly parallel trends.

Bivariate plots of height and volume show that height and volume are also strongly positively correlated, though regression line analysis shows that a change in height does not affect as much of a change in volume as does a change in diameter evidenced by lower r^2 values for the regression lines (Figure 16). Shields measured by Baptista et al. (2008) have greater volumes for their heights given than any other terrestrial shields as well as our measurements of Syria Planum shields using HRSC DEMs. Although their heights are comparable to terrestrial cones, Snake River Plain and Syria Planum low-shields have larger volumes for a given height because of their larger diameters (Figure 16c). Though visually Syria Planum shields appear to follow the same H/V trend as ash-flow calderas (Figure 16d), the Syria Planum-Snake River Plain regression line has a slope that is 1.16 times steeper than that of ash-flow calderas. However, Syria Planum and Snake River Plain low-shields do have an H/V trend that is nearly parallel to that of terrestrial stratocones with summit craters.

When diameters and slopes are compared (Figure 17), Snake River Plain and Syria Planum low-shields continue to form a distinctive group that has lower slopes for a given diameter than many other types of volcanoes. Slopes of regression lines are reported in Table 7. The only terrestrial volcanoes that have significant overlap with Snake River Plain and Syria Planum low shields are the Icelandic shields of Rossi (1995) and large maars (Pike and Clow, 1981). Interestingly, all volcanic types show an inverse relationship of varying degrees between slope and diameter except the shields studied by Baptista et al. (2008), though this relationship

may be due to an outlier. This is consistent with our suggestion that the measurements are flawed in some way related to the very low heights (and consequently flank slopes: < 1°) estimated for these shields using MOLA elevations.

As with the diameter and slope relationships, Snake River Plain and Syria Planum low-shields have little to no overlap with most terrestrial volcanoes. They do occupy a similar height/slope morphospace as olivine tholeiites (Rossi, 1995), though Syria Planum low-shields are larger in height (Figure 18). Snake River Plain low-shields also show some overlap with terrestrial maars and Syria Planum low-shields overlap with the smaller terrestrial stratocones with summit calderas.

Bivariate plots and regression analysis of morphometric features show similar trends for both Snake River Plain and Syria Planum low-shields (Table 7). The volcanoes from the two regions form the upper and lower bounds of the same trends. This interplanetary low-shield group is separate and distinct form other volcanic structures; they are most similar to the olivine tholeiite shields of Rossi (1995) and similar in some respects to small steep shields (Pike and Clow 1981), many of which are from Iceland. The similarity of morphometric characteristics leads us to conclude that Snake River Plain shields are the most appropriate terrestrial analogs for the volcanoes on Syria Planum. Even so, Syria Planum shields are consistently larger in diameter, volume, and height than those of the Snake River Plain.

3.4. Elongation and structure of vents and shields

3.4.1. Orientations of shields and craters

The first eigenvector solution to a best fit ellipse with same area as the base area of the shield was used to calculate the orientation of each shield and pit crater. These orientations were

then divided into ten degree bins (0°-10°, 10°-20°, etc.) and plotted on rose diagrams to highlight significant orientation trends (Figure 19). Significant trends are defined as being one standard deviation above the mean (the average number of volcanoes per bin) and minor trends are defined as being above the mean but less than one standard deviation above the mean. The rose plot for the elongation directions of Snake River Plain shields shows significant orientation trends in the north-east, at 20° - 50° and 120° - 130°. Minor trends are seen at 60° - 90° as well as 160° - 170°. Snake River Plain crater orientations have significant trends at 0° - 10°, 110° - 120°, and 170° - 180°, with minor trends at 50° - 60°, 100° - 110°, and 140° - 170°. The dominant NE orientation of the shields is consistent with the orientation of the central axis of the plain probably defined by the direction of plate motion over a more or less fixed plume or plume channel (Schutte et al. 1998). On the other hand, the orientation of the vent craters are consistent with the orientations of the basin and range faults near the plain as well as trends seen in two-point azimuth analysis (Fig. 11). There is a regional slope to the plain; it is higher in the NE of the plain. This regional slope, as well as preexisting topography (e.g. older, buried shields), likely influenced the NE-elongation of the shields. However, the orientations of the craters were perhaps controlled by the basin and range faults crossing the plain that must act as conduits for the rising lavas and define elongated vents now marked by pit craters. Alternately, the regional stress field created dikes that follow this orientation and shaped the vents.

Syria Planum shields are elongated EW and broadly scattered between 60° to 120° (Figure 19) which has no particular alignment with any of the surrounding extensional features, which could control conduit geometry, or with the regional slope, which controls lava flow directions. Syria Planum pit craters are elongated NE at 10° – 20° and SE between 120° and 150° with minor trends at 0° – 10°, 40° – 60°, and 170° – 180°. These trends align with the principal

extensional features of eastern Noctis Labyrinthus (east of Syria Planum, Figure 2, 12) for the 10° – 20° trend and Claritas Fossae (on the west) for the 120° – 150° trend. The elongation directions of the pit craters also coincide with two-point azimuth analysis of all shields on the planum which shows strong SE alignments as well as some NE alignments (Figure 12). We suggest that these extensional features shaped dikes or could be used as conduits for erupting lavas elongating both shields and pit craters as they do on the Snake River Plain. Syria Planum has no narrow zone of concentrated volcanism like the Snake River Plain; thus lava field interactions occur far from the elevated vent areas and exert little control on the shape of the shields. Apparently, a strong relationship in the orientation of the volcanic vents with the existing fault systems in the region, just as it does for the eastern Snake River Plain.

3.4.2. Vent structures

Over half of the vent structures on the Snake River Plain and Syria Planum shields are simple pit craters. These are circular or elliptical depressions generally at or near the topographic summit of the shield. Shields with multiple pit craters are frequent on both the Snake River Plain and Syria Planum; however, multiple pit craters on Syria Planum shields tend to form chains (a series of craters in a linear alignment). Snake River Plain pit craters often have raised rims or spatter ramparts associated with them, where Syria Planum pit craters have no observable raised rims or spatter ramparts.

Similar to the shield diameter and height trends, Snake River Plain and Syria Planum craters form a distinctive group that is separate or has little overlap with other terrestrial volcanic craters with the exception of pit craters on Icelandic shields (Pike and Clow, 1981). Syria Planum craters are generally larger in diameter (>1000 m) than Snake River plain craters (50 to 1,000 m). They largely overlap in depth, but the deepest (>100 m) are on Syria Planum and the

shallowest (<8 m) are on the Snake River Plain (Figure 20a) (The absence of shallow craters may be a resolution problem on Mars.) The average ratio of crater diameter (D_{crater}) to shield diameter (D_{shield}) for Snake River Plain low shields is 0.11 +/- 0.1 and Syria Planum has a similar ratio of 0.12 +/- 0.06. This is nearly twice the published D_{crater}/D_{shield} ratio for Icelandic shields of 0.06, equivalent to the ratio for steep shields 0.12, and 1.5 times larger than the published ratio for low-shields of 0.08 (Wood, 1979). These ratios are also larger than the 0.03 +/- 0.02 ratio calculated from the crater measurements made on martian low shields from other regions by Hauber et al. (2009).

Using the same comparison criteria as Bemis (1995), we plot crater diameter and crater depth (Figure 20a), volcano diameter and the ratio of crater and volcano diameter (Figure 20b), as well as the volcano diameter and the crater diameter (Figure 20c). The plot of crater diameter and depth shows that both Snake River Plain and Syria Planum craters are similar to other terrestrial cones as well as small steep and Icelandic shields (Pike and Clow, 1981) and are distinctly different from stratocones and ash flows (Pike and Clow, 1981). However, when the ratio of crater diameter to volcano diameter is plotted against the volcano diameter, Snake River Plain shields and Syria Planum shields are shown to be distinctly different from terrestrial cones (cinder cones, etc.) and have very little overlap with lava cones as compiled by Wood (1979). With this particular comparison, Snake River Plain and Syria Planum shields show more overlap with stratocones with summit craters (Pike and Clow, 1981) and fit nicely with small steep and Icelandic shields. When crater diameter is plotted against volcano diameter, Snake River Plain and Syria Planum low-shields appear to follow the same trends as both other terrestrial shields and stratocones and distinctly different from terrestrial cones. From this we see that while craters on Snake River Plain low-shield are smaller than those on Syria Planum low-shields, they follow

the same morphometric trends, and their craters are proportionately similar to terrestrial shields and stratocones.

4. Discussion

Through our comparison of morphometric characteristics, cluster analysis, principal component analysis, and vent structure analysis, we conclude that the low-shield volcanoes of the eastern Snake River Plain and Syria Planum are similar in their morphometry. Cluster analysis of a dataset combining Snake River Plain and Syria Planum low-shields with other terrestrial volcanoes measured by Pike and Clow (1981) and Rossi (1995) shows that Syria Planum low shield are most similar to Snake River Plain low shields in height, area, volume and flank slope. Syria Planum low shields follow the same trends in diameter to volume, diameter to height, and diameter to slope relationships as Snake River Plain low-shields. When compared to other terrestrial volcanoes the low-shields consistently group together because of their small sizes and low flank slopes. While the morphometric characteristics of Snake River Plain and Syria Planum low shields do follow the same trends, Syria Planum low-shields are systematically larger (in height, base area, volume), though equivalent in shape (slope and eccentricity). They also follow the same volumetric trends but volumes of Snake River Plain low-shields average 20 times smaller than those on Syria Planum (Table 1). The Snake River Plain covers an area of approximately 33,000 km^2 where Syria Planum is roughly 700,000 km^2 which is approximately 7.5 shields per 1,000 km^2 for the Snake River Plain and approximately 0.4 shields per 1,000 km^2 on Syria Planum. The similar number of shields in the comparatively smaller area of the Snake River Plain forces more overlap of flow fields and burial of shields. Over 58% of the shields on the Snake River Plain are buried by younger or adjacent flows on more than 75% of their flanks where only about 10% are completely unburied. Thus, a majority of the shields are obscured and

true volumes and diameters are difficult to obtain, making the volumes of Snake River Plain shields reported by this study minimum estimates. Because of this we can postulate that Snake River Plain and Syria Planum low-shields may be even more similar in size than what is reported here. While a set of morphometric characteristic boundaries can be defined that would contain the set of terrestrial and martian shields, Snake River Plain and Syria Planum low-shields define an even smaller, well defined subset within these morphometric characteristic boundaries; supporting the conclusion that Syria Planum low-shields are most similar to Snake River Plain low-shields of all the volcano types considered here. Using this morphometric similarity between the two volcanic provinces, we can infer similarities in eruption and emplacement mechanisms and possibly the crustal and lithospheric structure of Syria Planum.

Hughes et al. (2002) stated that the style of magmatism found on the eastern Snake River Plain is dependent on crustal extension. Crustal extension is evidenced by the Basin and Range fault systems that are found on the north and south of the plain but do not propagate through the plain. Instead, according to Kuntz et al. (1992), volcanic rift zones that are parallel but not co-linear with the Basin and Range faults are where this extension is accommodated through dike injection instead of normal faulting. Our two-point azimuth analysis and crater elongations (Fig. 11, 20) agree with the locations of these volcanic rift zones. This implies that the emplacement of the low-shields in the Snake River Plain was tectonically controlled by extension. However, the major control is not the NW trending Basin and Range faults, but the NE-trending axis of the plain which most investigators conclude is the trace of the Yellowstone plume. The alignment is not as strong in the western part of the Snake River Plain where the volcanoes are more scattered and farther apart.

Similarly, our two-point and crater elongation analyses of Syria Planum low-shields agree with Baptista et al. (2008) and Richardson et al. (2013) that there is an underlying extensional tectonic control on their emplacement and morphology. Zhong (2002) concluded that a thermal plume does not completely explain the topography and geoid of the Tharsis region and the tectonic deformation, flexural loading, and crustal deformation of the area are best explained by volcanism (Banerdt and Golombek, 2000, Zuber et al., 2000, Phillips et al., 2001, Zhong and Roverts, 2003). However, the volcanism still requires a source. The major features of the Snake River Plain are plume related. The morphometric similarity of the Syria Planum shields to the Snake River Plain shields implies that their sources may be similar. The Syria Planum volcanoes are at the summit of a long-lived dome, which indicates the possibility of a mantle upwelling of some sort. Schumacher and Breuer (2007) suggest that the initial stages of volcanism on Syria Planum were due to a mantle plume that eventually died out. The volcanism sourced from the plume thickened the crust so that upper mantle was insulated sufficiently to continue to generate zones of partial melt (Figure 21). The regional extension on both planets is possibly a secondary control on the vent locations.

Bemis (1995) conducted a comprehensive study of shield volcanoes in three tectonically different regions and concluded that shapes and growth trends within a volcanic class (e.g. shield volcanoes, stratocones, etc.) may be due to factors other than eruptive style, namely the tectonic setting. She noted differences in size but primarily shape between the shields in Guatemala, Iceland, and the Snake River Plain. Guatemalan shields are in a subduction-related back-arc extensional graben and the lavas have higher SiO_2 contents (~52% vs. ~48% for the eastern Snake River Plain). Iceland is a mid-ocean rift zone influenced by a mantle plume, and the Snake River Plain is the track of a continental mantle plume trace influenced by Basin and Range

extension. Bemis (1995) concluded that the different tectonic settings influence magma supply rates, temperatures, fractionation of magma, and the duration of eruptions in each setting. She suggests a higher starting SiO_2 content and a single magma system that evolves over time for the subduction-related shields, resulting in steeper volcanoes (8° +/- 3° vs 2.5° +/- 1° for the eSRP). For the mid-range (in both size and flank slope in comparison to the Guatemalan and Snake River Plain shields she cataloged) Icelandic shields she points to the relatively consistent plate motion away from the source limiting the persistence of eruption at any one location that possibly reflects variation in composition and volume in the magma supply. However, she states the consistency of the size and shape of the Icelandic shields suggests consistency in the average composition and temperature of the magma source. For the Snake River Plain she suggests larger volumes of magma rise through the crust faster than either Guatemala or Iceland resulting in less evolved magmas erupting at higher temperatures, which produces shields with lower flank slopes.

Hauber et al. (2009) cataloged low-shields found in four different areas on Mars: Syria Planum, Tempe Terra, the Ceraunius Fossae region, and south and east of Pavonis Mons. Richardson et al. (2015) also identified low-shields within the caldera of Arsia Mons. Hauber et al. (2009) state that there is no obvious spatial correlation between the low-shields found in these provinces and major geologic structures but local tectonic trends control and influence the elongation of shields and craters.

We propose that the similarity between the Snake River Plain and Syria Planum low-shields is sufficiently strong to imply similar eruption mechanisms and magma sources. Hughes et al. (2002) proposed a scenario based on partial melting and requires small portions of partial melt to be extracted from the parent source located in the upper mantle and rise through the

upper crust in dikes, and suggest separate, low-volume batches of melt extracted from local reservoirs dispersed beneath the plain for each of the shields. These partial melts may stall in the middle crust and may be where the magma can differentiate into a denser Fe-rich magma (Christiansen and McCurry, 2008) (Figure 21). Zones of regional extensional stress may facilitate dike propagation feeding fissure eruptions that eventually localized to one point to form the shields of the Snake River Plain. This proposal of magma source for the Snake River Plain shields is similar to that proposed by Hauber (2009) for Syria Planum low-shields, which we conclude to be a reasonable explanation for both regions of volcanism.

Morphometric characteristic comparison of Snake River Plain and Syria Planum low-shields shows that they are members of the same spectrum of shield volcanoes, with Syria Planum low-shields systemically larger than Snake River Plain shields. This size difference is likely a complex relationship of intrinsic and extrinsic factors linked to the different sizes of the planets. Intrinsic factors such as temperature, composition, rheology, and content of dissolved gasses are affected by the location at which the planet accreted. Earth and Mars are both "rocky" planets with similar bulk compositions, although Mars contains higher concentrations of moderately volatile elements and has a mantle that is richer in oxidized iron (Taylor, 2013). The two planets also have basaltic magmas that presumable have similar rheology and likely similar eruption temperatures (Francis, 1993, Baptista et al. 2008, Hauber et al., 2009, Lopes, 2013). The extrinsic factors imposed by gravity and the atmosphere are affected by the size of the planet itself. Smaller planets have less mass and therefore smaller gravity. With less mass, smaller planets are less able to maintain substantial atmospheres. Gravity factors into many geologic processes such as the depth of melting in a planetary mantle to the maximum height of a pyroclastic projectile and everything in between (Lopes, 2013). Also important to note is the

affect gravity has on the minimum ascent rates required for magmas to reach the surface of a planet.

Buoyancy is the force that causes magma to rise within a planet and is defined as $F_b = g(\rho_r - \rho_m)V$; where F_b is the buoyant force, g is gravity, ρ_r is country rock density, ρ_m is magma density, and V is the volume of the magma. Densities of basaltic magma on Earth and Mars are unlikely to differ by more than 10% (Best, 2003). If we let the density difference between country rock and magma be proportionally equal for both planets and assume the same force is necessary for magma to rise, then the volume of a magma batch on Mars must be a maximum of 2.66 times larger than those on Earth. The ratio of the gravitational forces of the two planets is 2.66 (Figure 22). In addition, because the gravity on Mars is less, ascent rates would be slower for similar sized magma batches, requiring larger magma batches to avoid excessive cooling during ascent (Lopes et al., 2013). The lower gravity on Mars also produces less crustal compaction resulting in deeper neutral buoyancy zones, requiring wider dikes for magma transport to the surface (Francis, 1993, Lopes, 2013). However, dikes are limited in their vertical extent by the elastic deformation of the country rock, implying only a fixed quantity of magma can rise at any given time (Melosh, 2011). Melosh (2011) derived a formula for the length of a dike in terms of the volume, viscosity, and density difference which also shows that the volume of magma erupted increases as gravity decreases. This equation, $L_c = \frac{E^{1/2}(2Q_d\eta)^{1/6}}{(\Delta\rho g)^{2/3}}$ (L_c = length of the crack, E = Young's modulus, Q_d = volume discharge, η = viscosity, $\Delta\rho$ = density difference, g = gravity). These conditions promote higher eruption velocities and volumes on smaller planets. These higher effusion rates in combination with a thin atmosphere would cause surface flows to cool more slowly and flow farther, thus forming the larger, shallow sloped edifices like those on Syria Planum.

5. Conclusions

This study quantitatively reinforces previous qualitative conclusions that the low-shield volcanoes of Syria Planum and the Snake River Plain are similar. We also show that higher resolution topographic data (HRSC) produce measurements with greater similarities to the morphometric trends defined by the volcanoes of the Snake River Plain. Consequently, insight into the development of such volcanoes can be developed by comparison with Snake River Plain volcanoes. The volcanoes probably have similar eruption mechanisms, rates, and durations, and lavas with similar viscosities and compositions.

The larger sizes of the shields on Syria Planum than on the Snake River Plain may be linked to the smaller size of Mars. Because it is smaller, it has a lower gravitational force, which also results in lower buoyancy forces for batches of magma rising through the lithosphere. The force required for breaking through the crust is probably about the same on Earth and on Mars. Since the buoyancy force for a given volume of magma is smaller on Mars, the total volume of rising magma must be greater than on Earth to overcome the strength of the brittle crust. The resultant larger magma batches could lead to larger volcanoes, higher eruption rates, and longer lava flows as observed for Syria Planum.

References

Anders, M.H., Geissman, J.W., Piety, L.A., and Sullivan, J.T., 1989, Parabolic distribution of circumeastern Snake River Plain seismicity and latest Quaternary faulting: Migratory pattern and association with the Yellowstone hotspot: Journal of Geophysical Research: Solid Earth (1978–2012), v. 94, no. B2, p. 1589-1621.

Anders, M.H., Rodgers, D.W., Hemming, S.R., et al., 2014, A fixed sublithospheric source for the late Neogene track of the Yellowstone hotspot: Implications of the Heise and Picabo volcanic fields: Journal of Geophysical Research: Solid Earth, v. 119, no. 4, p. 2871-2906.

Baptista, A.R., Mangold, N., Ansan, V., et al., 2008, A swarm of small shield volcanoes on Syria Planum, Mars: Journal of Geophysical Research: Planets (1991–2012), v. 113, no. E9.

BEMIS, K., 1995, A morphometric study of volcanoes in Guatemala, Iceland, the Snake river plain and the South Pacific.-253 págs: State Univ.New Jersey [Tesis Ph.D].

Best, M.G., 2013, Igneous and metamorphic petrology, John Wiley & Sons.

Basaltic Volcanism Study Project, 1981, Basaltic Volcanism on the Terrestrial Planets, Pergamon Press, Inc., New York.

Carr, M. H., 1981, The Surface of Mars: Yale Univ. Press, New Haven, Conn., chap. 7, p. 87–113.

Carr, M. H., 1975, The volcanoes of Mars: Scientific American, v. 234, p. 32– 43.

Carr, M.H., 1974, Tectonism and volcanism of the Tharsis region of Mars: Journal of Geophysical Research, v. 79, no. 26, p. 3943-3949.

Carr, M.H., 1973, Volcanism on mars: Journal of Geophysical Research, v. 78, no. 20, p. 4049-4062.

Carr, M., Feigenson, M., Patino, L., and Walker, J., 2003, Volcanism and geochemistry in Central America: Progress and problems: Inside the subduction factory, p. 153-174.

Cas, R.A., and Wright, J.V., 1987, Volcanic successions: modern and ancient, Springer Science & Business Media.

Champion, D.E., Lanphere, M.A., Anderson, S.R., and Kuntz, M.A., 2002, Accumulation and subsidence of late Pleistocene basaltic lava flows of the eastern Snake River Plain, Idaho: SPECIAL PAPERS-GEOLOGICAL SOCIETY OF AMERICA, p. 175-192.

Christensen, P.R., Jakosky, B.M., Kieffer, H.H., et al., 2004, The thermal emission imaging system (THEMIS) for the Mars 2001 Odyssey Mission: Space Science Reviews, v. 110, no. 1-2, p. 85-130.

Christiansen, E.H., and McCurry, M., 2008, Contrasting origins of Cenozoic silicic volcanic rocks from the western Cordillera of the United States: Bulletin of Volcanology, v. 70, no. 3, p. 251-267.

Christensen, P., Enle, E., Anwar, S., Dickenshield, S., Noss, D., Gorelick, N., Weiss-Malik, M., JMARS – A Planetary GIS, http://adsabs.harvard.edu/abs/2009AGUFMIN22A..06C.

DeNosaquo, K.R., Smith, R.B., and Lowry, A.R., 2009, Density and lithospheric strength models of the Yellowstone–Snake River Plain volcanic system from gravity and heat flow data: Journal of Volcanology and Geothermal Research, v. 188, no. 1, p. 108-127.

Fagents, S.A., Gregg, T.K., and Lopes, R.M., 2013, Modeling volcanic processes: the physics and mathematics of volcanism, Cambridge University Press.

Francis, P., 1993, Volcanoes. A planetary perspective: Volcanoes.A planetary perspective., by Francis, P. Clarendon Press, Oxford (UK), 1993, 452 p., ISBN 0-19-854452-9, ISBN 0-19-854033-7 (paper)., v. 1.

Gesch, D., Evans, G., Mauck, J., Hutchinson, J., and Carswell Jr, W.J., 2009, The national map: Elevation: US geological survey fact sheet, v. 3053, no. 4.

Greeley, R., 1982, The Snake River Plain, Idaho: representative of a new category of volcanism: Journal of Geophysical Research: Solid Earth (1978–2012), v. 87, no. B4, p. 2705-2712.

Greeley, R., and Spudis, P.D., 1981, Volcanism on Mars: Rev. Geophys, v. 19, no. 1, p. 13-41.

Hackett, W., and Smith, R., 1992: Quaternary volcanism, tectonics, and sedimentation in the Idaho National Engineering Laboratory area.

Hauber, E., Bleacher, J., Gwinner, K., Williams, D., and Greeley, R., 2009, The topography and morphology of low shields and associated landforms of plains volcanism in the Tharsis region of Mars: Journal of Volcanology and Geothermal Research, v. 185, no. 1, p. 69-95.

Hughes, S.S., Wetmore, P.H., and Casper, J.L., 2002, Evolution of Quaternary tholeiitic basalt eruptive centers on the eastern Snake River Plain, Idaho: Tectonic and Magmatic Evolution of the Snake River Plain Volcanic Province: Idaho Geological Survey Bulletin, v. 30, p. 363-385.

Jaumann, R., Neukum, G., Behnke, T., et al., 2007, The high-resolution stereo camera (HRSC) experiment on Mars Express: Instrument aspects and experiment conduct from interplanetary cruise through the nominal mission: Planetary and Space Science, v. 55, no. 7, p. 928-952.

Kuntz, M.A., Covington, H.R., and Schorr, L.J., 1992, An overview of basaltic volcanism of the eastern Snake River Plain, Idaho: Geological Society of America Memoirs, v. 179, p. 227-268.

Kuntz, M.A., Skipp, B., Champion, D.E., Gans, P.B., Van Sistine, D.P., and Snyders, S.R., 2007, Geologic Map of the Craters of the Moon 30′ X 60′ Quadrangle, Idaho, US Geological Survey.

LaPoint, P., 1977, Preliminary Photogeologic map of the Eastern Snake River Plain, Idaho. Miscellaneous Field Studies Map MF-850. Denver: United States Geologic Survey, scale 1:250,000.

Leeman, W.P., , Magic Reservoir eruptive center: Snake River Plain-Yellowstone Volcanic Province: Jackson, Wyoming to Boise, Idaho July 21-29, 1989, p. 62-68.

Leeman, W., Ma, M., Murali, A., and Schmitt, R., 1978, Empirical estimation of magnetite/liquid distribution coefficients for some transition elements: Contributions to mineralogy and petrology, v. 65, no. 3, p. 269-272.

Lewis, R., Link, P., Stanford, L., Long, S., 2012, Geologic map of Idaho: faults (shear displacement structure), Idaho Geological Survey Map 9, scale 1:750,000.

Lopes, R. M. C., Fagents, S. A., Gregg, T. K., 2013, Modeling Volcanic Processes: the physics and mathematics of volcanism: New York, Cambridge University Press, 421 p.

Malin, M.C., Bell, J.F., Cantor, B.A., et al., 2007, Context camera investigation on board the Mars Reconnaissance Orbiter: Journal of Geophysical Research: Planets (1991–2012), v. 112, no. E5.

Melosh, H.J., 2011, Planetary surface processes, Cambridge University Press 13.

Mouginis-Mark, P.J., Wilson, L., and Zuber, M.T., 1992, The physical volcanology of Mars: Mars, v. 1, p. 424-452.

Mutch, T.A., Arvidson, R.E., Head III, J., Jones, K.L., and Saunders, R.S., 1976, The geology of Mars: Princeton, NJ, Princeton University Press, 1976.409 p., v. 1.

Noe-Nygaard, A., 1968, On extrusion forms in plateau basalts, Shield volcanoes of 'Scutulum' type: Science in Iceland Anniversary, Societas Scientiarum Islandica, Rekjavik, v. 10-13.

Pedersen, G., and Grosse, P., 2014, Morphometry of subaerial shield volcanoes and glaciovolcanoes from Reykjanes Peninsula, Iceland: Effects of eruption environment: Journal of Volcanology and Geothermal Research, v. 282, p. 115-133.

Pierce, K.L., and Morgan, L.A., 1992, The track of the Yellowstone hot spot: Volcanism, faulting, and uplift: Geological Society of America Memoirs, v. 179, p. 1-54.

Pike, R.J., and Clow, G.D., 1981: Revised classification of terrestrial volcanoes and catalog of topographic dimensions, with new results of edifice volume.

Potter, K., 2010. Subsurface stratigraphy of the Arco-Big Southern Butte volcanic rift zone and implications for late Pleistocene rift zone development, Eastern Snake River Plain, Idaho. Pocatello: Idaho State University.

Putirka, K.D., Perfit, M., Ryerson, F., and Jackson, M.G., 2007, Ambient and excess mantle temperatures, olivine thermometry, and active vs. passive upwelling: Chemical Geology, v. 241, no. 3, p. 177-206.

Richardson, J., Bleacher, J., and Baptista, A., 2010, Identification of volcanic ridge in northern Syria Planum, Mars: Constraint on geologic history of Syria, *in* Lunar and Planetary Science Conference, p. 1427.

Richardson, J., Bleacher, J., Connor, C.B., and Connor, L., 2012, Using spatial density to characterize volcanic fields on Mars, *in* Lunar and Planetary Science Conference, p. 2314.

Richardson, J.A., Bleacher, J.E., and Glaze, L.S., 2013, The volcanic history of Syria Planum, Mars: Journal of Volcanology and Geothermal Research, v. 252, p. 1-13.

Rodgers, D.W., Hackett, W.R., and Ore, H.T., 1990, Extension of the Yellowstone plateau, eastern Snake River Plain, and Owyhee plateau: Geology, v. 18, no. 11, p. 1138-1141.

Schmincke, H., 2004, Volcanism, Springer Science & Business Media 28.

Schumacher, S., and Breuer, D., 2007, An alternative mechanism for recent volcanism on Mars: Geophysical Research Letters, v. 34, no. 14.

Schutt, D., Humphreys, E.D., and Dueker, K., 1998, Anisotropy of the Yellowstone hot spot wake, eastern Snake River Plain, Idaho. *in* Geodynamics of Lithosphere & Earth's Mantle, Springer, p.443-462.

Scott, D. H., and K. L. Tanaka, 1998, Geological map of the equatorial region of Mars: U.S. Geol. Surv. Misc. Invest. Map I-1802-A, scale:1:15,000,000.

Shervais, J.W., and Hanan, B.B., 2008, Lithospheric topography, tilted plumes, and the track of the Snake River–Yellowstone hot spot: Tectonics, v. 27, no. 5.

Smith, D.E., Zuber, M.T., Frey, H.V., et al., 2001, Mars Orbiter Laser Altimeter: Experiment summary after the first year of global mapping of Mars: Journal of Geophysical Research: Planets (1991–2012), v. 106, no. E10, p. 23689-23722.

Smith, R.P., 2004, Geologic setting of the Snake River Plain aquifer and vadose zone: Vadose Zone Journal, v. 3, no. 1, p. 47-58.

Smith, R.B., and Braile, L.W., 1994, The Yellowstone hotspot: Journal of Volcanology and Geothermal Research, v. 61, no. 3, p. 121-187.

Smith, R.B., Jordan, M., Steinberger, B., et al., 2009, Geodynamics of the Yellowstone hotspot and mantle plume: Seismic and GPS imaging, kinematics, and mantle flow: Journal of Volcanology and Geothermal Research, v. 188, no. 1, p. 26-56.

Spera, F. J., 2000, Physical Properties of Magma: Encyclopedia of Volcanoes, p. 171-190.

Tanaka, K.L., Skinner, J.A., Dohm, J.M., et al., 2014, Geologic map of Mars, US Department of the Interior, US Geological Survey.

Taylor, G.J., 2013, The bulk composition of Mars: Chemie der Erde-Geochemistry, v. 73, no. 4, p. 401-420.

Thordarson, T., and Larsen, G., 2007, Volcanism in Iceland in historical time: Volcano types, eruption styles and eruptive history: Journal of Geodynamics, v. 43, no. 1, p. 118-152.

Tolan, T.L., Reidel, S.P., Beeson, M.H., Anderson, J.L., Fecht, K.R., and Swanson, D.A., 1989, Revisions to the estimates of the areal extent and volume of the Columbia River Basalt Group: Geological Society of America Special Papers, v. 239, p. 1-20.

Walker, G.P., 2000, Basaltic volcanoes and volcanic systems: Encyclopedia of volcanoes, p. 283-289.

Walker, G.P., 1993, Basaltic-volcano systems: Geological Society, London, Special Publications, v. 76, no. 1, p. 3-38.

Wilson, L., and Head, J.W., 1994, Mars: Review and analysis of volcanic eruption theory and relationships to observed landforms: Reviews of Geophysics, v. 32, no. 3, p. 221-263.

Wood, C.A., 1980, Morphometric evolution of cinder cones: Journal of Volcanology and Geothermal Research, v. 7, no. 3, p. 387-413.

Wood, C.A., 1979, Monogenetic volcanoes of the terrestrial planets, *in* Lunar and Planetary Science Conference Proceedings, p. 2815-2840.

World Imagery, Sources: Esri, DigitalGlobe, GeoEye, i-cubed, USDA FSA, USGS, AEX, Getmapping, Aerogrid, IGN, IGP, swisstopo, and the GIS User Community.

Figure 1: Shield Types and Cross Section

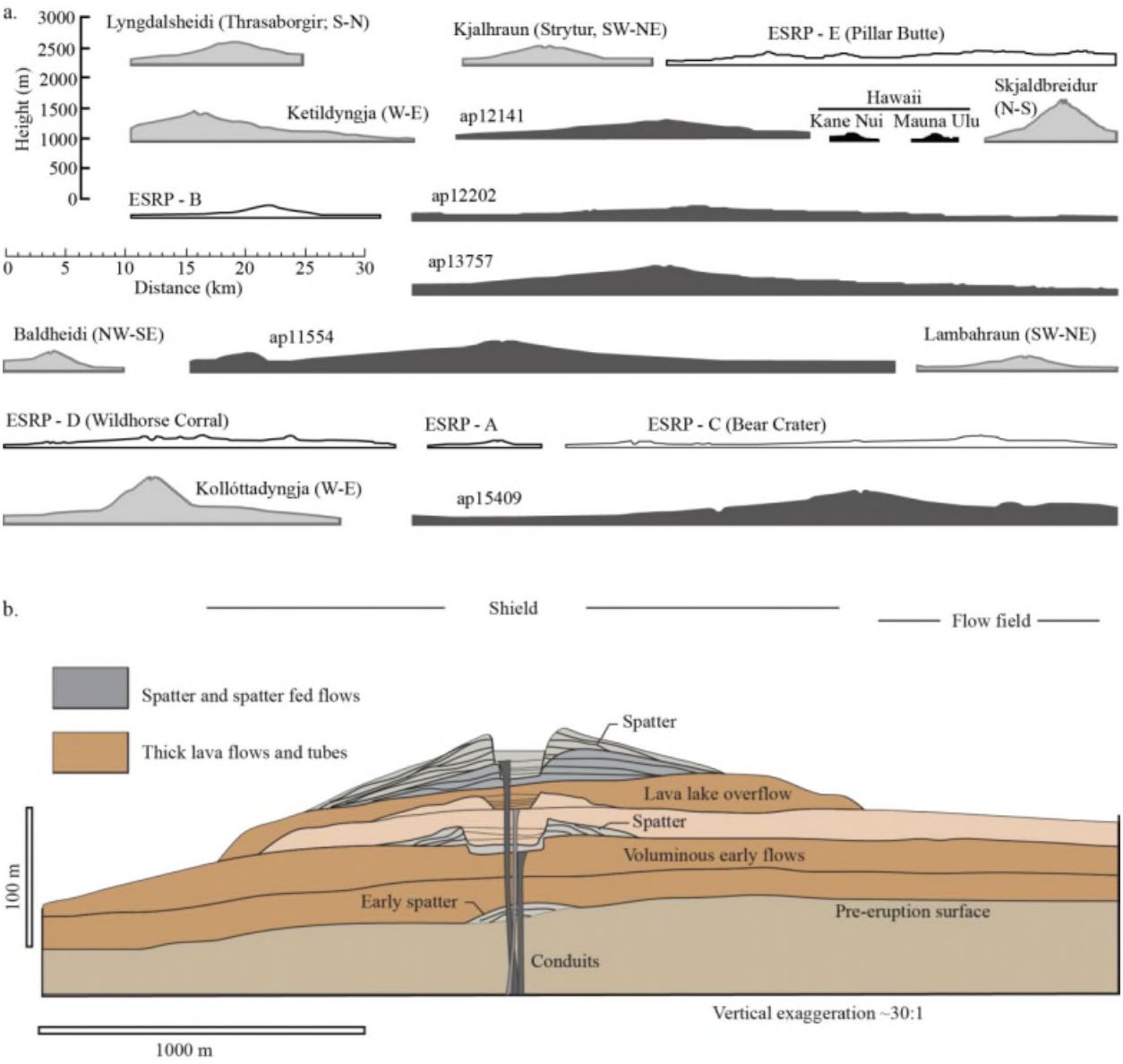

Figure 1: (a) Comparison between topographic profiles across low shields on Mars and Earth. Modified from Hauber et al (2009). Low shields on Mars (dark gray), though significantly smaller than large Martian shields like Olympus Mons, are still larger than Earth low shields (black outline: eSRP-eastern Snake River Plain; light gray: Iceland; black: Hawaii). The Snake River Plain low shields are the closest analogues to the Martian low-shields. The Snake River Plain is the type location for plains volcanism (Greeley, 1982). Martian profiles refer to MOLA orbit numbers (vertical exaggeration of all profiles is 5). (b) Idealized cross section of a low-shield volcano shows the basalt-flow morphology of a typical shield volcano in the Central and Eastern Snake River Plain. Also shown is an example of where we define the topographic shield and the flow apron.

Figure 2: Syria Planum Regional Map

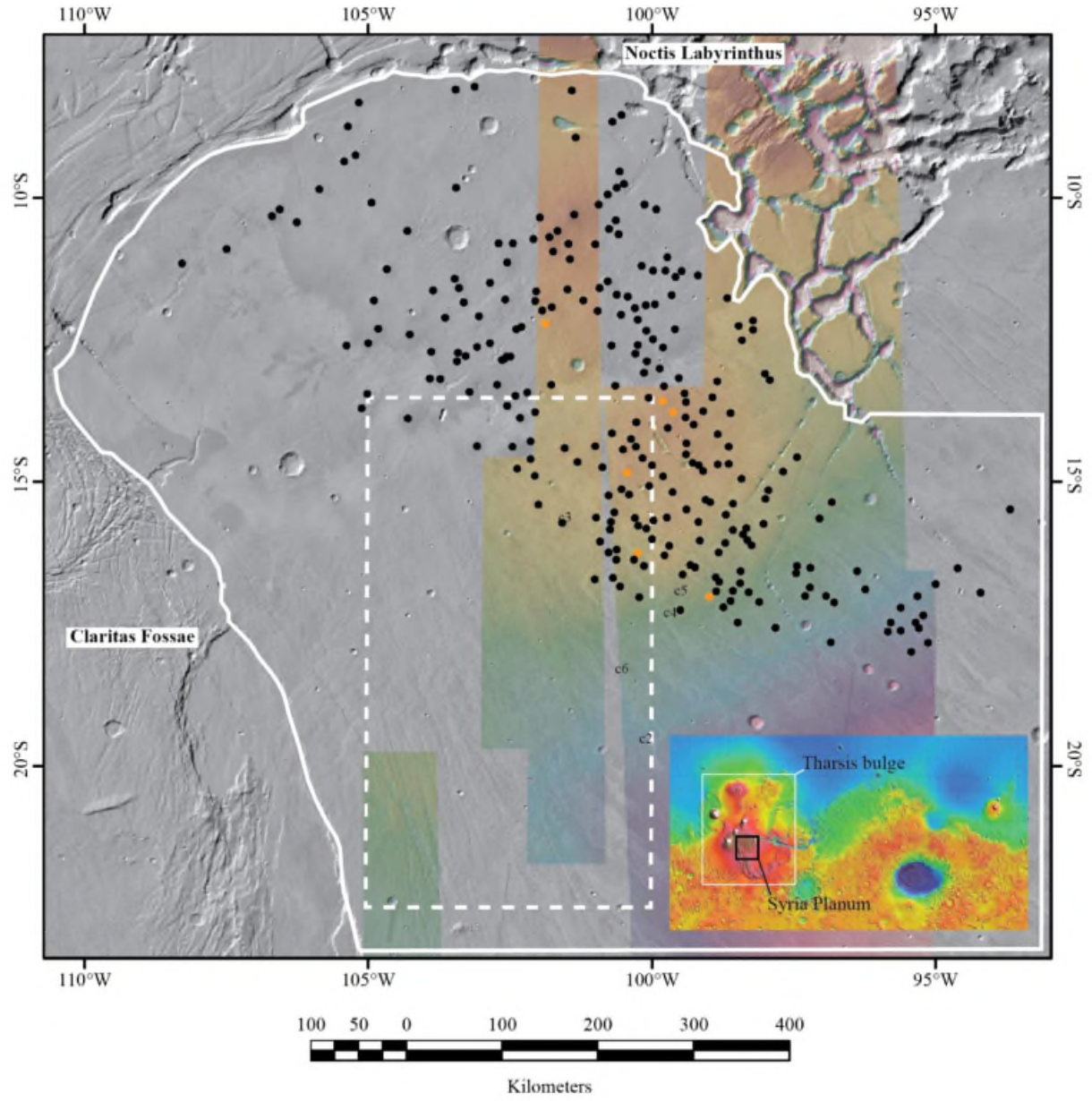

Figure 2: Shaded relief map of Syria Planum, Mars from combined MOLA DEM and THEMIS imagery. HRSC DEM coverage is shown, red showing higher elevation. Previous study areas are outlined, Richardson et al. (2013) by solid white line, Baptista et al. (2008) by dashed white line. Shields are marked with black dots, shields typifying clusters are marked in orange and label denotes the cluster. C1 is Shield 243. c2 is Shield 175, c3 is Shield 29, c4 is Shield 191, c5 is Shield 126, c6 is Shield 151.

Figure 3: eastern Snake River Plain Regional Map

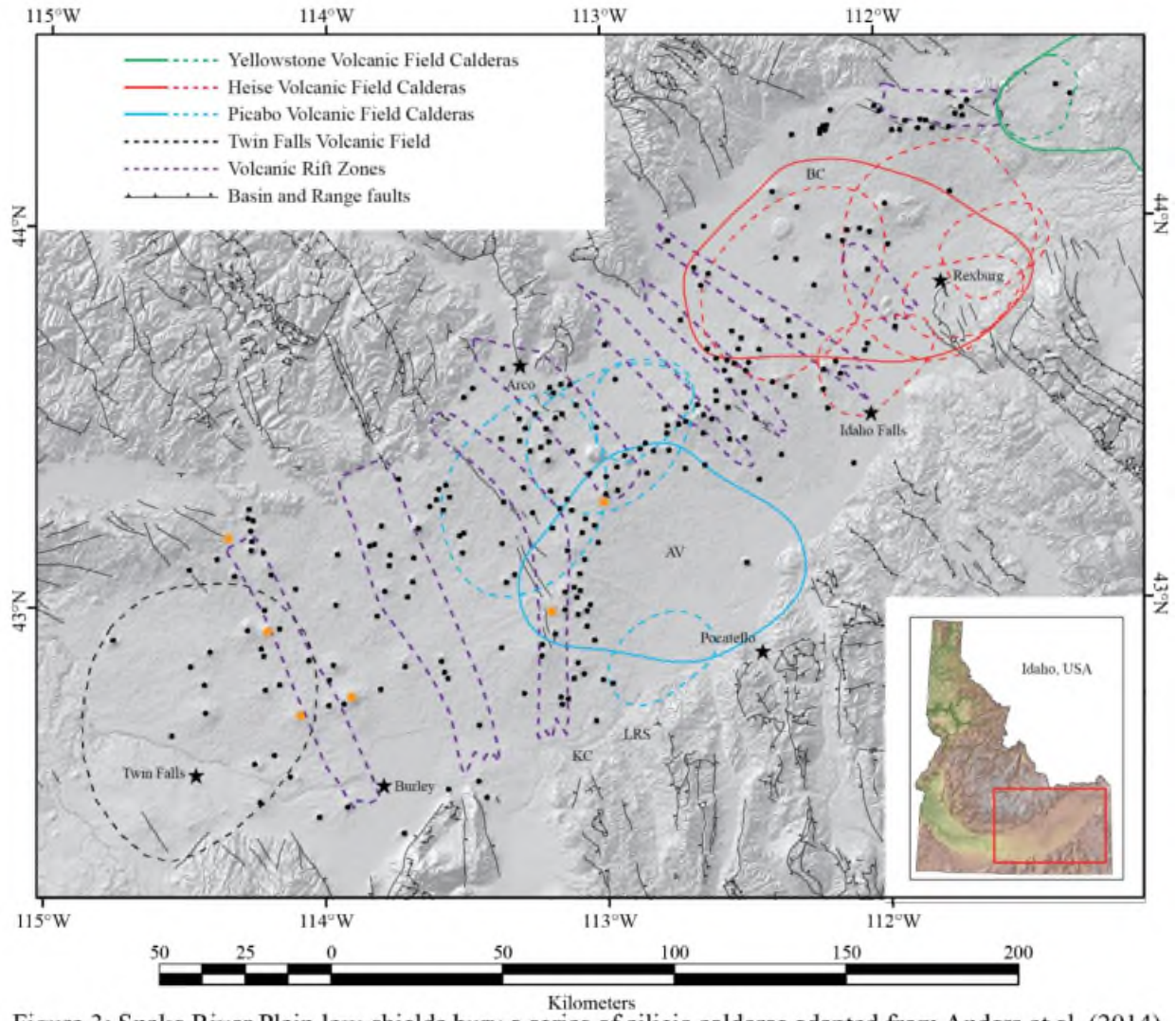

Figure 3: Snake River Plain low-shields bury a series of silicic calderas adapted from Anders et al. (2014). The ring faults for these calderas are highly speculative, but may influence the location of the basaltic volcanism. Some shields may also be aligned along the north and north-west edge of the Picabo calderas, along the west edge of the Arbon Valley Tuff Caldera (AV), as well as along the south edge of the Black-tail Creek Tuff (BC) caldera proposed by Morgan and McIntosh (2005). However, some of the caldera boundaries have been drawn on the assumption that they controlled shield locations. Some eruption sites may be aligned along basin-and-range faults and their corresponding volcanic rift zones proposed by Kuntz and others (1992). Yellowstone volcanic field calderas: Mesa Falls (MF, 1.30 Ma), Huckleberry Ridge Tuff (HR, 2.13 Ma), Lava Creek is not shown as it is just outside the bounds of this map. Heise volcanic field calderas: Kilgore Tuff (K, 4.61 Ma), Elkhorn Spring Tuff (ES, 5.52 Ma), Wolverine Creek Tuff (WC, 5.72 Ma), Conant Creek Tuff (CC, 6.01 Ma), Walcott Tuff (WT, 6.27 Ma), Blacktail Creek Tuff (BC, 6.66 Ma). Picabo volcanic field calderas: American Falls Tuff (AF, 7.58 Ma), Lost River Sinks Tuff (LRS, 8.87 Ma), Kyle Canyon Tuff (KC, 9.28 Ma), Little Chokecherry Canyon Tuff (LCC, 9.46 Ma), Arbon Valley Tuff (AV, 10.27 Ma). Twin Falls volcanic field (TFVF, 12.5 to 7.5 Ma), Magic Reservoir Volcanic Center (MRVC). Volcanic rift zones from west to east (Hughes, 2002): Richfield-Burley Butte, Borkum, The Great Rift, Arco-Big Southern Butte, Howe-East Butte, Lava Ridge-Hell's Half Acre, Circular Butte-Kettle Butte, Menan, Spencer-High Point.

Figure 4: eSRP Shield Profiles

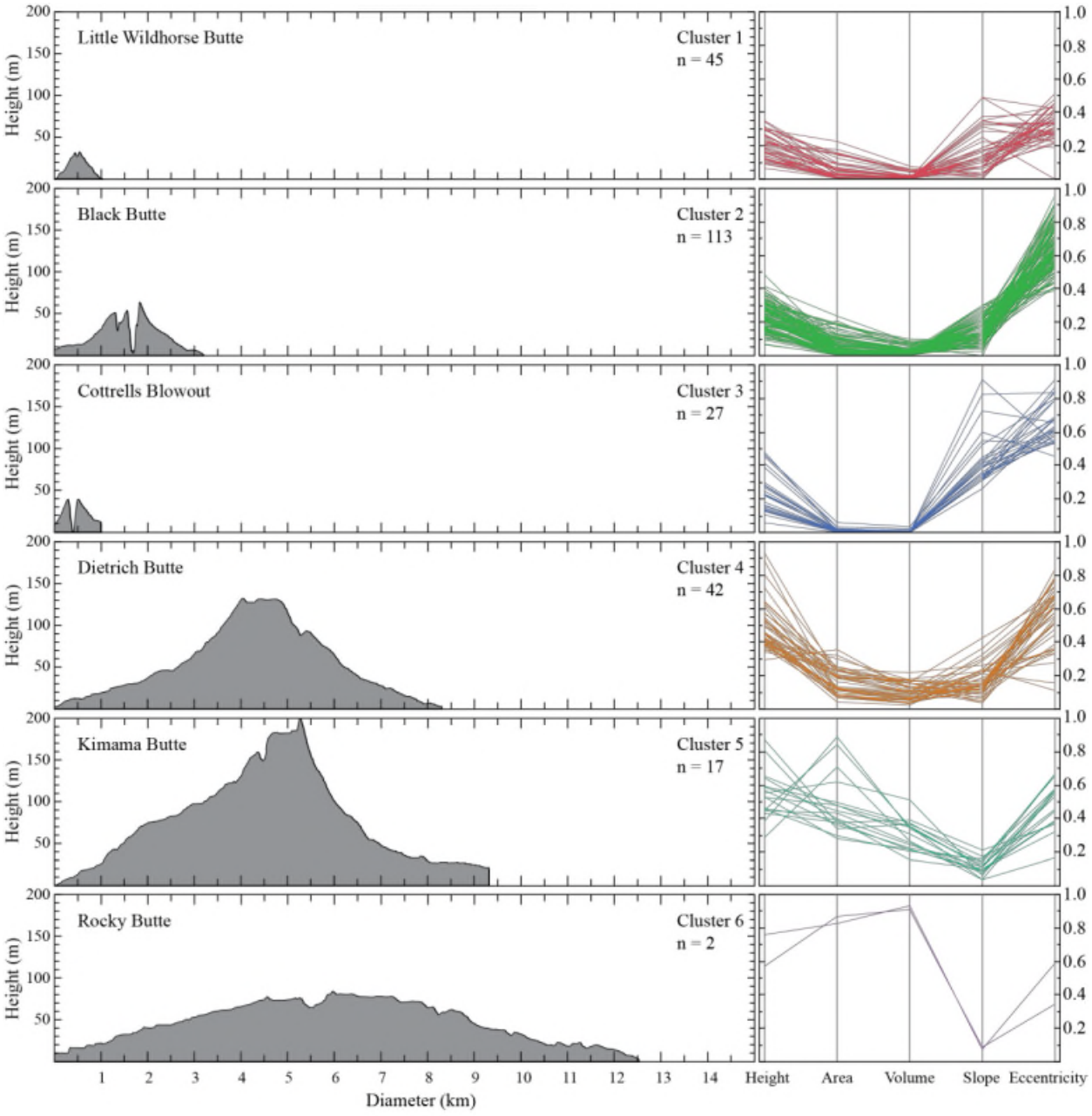

Figure 4: Topographic profiles from each of the six groups identified by cluster analysis of Snake River Plain low-shields. Also shown are the morphometric relation plots. These plots show the relative relationships between morphometric characteristics that describe each cluster of shields. Vertical exaggeration is approximately 18:1.

Figure 5: Histograms of Morphometric Characteristics

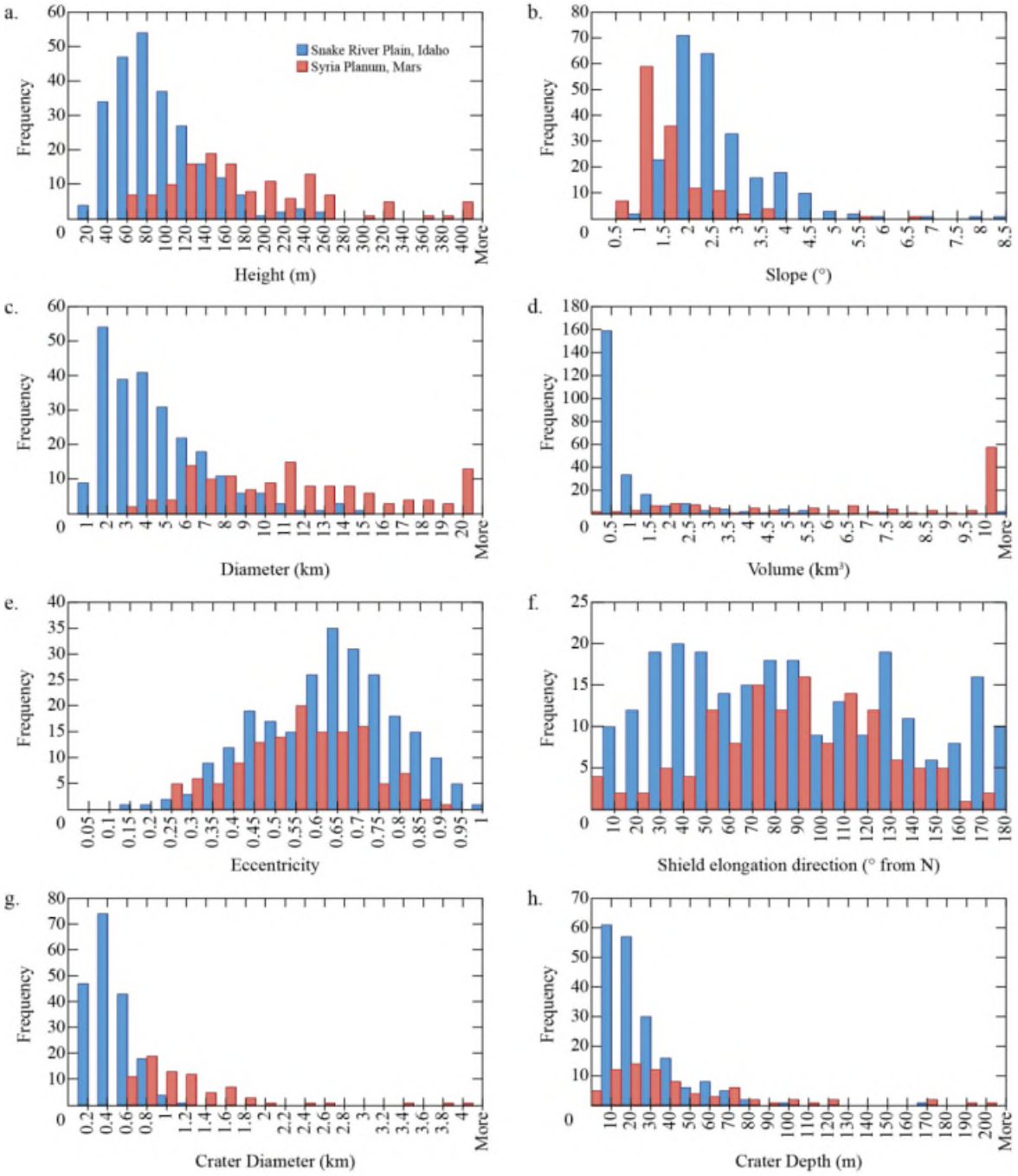

Figure 5: Histograms showing the height (a), slope (b), diameter (c), and volume (d) distributions for both Snake River Plain and Syria Planum low-shields. Shield eccentricity (e) and elongation (f) direction (in degrees from north) are also shown. Though there is considerable overlap in the distribution, the majority of Snake River Plain low-shields are smaller in height, diameter and volume than Syria Planum low-shields, and the majority of Syria Planum low-shields have smaller slopes than Snake River Plain shields. The majority of Snake River Plain volcanic craters are also smaller in diameter than Syria Planum craters (g). Crater depth (h) is fairly consistent between the two regions though Syria Planum does have a greater number of deeper craters than the Snake River Plain.

Figure 6: Elevation Dataset and Measurement Method Comparison

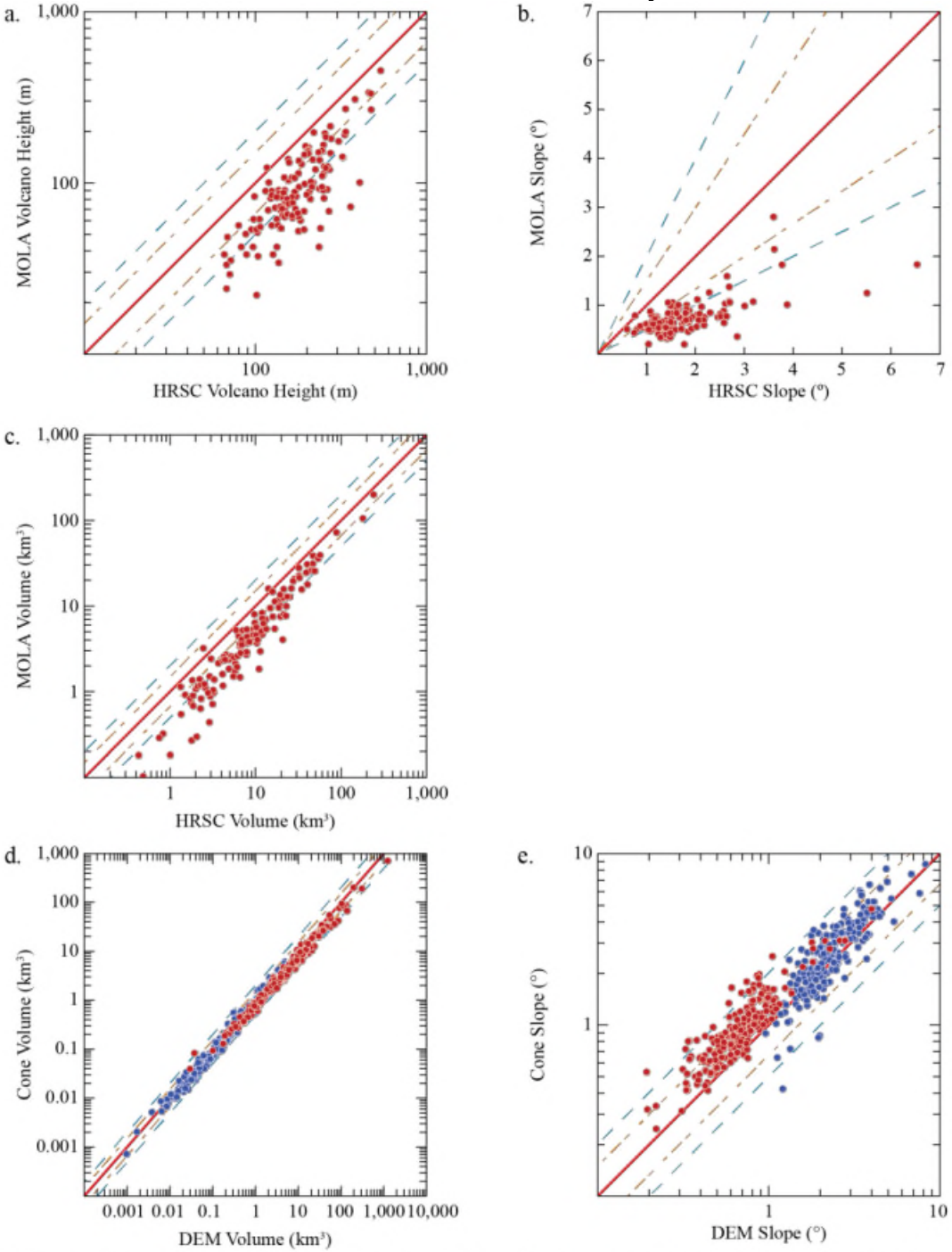

Figure 6: Comparisons of morphometric characteristics of volcanoes on Syria Planum derived from two different elevation datasets. Volcano heights using HRSC (High Resolution Stereo Camera) DEMs are larger (by as much as 2 times) than for heights measured on gridded MOLA (Mars Orbiting Laser Altimeter) DEMs; the calculated slopes are thus steeper and volumes larger if HRSC data are used. (d) Volumes measured using a DEM profile compared to the calculated volume of an idealized cone. Volumes are comparable, however, on average the cone method gives a smaller volume. (e) The average slopes of DEM profiles compared to slopes calculated from an idealized cone. The cone method gives steeper slopes (by as much as 2 times) than the averaged DEM profile.

Figure 7: Syria Planum Shield Profiles

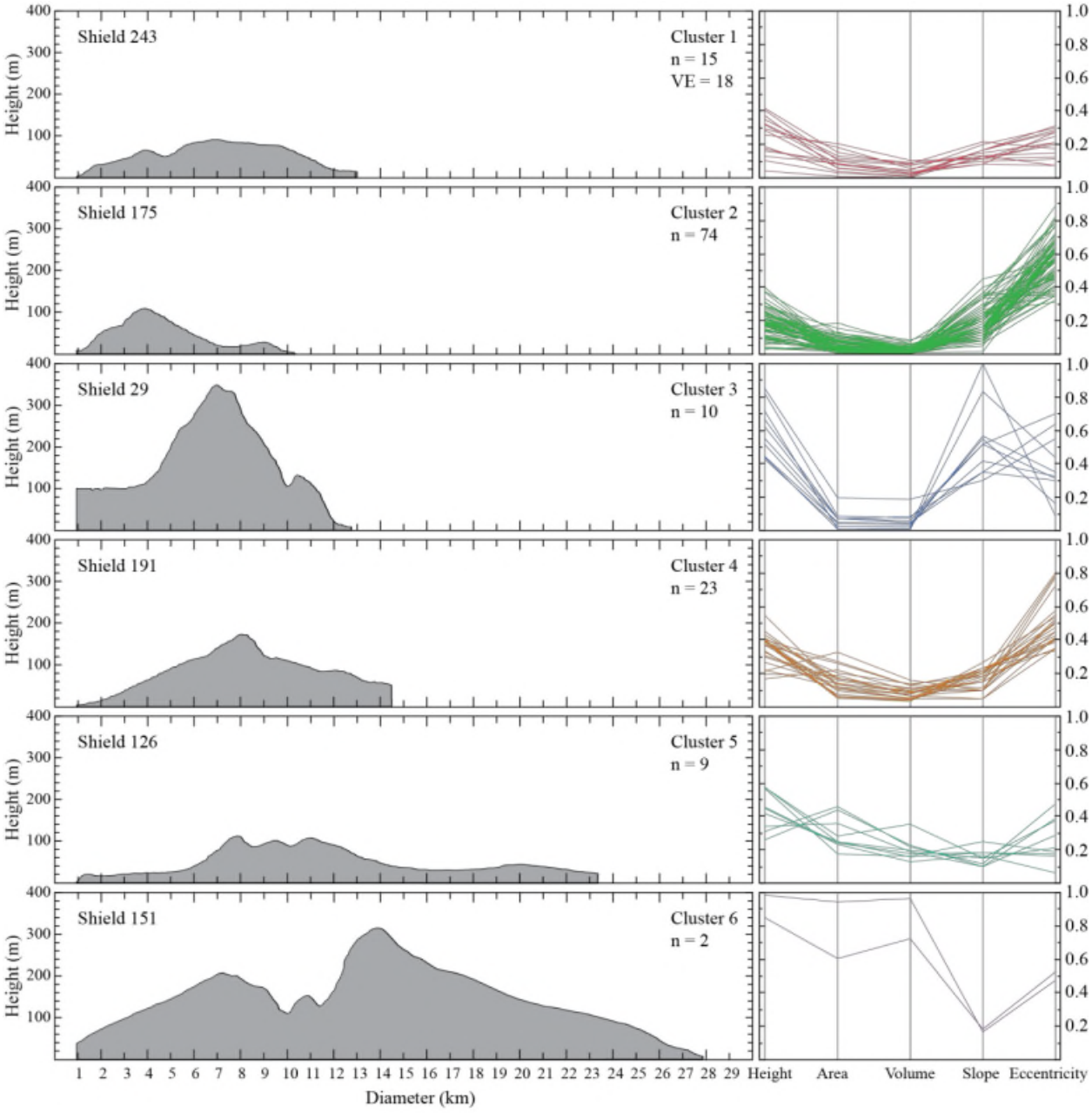

Figure 7: Topographic profiles from each of the six groups identified by cluster analysis of Syria Planum low-shields. Also shown are the morphometric relation plots. These plots show the relative relationships between morphometric characteristics that describe each cluster of shields. The scale used is twice that used for Snake River Plain low-shields.

Figure 8: Syria Planum Crater Types

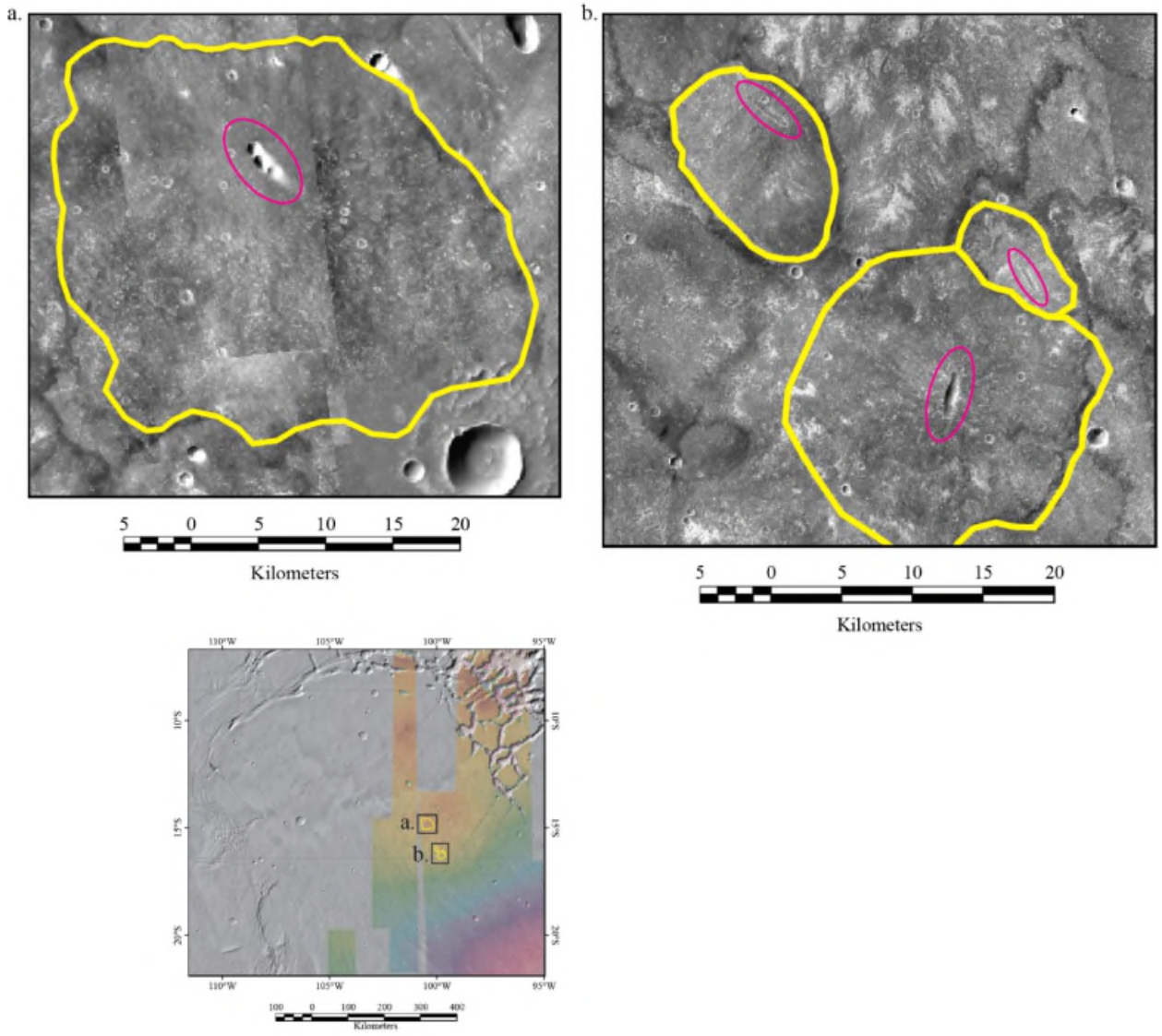

Figure 8: Types of volcanic craters on Syria Planum: (a) shield with multiple craters in a chain, (b) shields with fissure like vents. Vents are circled, yellow outlines the extent of the topographic shield.

Figure 9: Principal Component Analysis of all Volcano Types

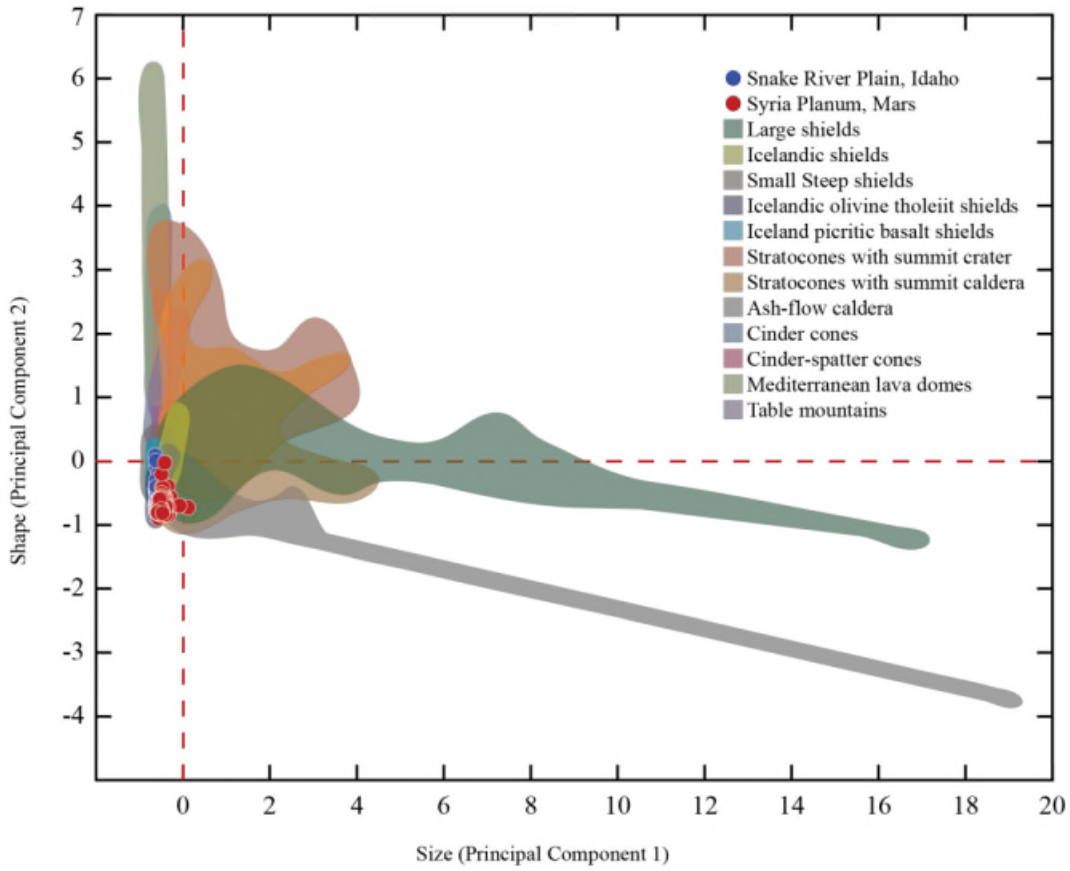

Figure 9: Score plot showing each volcano's position with respect to the first and second principal components. Principal component 1 is a rotational transformation of a linear combination of height, area, and volume which we term the size component. Principal component 2 retained only the slope and we term this the shape component. Snake River Plain, Syria Planum low-shields, other shields, stratocones, and other terrestrial cones are on separate layers that can be toggled on or off in PDF for better viewing and comparison. Large shields, Icelandic shields, small steep shields, stratocones, and terrestrial cone data is taken from Pike and Clow (1981). Icelandic olivine tholeiit and picrite basalt data is taken from Rossi (1995).

Figure 10a: Cluster Analysis of all Volcano Types

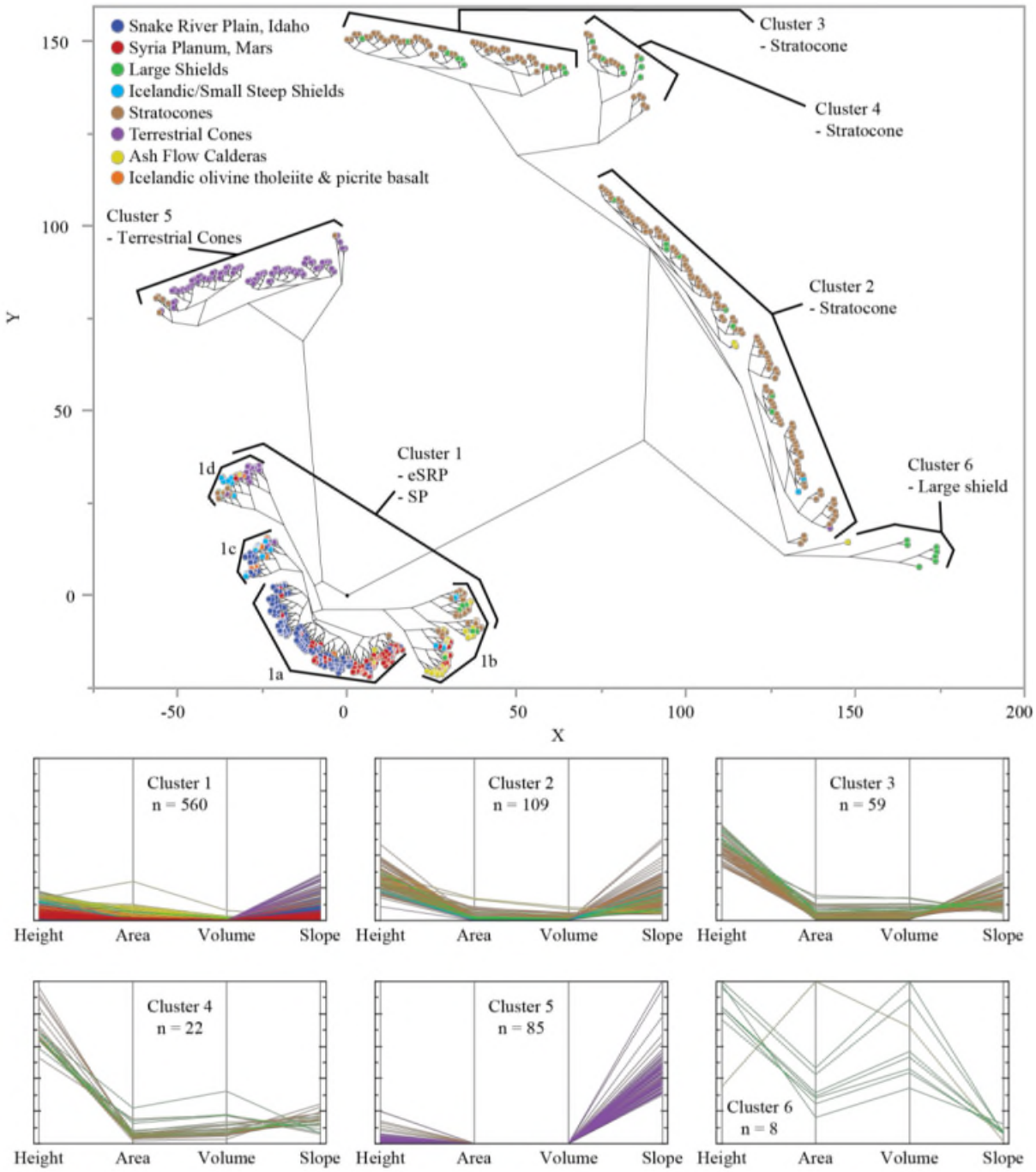

Figure 10a: Cluster analysis of Snake River Plain and Syria Planum low-shields in combination with other terrestrial volcanoes measured by Pike and Clow (1981) and Rossi (1995). We combine several of Pike and Clow's (1981) categories to simplify the diagram, see Table 3 for volcano categories. All eSRP and SP low-shields fall into cluster 1, and the majority of eSRP and SP shields form a sub-group within the cluster (1a). Though cluster 1 does contain examples from all other volcano classes, sub-group 1a containing eSRP and SP low-shields, shows that their morphometry is distinct from other terrestrial volcanoes and that SP low-shields are most similar to eSRP low-shields. Sub-group 1b contains the majority of the ash-flow calderas, 1c is a mixture of eSRP and Rossi (1995) shields. The parallel plots show the morphometric profile of each volcano in each cluster.

Figure 10b: Cluster Analysis of Snake River Plain Shield Volcanoes

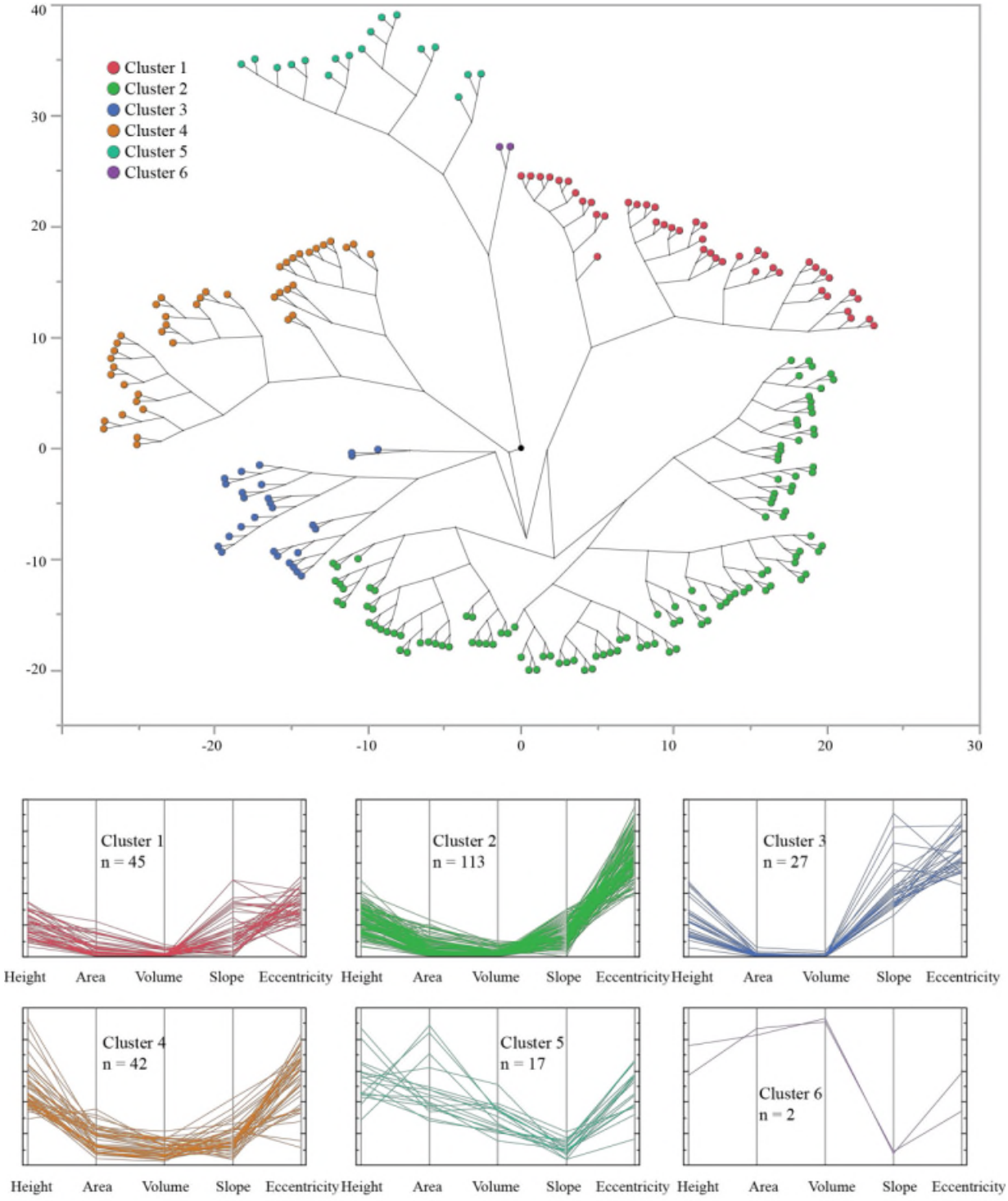

Figure 10b: Constellation plot and morphometric characteristic profiles of the six groups identified by cluster analysis of Snake River Plain low-shields.

Figure 10c: Cluster Analysis of Syria Planum Shield Volcanoes

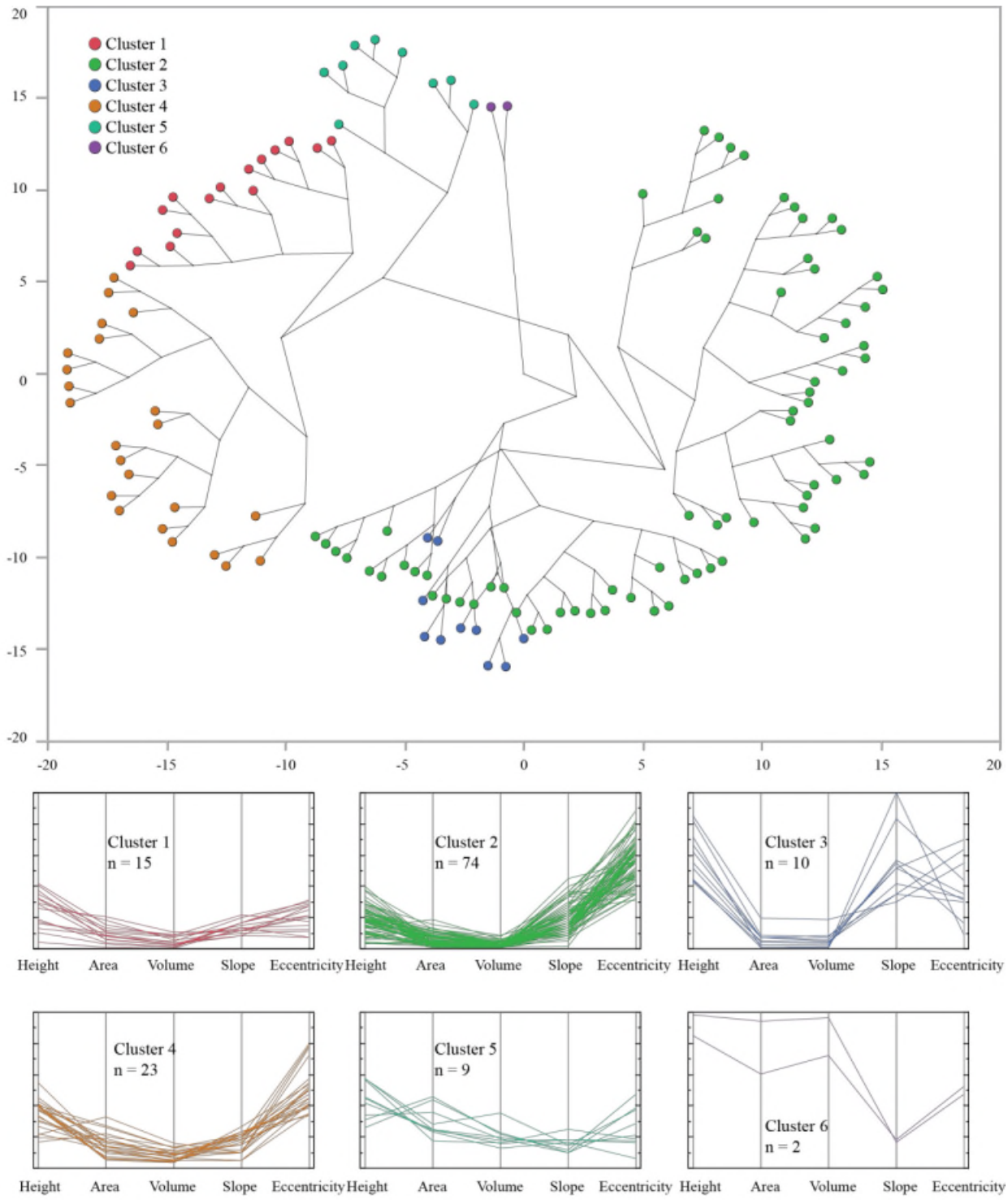

Figure 10c: Constellation plot and morphometric characteristic profiles of the six groups identified by cluster analysis of Syria Planum low-shields.

Figure 10d: Cluster Analysis of eSRP and SP Shield Volcanoes

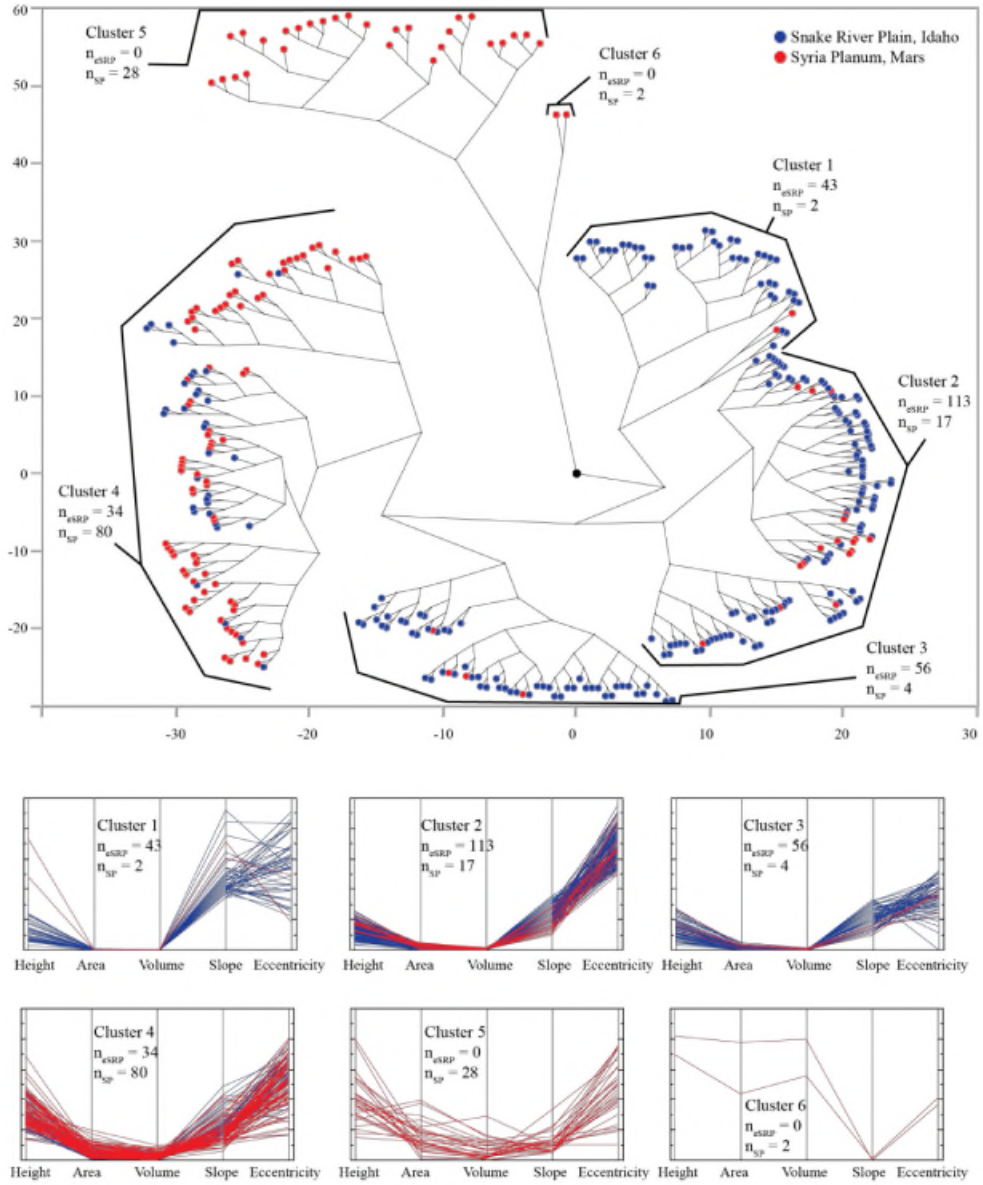

Figure 10d: Constellation plot and morphometric characteristic profiles of the six groups identified by cluster analyis of Snake River Plain and Syria Planum low-shields.

Figure 11: Map of Snake River Plain Cluster and Two-Point Azimuth Analysis

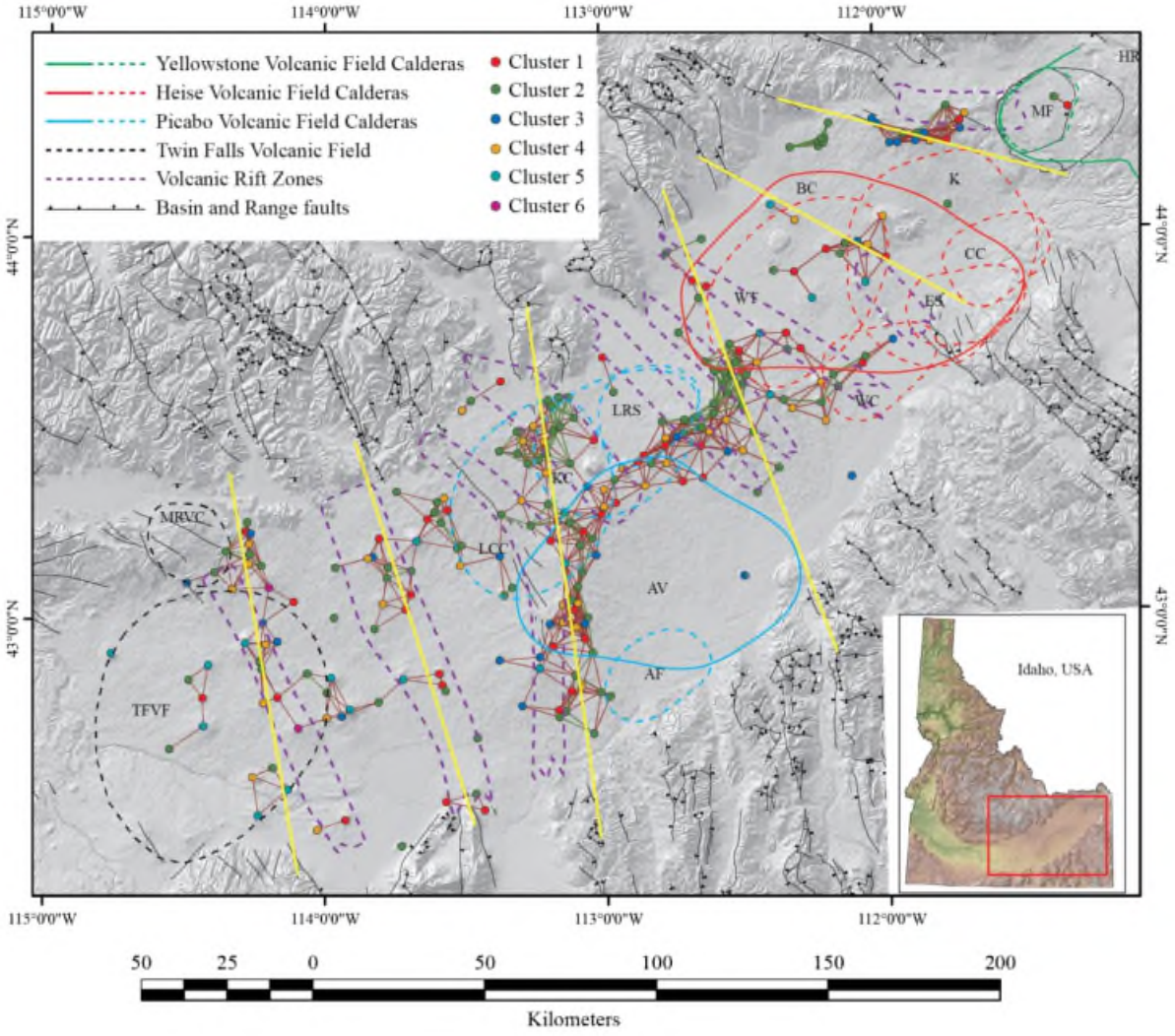

Figure 11: Two-point azimuth analysis (similar to that completed by Richardson et al., 2013) for all Snake River Plain low-shields is shown with dark red lines. These lines show possible structural controls, highlighted by yellow lines, that may stem from the surrounding Basin and Range fault systems. The six groupings identified by cluster analysis are shown and denoted by colored dots. Two-point analysis for individual clusters was conducted, cluster 2 is the only cluster that produced significant lineaments (shown with green lines). Also shown on this map are the Basin and Range faults, proposed caldera boundaries (Anders, 2014) and volcanic rift zones (Hughes, 2002, Kuntz and others, 1992).

Figure 12: Map of Syria Planum Cluster and Two-Point Azimuth Analysis

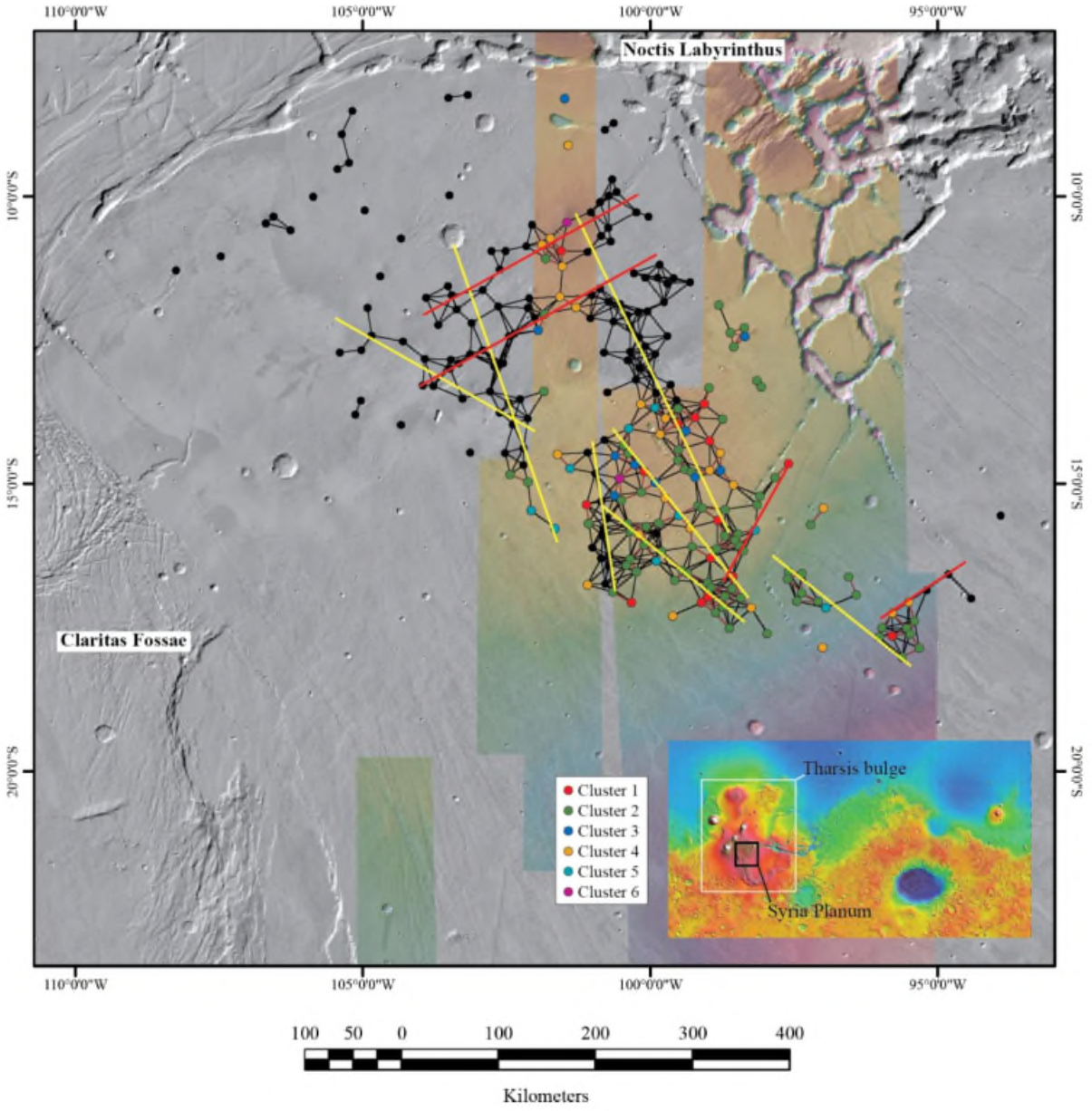

Figure 12: Two-point azimuth analysis (similar to that completed by Richardson et al., 2013) for all Syria Planum low-shields is shown with black lines HRSC azimuth lines are shown in dark red. These lines show possible structural controls, highlighted by yellow and red lines, that may stem from the surrounding stress regimens. The six groupings identified by cluster analysis are shown.

Figure 13: Shield Profiles for eSRP and SP Cluster Analysis

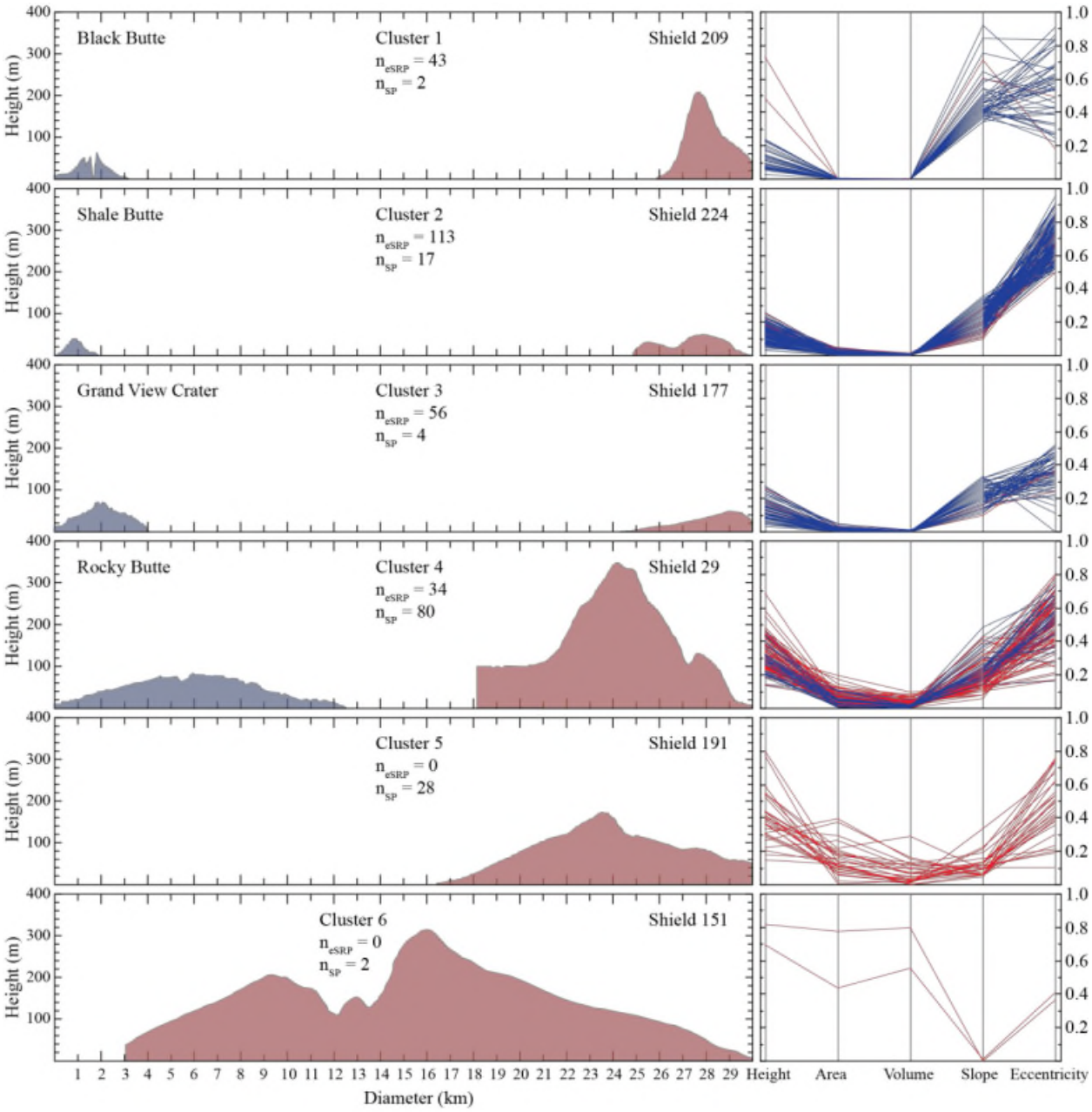

Figure 13: Topographic profiles from each of the six groups identified by cluster analysis of Snake River Plain and Syria Planum low-shields. Though similar in slope, Syria Planum low-shields are systemically larger in size than Snake River Plain low-shields. Vertical exaggeration is approximately 18:1.

Figure 14: Morphometric Characteristic Plot Diameter v. Height

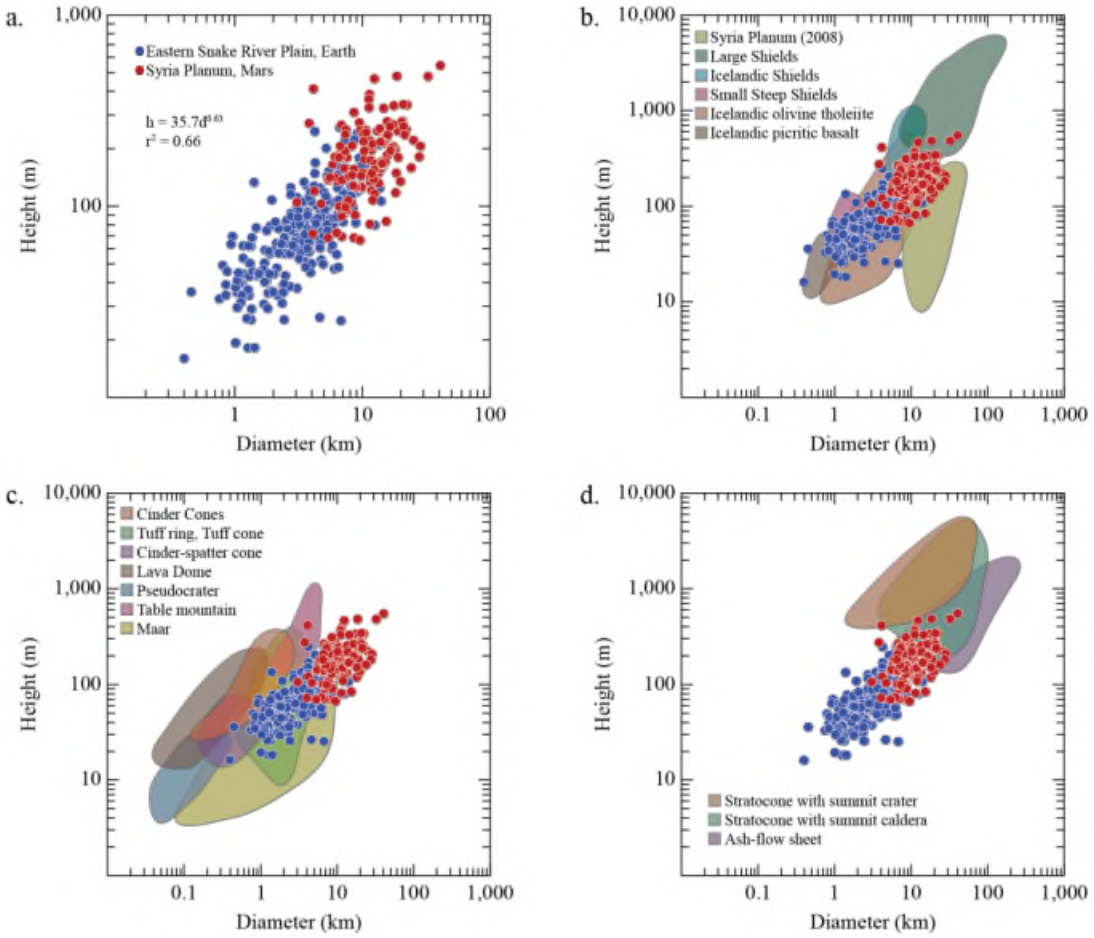

Figure 14: Morphometric comparison of volcano diameter and height. (a) Snake River Plain and Syria Planum low-shields form a continuous group with a positive correlation. Although volcanoes from both planets overlap, low-shields on Syria Planum are systematically bigger and higher. The equation for the regression line for eSRP and SP low-shields is listed with its r^2 value. (b) The low-shields are compared to other terrestrial shields defined by Pike and Clow (1981, see table 3 for descriptions and acronyms), Rossi (1995) and the 30 low-shields on Syria Planum studied by Baptista et al. (2008). SP and eSRP low-shields form a single distinct group that has little overlap with other shield types. The low-shields overlap somewhat with the small steep category that consists mostly of Icelandic shields as well as with Icelandic olivine tholeiites (Rossi, 1995). The measurements made by Baptista et al. (2008) used MOLA data and bear little resemblance to other volcanoes because of their low heights. (c) SP and eSRP shields are compared to various scoria cones, maars, and table mountains from Pike and Clow (1981). SP and eSRP shields form a distinct group that has an almost parallel trend to scoria cones but fall in with larger maars and with tuff rings. (d) SP and eSRP shields are also distinct from stratovolcanoes with summit craters measured by Pike and Clow (1981), there is some overlap of SP shields and some stratovolcanoes with summit calderas and ash flows.

Figure 15: Morphometric Characteristic Plot Diameter v. Volume

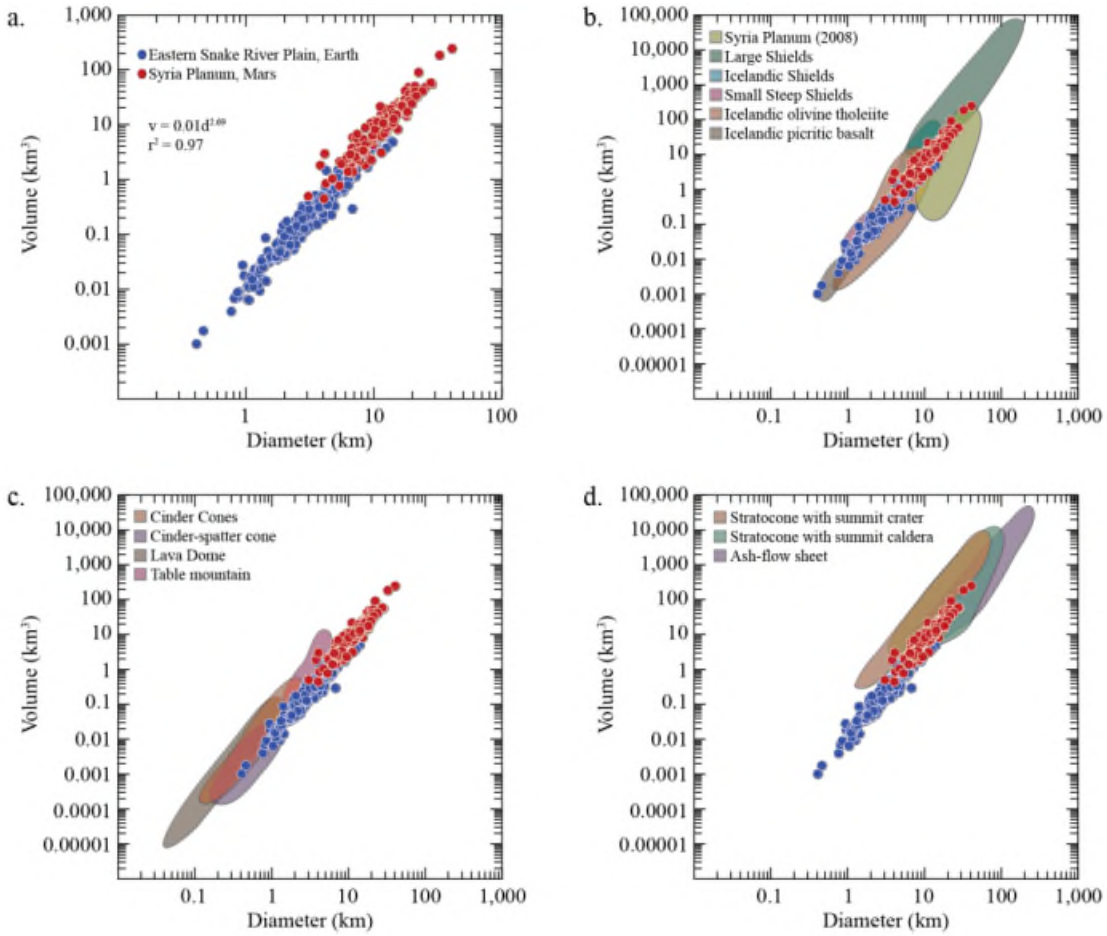

Figure 15: Morphometric comparison of volcano diameter and volume. (a) Snake River Plain and Syria Planum low-shields form the extremes of the same grouping with positive correlation between diameter and volume. (b) SP and eSRP shields are compared to terrestrial shields (Pike and Clow, 1981, Rossi, 1995) and the low-shields studied by Baptista et al. (2008). SP and eSRP shields form a single distinct group with little overlap with other shield types as measured by Pike and Clow (1981), but do overlap considerably with Icelandic olivine tholeiites measured by Rossi (1995). Where overlap occurs with Pike and Clow (1981) both eSRP and SP are smaller than other terrestrial shields. (c) SP and eSRP are compared to various cones, table mountains, and Mediterranean lava domes (Pike and Clow, 1981) showing eSRP and SP forming a distinct grouping that is nearly parallel to other terrestrial small cones. This relationship shows eSRP and SP shields to have smaller volumes for a given diameter. (d) SP and eSRP low-shields are compared to stratocones and ash-flows (Pike and Clow, 1981). SP and eSRP low-shields appear to follow the same trend as ash-flows and have a similar diameter to volume relationship with stratocones as they do with terrestrial cones. While SP low-shields are comparable in diameter to terrestrial stratocones, they are smaller in volume.

Figure 16: Morphometric Characteristic Plot Height v. Volume

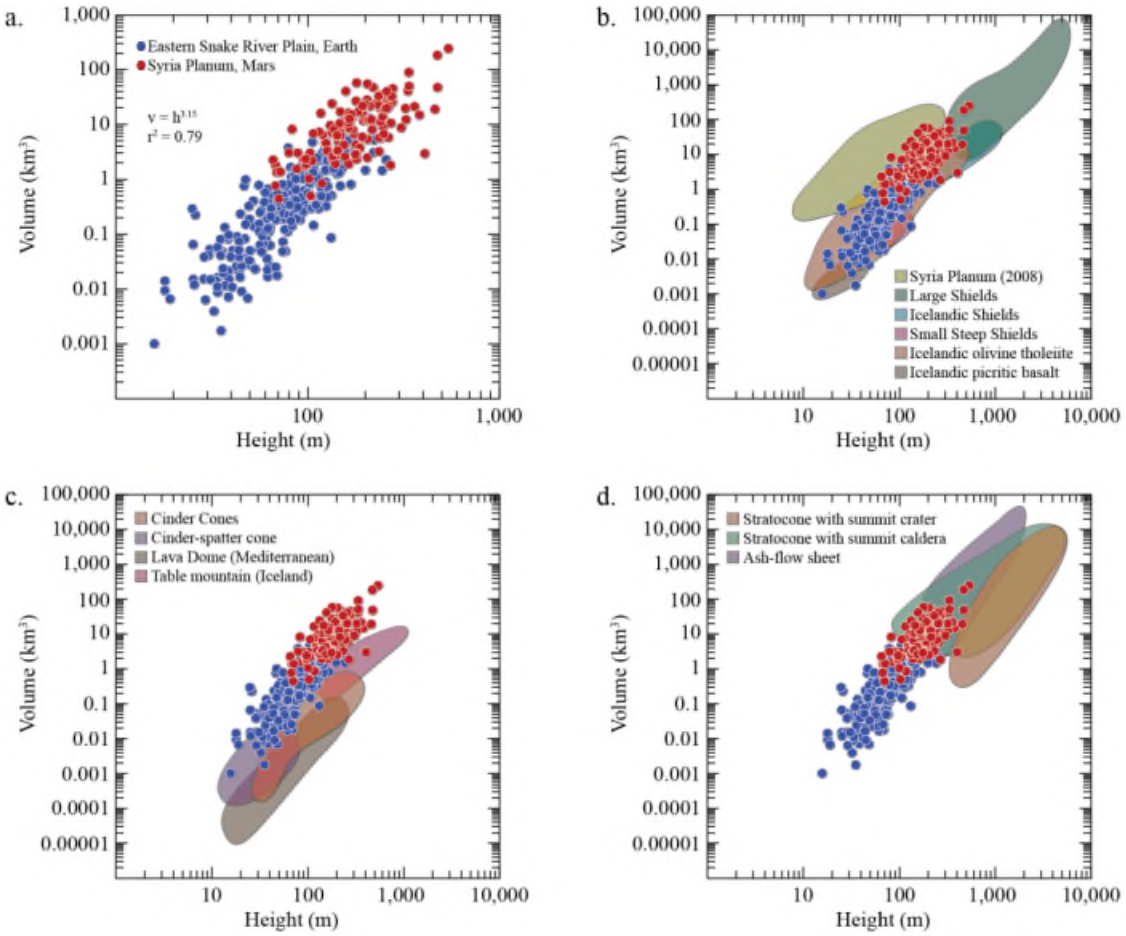

Figure 16: Morphometric characteristic comparison plot of height and volume. (a) This plot shows that though the two areas follow the same height/volume relationship trend, Snake River Plain low-shields are still considerably smaller in volume than Syria Planum low-shields. (b) This plot shows that both eSRP and SP low-shields are distinctly different than other terrestrial shields as measured by Pike and Clow (1981), but occupies the same spread as the olivine tholeiites as measured by Rossi (1995). This also shows that measurements made by this study are not in agreement with those made by Baptista et al. (2008). (c) SP and eSRP shields are of comparable height and volume to cinder/spatter cones as measured by Pike and Clow (1981), where measurements made by Baptista et al. (2008) are similar to tuff rings/cones. (d) This plot shows that eSRP and SP low-shields are distinct from terrestrial stratocones and may follow the same trend as ash-flows.

Figure 17: Morphometric Characteristic Plot Diameter v. Slope

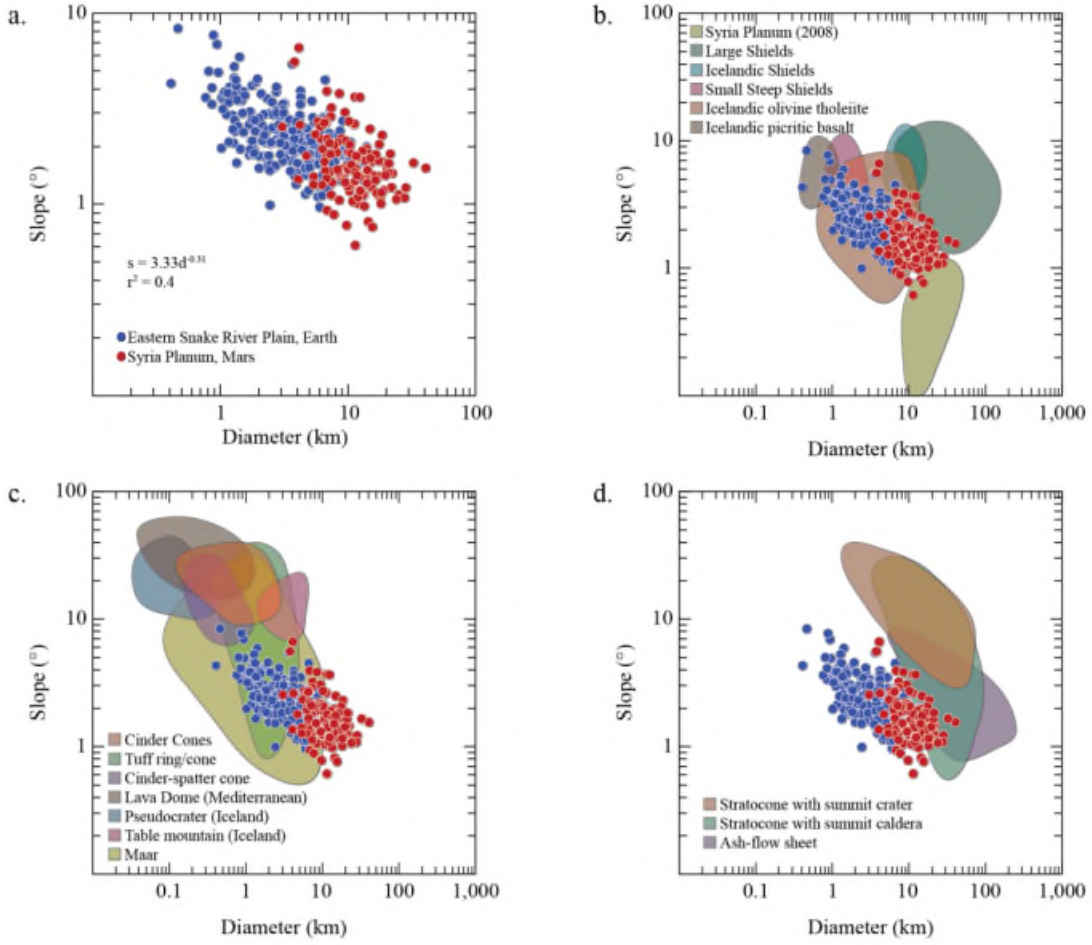

Figure 17: Morphometric comparison of volcano diameters and slope. (a) Snake River Plain and Syria Planum low-shields form extremes of the same grouping that shows a decrease in slope with increasing diameter. (b) SP and eSRP low-shields are compared to other terrestrial shield volcanoes measured by Pike and Clow (1981) and Rossi (1995) as well as SP low-shields measured by Baptista et al. (2008). This plot shows that SP and eSRP low-shields have distinctly smaller slopes than other terrestrial shields for a given diameter except Icelandic olivine tholeiites (Rossi, 1995). The shields measured by Baptista et al. (2008) may follow the same trend as SP and eSRP shields, but possible outliers give an anomalous trend. (c) SP and eSRP low-shields are compared to terrestrial cones, maars, and table mountains. This plot shows that SP and eSRP low-shields have distinctly lower slopes than terrestrial cones, with the exception of large terrestrial maars. (d) SP and eSRP low-shields are compared to terrestrial stratocones (Pike and Clow, 1981). SP and eSRP low-shields have systemically smaller slopes for any given diameter.

Figure 18: Morphometric Characteristic Plot Height v. Slope

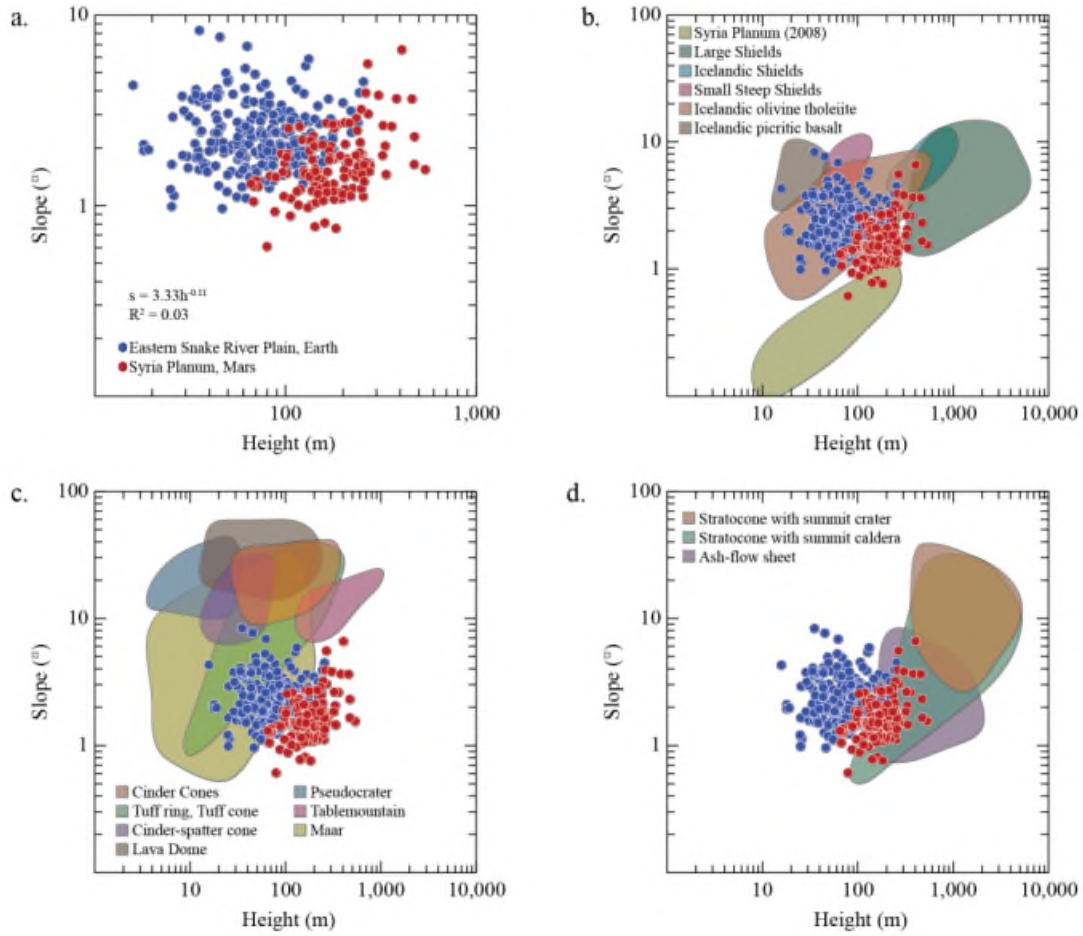

Figure 18: Morphometric characteristic comparison plot of height and slope. (a) On average Snake River Plain and Syria Planum low-shields are of comparable slopes though Syria Planum low-shields tend to be taller than Snake River Plain low-shields. (b) SP and eSRP shields are compared to other terrestrial shields (Pike and Clow, 1981, Rossi, 1995) and Syria Planum low-shields measured by Baptista et al. (2008). SP and eSRP low-shields have distinctly smaller slopes than other terrestrial shields as calculated from measurements made by Pike and Clow (1981), but overlap with Icelandic olivine tholeiites (Rossi, 1995). Measruements made by Baptista et al. (2008) also show Syria Planum low-shields as having distinctly smaller slopes. However, this plot shows that their slopes follow a similar height/slope trend as large terrestrial shields as calculated from Pike and Clow (1981). (c) This shows that eSRP and SP low-shields from their own distinct grouping as compared to terrestrial small cones, though eSRP shields overlap with maars and tuff rings in both height and slope. (d) Again, eSRP and SP shields are distinctly smaller in both slope and height than terrestrial stratocones as measured by Pike and Clow (1981), though SP shields do overlap in height and slope with ash flows.

Figure 19: Rose Diagrams

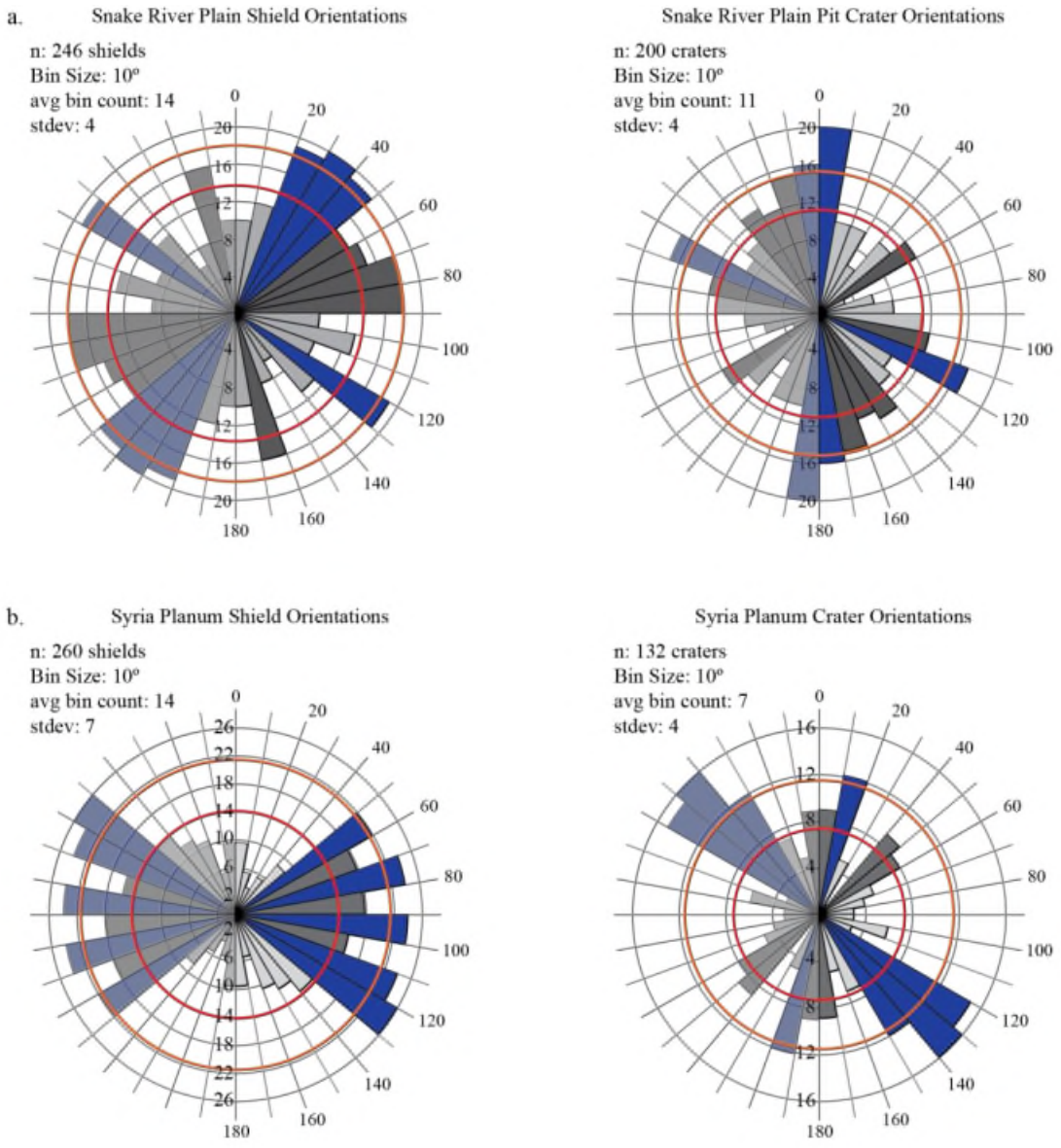

Figure 19: Elongation directions of low-shields and their craters are shown on rose diagrams. (a) Orientations of Snake River Plain low-shields and craters. Shields are elongated in the NE and SE directions, which correspond to the axis of the plain and basin and range faults respectively. Craters show significant orientations in the N and SE directions which correspond well with basin and range faults. (b) Orientations of Syria Planum low-shields and craters covered by MOLA elevation dataset (compare with Fig. 3, 12). Shields show four significant orientations, where craters show only two.

Figure 20a: Crater Analysis, Depth v. Diameter

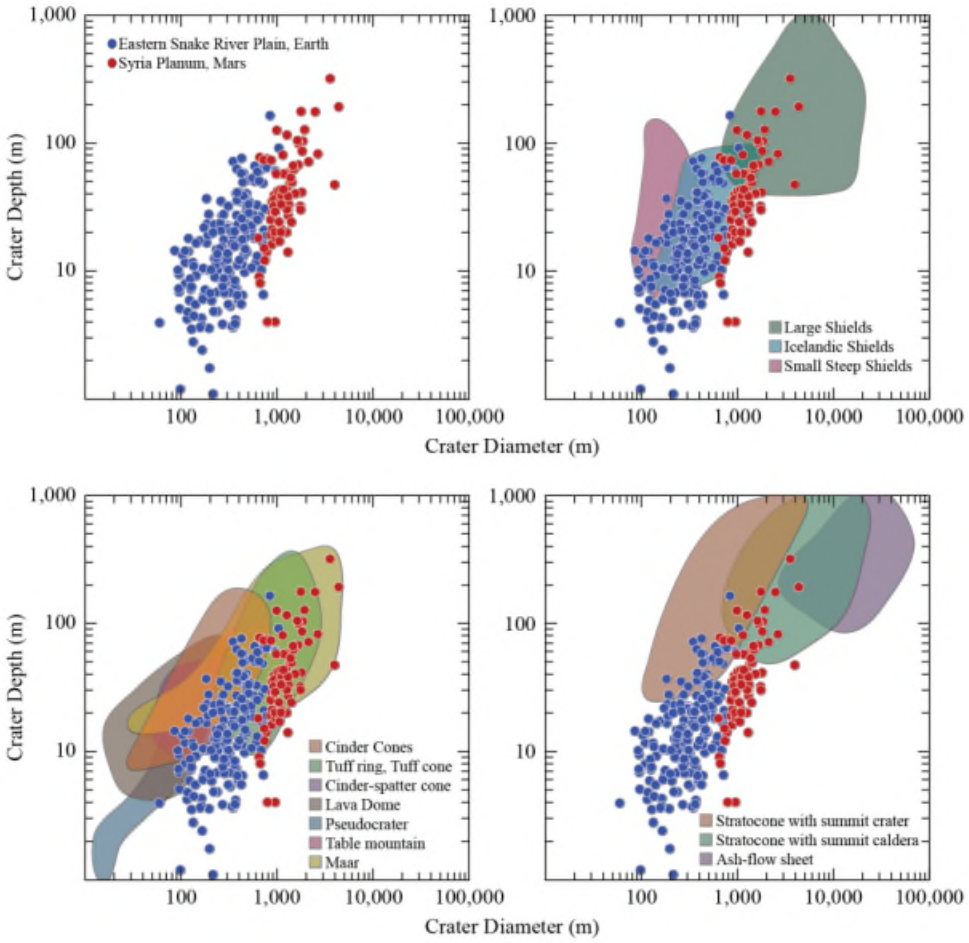

Figure 20a: Snake River Plain and Syria Planum low-shields have similar crater diameter to crater depth relationships as Icelandic and small steep shields, and appear to follow the same trend as large shields (Pike and Clow, 1981) with smaller craters. SP and eSRP craters and distinctly smaller than those of stratocones, though they follow parallel trends to stratocones with summit craters, and appear to follow the same trend as stratocones with summit calderas.

Figure 20b: Crater Analysis, Volcano Diameter v. Ratio of Crater Diameter to Volcano Diameter

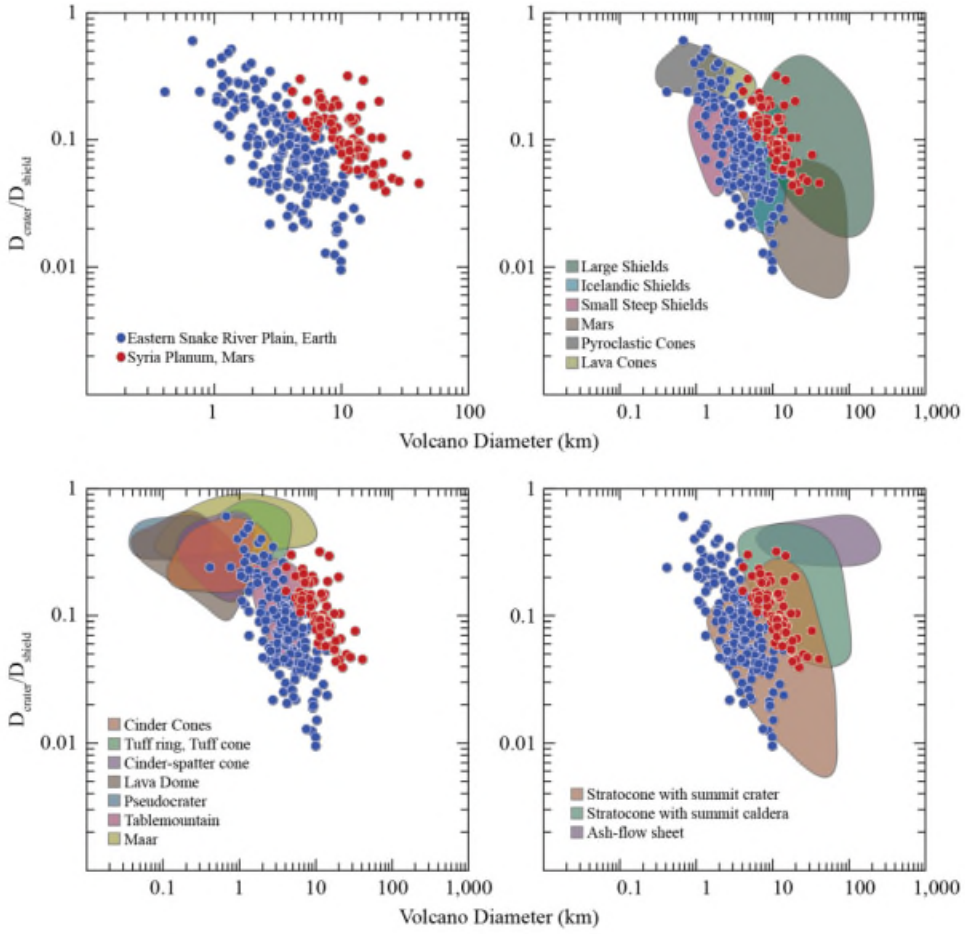

Figure 20b: The parallel trends of Syria Planum and Snake River Plain ratios of crater diameter to volcano diameter plotted against the volcano diameter shows that the two groups of shields have similar ratios, but Syria Planum is proportionately larger. Both eSRP and SP low-shields have similar ratios to terrestrial Icelandic, small steep shields, table mountains, and smaller stratocones with summit craters. While there is some overlap with the martian low-shields measured by Hauber et al. (2009) the majority of those shields have smaller crater to shield ratios.

Figure 20c: Crater Analysis, Volcano Diameter v. Crater Diameter

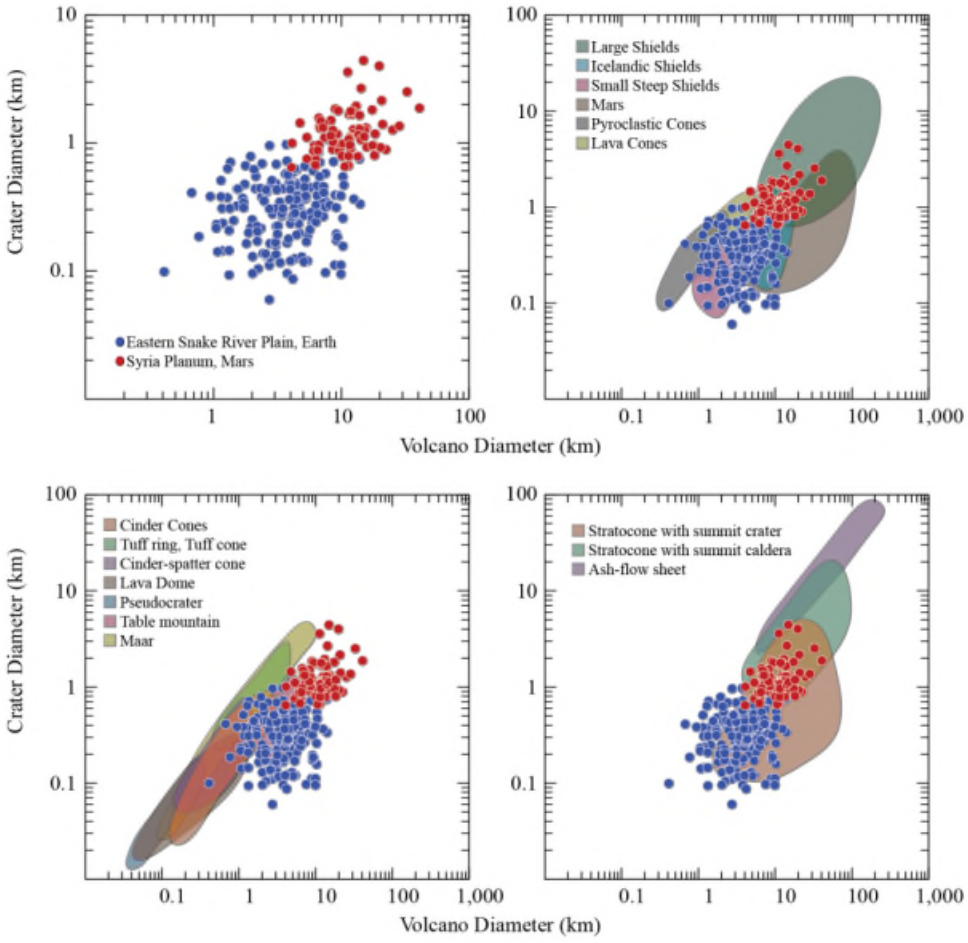

Figure 20c: Plots of crater diameter against volcano diameter. Snake River Plain and Syria Planum low-shield craters are comparable to Icelandic and small steep shields and have considerable overlap with stratocones as measured by Pike and Clow (1981). SP and eSRP low-shields have smaller craters for any given edifice diameter than most terrestrial cones, though comparable to those found on Icelandic table mountains as measured by Pike and Clow (1981).

Figure 21: Possible Magma Source

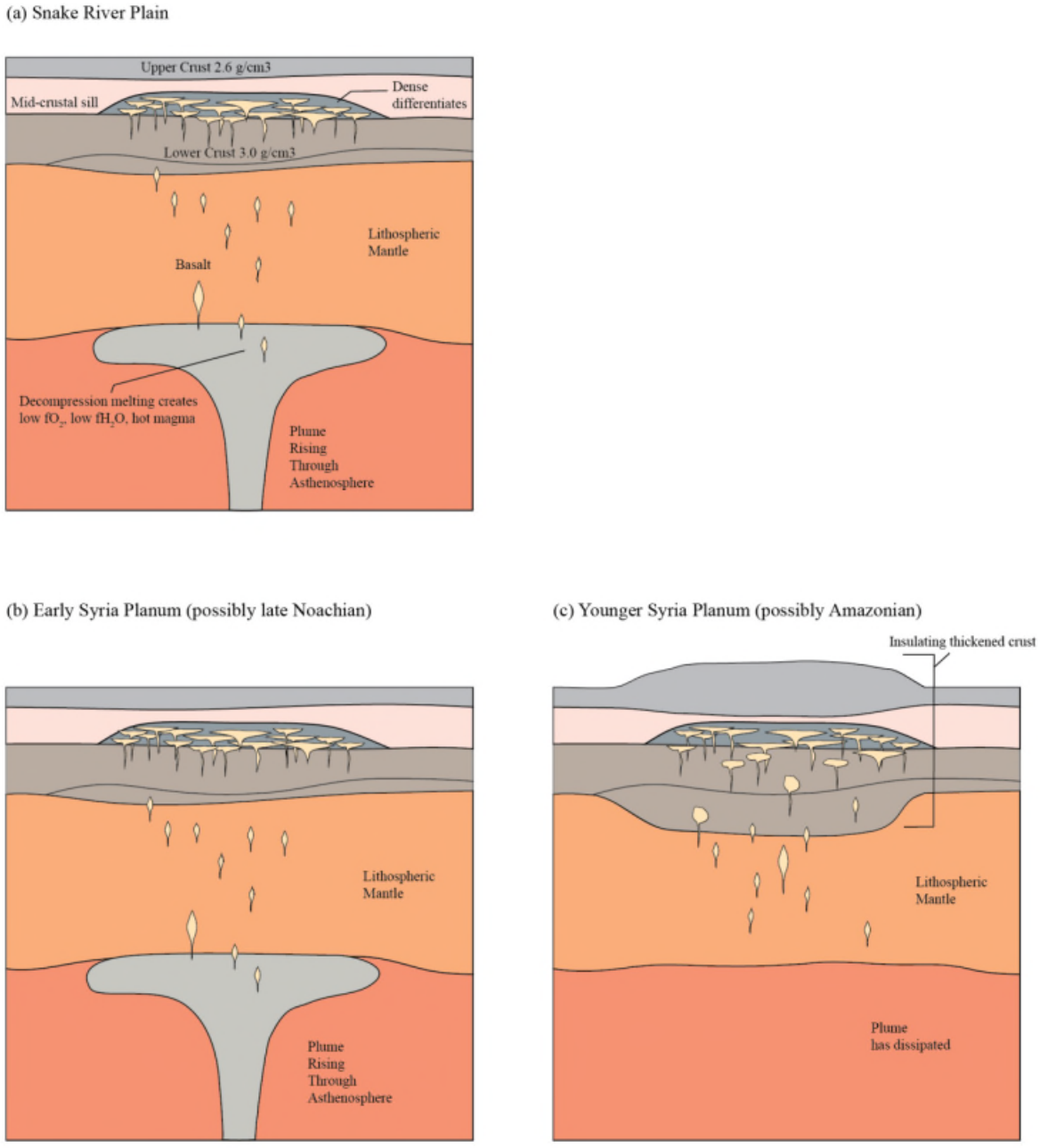

Figure 21: (a) Schematic lithospheric cross-section for the Snake River Plain adapted from Christiansen and McCurry (2008). (b) Schematic lithospheric cross-section for Syria Planum. Initial stages of volcanism are plume related and thickens the crust. (c) Eventually the plume terminates and the thickened crust insulates the upper mantle allowing volcanism to continue.

Figure 22: Buoyancy Cross Section

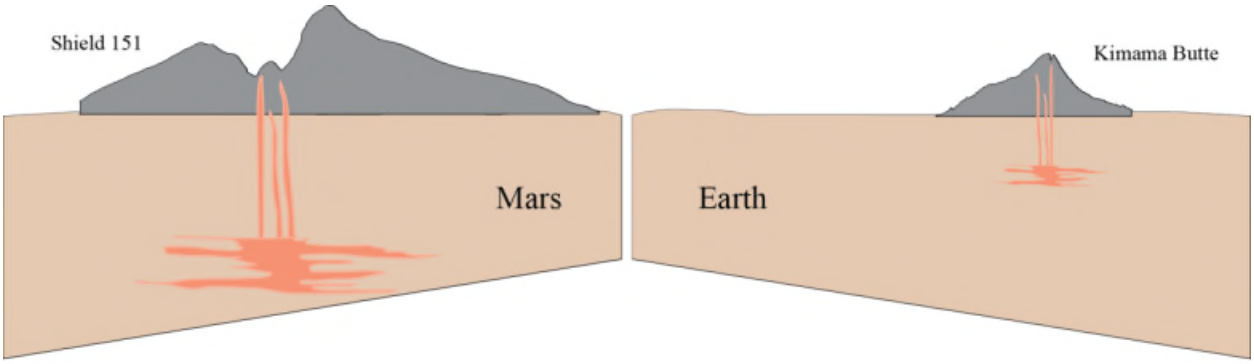

Figure 22: Buoyancy is an important force that drives magma ascent and is dependent on a planet's gravity. Assuming the forces resisting magma rise are equal on both planets (e.g. strength of the lithosphere), the volume of a batch of rising magma must be greater on Mars than on Earth to break through the overlaying lithosphere. These larger magma batches could lead to larger martian volcanoes, higher eruption rates, and longer lava flows. This could explain the larger diameters and volumes of Syria Planum low-shields than those of Snake River Plain low-shields even though they have comparable flank slopes. Scale does not extend below the surface, vertical exaggeration is approximately 18:1.

Table 1: Statistical Summary of Shield Morphometric Characteristics

Eastern Snake River Plain Low-shields							
n = 246	**Height (m)**	**Slope (°)**	**Diameter (km)**	**Area (km^2)**	**Volume (km^3)**	**Eccentricity**	**Orientation**
Avg	83	2	4	19	0.8	0.6	83
Min	16	1	0.4	0.1	0.001	0.1	1
Max	257	8	14	156	13	1.0	180
Std dev	44.5	1.1	2.7	26.1	1.6	0.2	49.6
Syria Planum Low-shields (HRSC)							
n = 133	**Height (m)**	**Slope (°)**	**Diameter (km)**	**Area (km^2)**	**Volume (km^3)**	**Eccentricity**	**Orientation**
Avg	191	2	12	148	16	0.6	91
Min	66	0.6	3	7	0.4	0.3	2
Max	542	7	41	1320	241	0.9	176
Std dev	87.7	0.8	6.0	166.7	28.1	0.1	37.8
Syria Planum Low-shields (MOLA)							
n = 260	**Height (m)**	**Slope (°)**	**Diameter (km)**	**Area (km^2)**	**Volume (km^3)**	**Eccentricity**	**Orientation**
Avg	115	0.7	14	185	18	0.6	95
Min	19	0.2	2	4	0.03	0.2	0.7
Max	791	4	58	2662	1249	0.9	179
Std dev	82.8	0.4	7.2	243.6	81.9	0.2	42.4
Syria Planum Low-shields (Baptista et al, 2008)							
n = 30	**Height (m)**	**Slope (°)**	**Diameter (km)**	**Area (km^2)**	**Volume (km^3)**		
Avg	93	0.5	23	470	21		
Min	9	0.1	10	78	0.2		
Max	248	1	43	1431	153		
Std dev	62.7	0.2	8.9	337.5	33.4		

Table 2: Statistical Summary of Crater Morphometric Characteristics

Eastern Snake River Plain Craters						
n = 187	**Height (m)**	**Diameter (km)**	**Eccentricity**	**Orientation**	**h/d**	**D_{crater}/D_{shield}**
Avg	21	0	0.7	94	0.1	0.1
Min	1	0.1	0.3	0	0.01	0.01
Max	163	1	1.0	180	0.2	0.6
Std dev	19.7	0.2	0.1	55.6	0.04	0.1
Syria Planum Craters (HRSC)						
n = 76	**Height (m)**	**Diameter (km)**	**Eccentricity**	**Orientation**	**h/d**	**D_{crater}/D_{shield}**
Avg	52	1	0.8	103	0.0	0.1
Min	4	0.6	0.4	1	0.00	0.04
Max	316	4	1.0	178	0.1	0.3
Std dev	49.6	0.7	0.2	55.4	0.03	0.1
Syria Planum Craters (MOLA)						
n = 132	**Height (m)**	**Diameter (km)**	**Eccentricity**	**Orientation**	**h/d**	**D_{crater}/D_{shield}**
Avg	16	2	0.8	96	0.01	0.1
Min	0	0.6	0.3	1	0	0.03
Max	140	4	1.0	178	0.1	0.3
Std dev	25.5	0.8	0.2	55.3	0.01	0.1

Syria Planum Craters (Hauber, 2009)		
n = 55	**Diameter (km)**	**D_{crater}/D_{shield}**
Avg	1	0.03
Min	0.2	0.01
Max	3	0.1
Std dev	0.6	0.0

Wood (1978)				
Type	**Volume (10^6 m^3)**	**Diameter (km)**	**h/d**	**D_{crater}/D_{shield}**
Pyroclastic Cones				
Spattercone	0.06	0.08	0.22	0.36
Cinder Cone	40	0.8	0.18	0.4
Pseudocrater	0.02	0.08	0.1	0.42
Maar	25	1.38	0.02	0.6
Lava Cones				
Icelandic Shield	9200	8.6	0.06	0.06
Steep Shields	50	1.6	0.04	0.12
Low Shields	450	4.8	0.02	0.08

Table 3: Statistical Summary of eSRP Morphometric Characteristics by Bury Category

*Eastern Snake River Plain Bury Category 0**					
n = 25	**Height (m)**	**Slope (°)**	**Diameter (km)**	**Area (km^2)**	**Volume (km^3)**
Avg	109	2	7	44	2.3
Min	58	1	2	3	0.05
Max	240	3	14	156	12.8
Std dev	44.7	0.5	3.4	43.7	3.0
Eastern Snake River Plain Bury Category 1					
n = 25	**Height (m)**	**Slope (°)**	**Diameter (km)**	**Area (km^2)**	**Volume (km^3)**
Avg	94	2	5	23	1
Min	39	1.3	0.9	0.6	0.01
Max	257	4	10	84	5
Std dev	52.1	0.8	2.4	21.5	1.2
Eastern Snake River Plain Bury Category 2					
n = 25	**Height (m)**	**Slope (°)**	**Diameter (km)**	**Area (km^2)**	**Volume (km^3)**
Avg	77	2	4	15	1
Min	31	1.3	1.2	1.1	0.02
Max	157	3	8	44	2
Std dev	26.4	0.4	1.6	10.8	0.5
Eastern Snake River Plain Bury Category 3					
n = 25	**Height (m)**	**Slope (°)**	**Diameter (km)**	**Area (km^2)**	**Volume (km^3)**
Avg	86	2	4	17	1
Min	35	1	1.2	1	0.02
Max	221	4	8	56	3
Std dev	39.6	0.7	2.0	14.4	0.7
Eastern Snake River Plain Bury Category 4					
n = 146	**Height (m)**	**Slope (°)**	**Diameter (km)**	**Area (km^2)**	**Volume (km^3)**
Avg	79	3	4	16	0.7
Min	16	1	0.4	0.1	0.001
Max	244	8	14	147	13
Std dev	44.6	1.2	2.6	24.5	1.5

*Category 4 shields are buried on 75-100% of their flanks, category 3 shields are buried on 50-75% of their flanks, category 2 shields are buried on 25-50% of their flanks, category 1 shields are buried on less than 25% of their flanks, category 0 shields are not buried.

Table 4: Volcano Type Index

Class This study	Class Pike & Clow (1981)		Example	Description
SCr	SA	Stratocone with summit crater: Alkalic affinity	Stromboli Etna Mt. Erebus	Composite volcano; crater only enlarged conduit, less than 1 to 1.5 km across; proportions lava/tephra may be equal, but are highly variable. Trachyte, some basalt and phonolite.
	SC	Stratocone with summit crater: Calc-alkalic affinity	Mayon Lassen Cotopaxi	As for SA, but rocks are mainly andesite, with some basalt, rhyolite and dacite.
	SCL	Stratocone with summit amphitheater: Calc-alkalic affinity	Mt. St. Helens Bezymianny	As for SC, but large horseshoe-shaped crater from directed lateral eruption engulfing much os summit.
Kca	KA	Stratocone with summit caldera: Alkalic affinity	Mt. Elgon Tambora Faial	Composite volcano; caldera is major collapse depression much broader than conduit, and over 1 to 1.5 km across; proportions of lava and tephra may be equal, but are highly variable. Trachyte, some basalt and phonolite.
	KAS	Stratocone with caldera: Alkalic affinity, more silica & pyroclastics	Katmai Hakone Batur	As for KA, but rocks are mainly andesite, with some basalt, rhyolite, and dacite.
	KC	Stratocone with summit caldera: Calc-alkalic affinity	Lago di Bolsena Tarso Voon Fantale	Composite volcano; conspicuously more tephra than SA, SC, KA, and KC; tephra commonly is more silicic than lava. Trachyte and phonolite, with some basalt.
	KCS	Stratocone with caldera: Calc-alkalic affinity, more silica & pyroclastics	Crater Lake Krakatau	As for KAS, but rocks are mainly andesite and dacite, with rhyolite and some basalt.
AF	AA	Ash-flow sheet with central caldera: Alkalic affinity	Ngorongoro Gadamsa	Voluminous sheets of ignimbrite around central caldera; may have resurgent dome; typically little lava. Mainly trachytic or phonolitic pumice.
	AP	Ash-flow sheet with central caldera: Calc-alkalic affinity	Yellowstone Aso Rotorua	As for AA, but much larger edifice and rocks mainly rhyolitic or dacitic ignimbrite; some called "Volcano-tectonic depressions".
LS	KTH	Oceanic shield with caldera, predominantly tholeiitic lava: Hawaii	Kilauea Olokele	Shield volcano; caldera much broader than conduit. Olivine-free or olivine-poor basalts of the calc-alkalic affinity; minimal tephra and perhaps non-tholeiitic basalt. Conspicuously larger than KTG and KTU; rift zones common on summit; caldera highly acircular.
	KTG	Oceanic shield with caldera, predominantly tholeiitic lava: Galapagos	Fernandina Alcedo	As for KTH, but more alkalic basalt and edifice smaller; circumferential ring-fractures conspicuous on summit.
	KTU	Oceanic shield with caldera, predominantly tholeiitic lava: Location varies	Niuafo'ou Karthala	As for KTG, but ring 0fractures not necessarily well developed on summit.
	KMA	Continental shield with caldera, predominantly non-tholeiitic lava	Askja Medicine Lake	As for KTG and KTU, but smaller edifice. Mostly alkalic basalt or mixture of alkalic and tholeiitic basalts; tephra content variable but higher than KMM. Formed on land; lower, less steep edifice than KMM.
	KMM	Oceanic shield with summit caldera, predominantly non-tholeiitic lava	Aoba Ambrym	As for KTG and KTU, but smaller edifice. Mostly alkalic basalt or mixture of alkalic and tholeiitic basalts; tephra content low and variable. Emergent submarine shield; higher, steeper edifice than KMA.
SI	SI	Shield volcano with summit crater: Icelandic type	Skjaldbreidur Whaleback	Conspicuously larger than SS or SL; basaltic lava with little (basaltic) tephra. Crater little more than enlarged vent or conduit.
SS	SS	Shield volcano with summit crater: small, steep type	Mauna Ulu Mt. Hamilton	Conspicuously smaller than SI and much steeper than SL; basaltic lava with little (basaltic) tephra.

Class This study	Class Pike & Clow (1981)		Example	Description
C	C	Cinder cone	Sunset Crater Puy de Pariou Paricutin	Scoria cone, tephra cone. Crater seldom intersects ground surface. Collapse of crater very rare; basaltic tephra not saturated by water; minimal lava spatter. Usually larger than A.
T	T	Tuff ring, Tuff cone	Diamond Head Solfatara Hverfjall	Tuff cone. Rarely intersects ground surface but often may approach it; occasional collapse of crater; basaltic tephra, mostly water-saturated; much more juvenile material than in E.
M	E	Maar	Pulvermaar Ubehebe Tower Hill Basotu	Crater intersects ground surface, characteristically as a result of collapse; basaltic tephra, virtually all water-saturated; much less juvenile material than in T.
Cs	A	Cinder-spatter cone	Capelinhos (inner cone) Lilewa	Smaller than C; crater may intersect ground surface; basaltic spatter and tephra, in varying relative proportions; more tephra in larger cones.
D	D	Lava dome with summit depression (Mediterranean)	Kameno Vouno Mikra	Mostly andesitic and dacitic lava; little tephra (same lithology); Mediterranean area.
P	P	"Pseudocrater" (Iceland)	Vesturhofdi Haey	Rootless cone of basaltic tephra within basaltic lava flow in Myvatn district of Iceland; tephra is water-saturated.
Tm	M	Cratered Tablemountain (Iceland)	Herdhubreidh Baejarfjall	Tuya. Steep-sided, characteristically flat-topped edifice of subaqueously deposited "moberg" surmounted by subaerial basaltic lava that may form low shield.
OT	Rossi (1995)	Olivine Tholeiite		
PI	Rossi (1995)	Picrite Basalt		

* Dimensions reported by Pike & Clow (1981) are consistent with this study's measurements so they are not included in plots.

Table 5: Statistical Summary of eSRP and SP Morphometric Characteristics by Cluster

Eastern Snake River Plain Low-shields Cluster 1							
n = 66	**Height (m)**	**Slope (°)**	**Diameter (km)**	**Area (km^2)**	**Volume (km^3)**	**Eccentricity**	**Orientation**
Avg	115	2	6	29	1.2	0.6	89
Min	56	1	3.1	7.4	0.230	0.2	4
Max	257	4	9	69	3	0.8	175
Std dev	38.8	0.6	1.4	14.1	0.7	0.1	52.1
Eastern Snake River Plain Low-shields Cluster 2							
n = 87	**Height (m)**	**Slope (°)**	**Diameter (km)**	**Area (km^2)**	**Volume (km^3)**	**Eccentricity**	**Orientation**
Avg	62	2	3	9	0.3	0.7	81
Min	18	1	1.0	0.8	0.007	0.5	1
Max	133	3	7	37	1	1.0	174
Std dev	23.6	0.5	1.4	7.8	0.3	0.1	50.4
Eastern Snake River Plain Low-shields Cluster 3							
n = 42	**Height (m)**	**Slope (°)**	**Diameter (km)**	**Area (km^2)**	**Volume (km^3)**	**Eccentricity**	**Orientation**
Avg	69	4	2	3	0.1	0.6	82
Min	16	3	0.4	0.1	0.001	0.5	5
Max	132	8	4	11	0	0.9	180
Std dev	28.4	1.2	0.9	2.7	0.1	0.1	46.7
Eastern Snake River Plain Low-shields Cluster 4							
n = 34	**Height (m)**	**Slope (°)**	**Diameter (km)**	**Area (km^2)**	**Volume (km^3)**	**Eccentricity**	**Orientation**
Avg	51	2	3	6	0.1	0.4	87
Min	18	1	0.8	0.5	0.004	0.1	7
Max	96	5	5	17	1	0.5	171
Std dev	21.1	0.9	1.2	5.2	0.1	0.1	48.2
Eastern Snake River Plain Low-shields Cluster 5							
n = 16	**Height (m)**	**Slope (°)**	**Diameter (km)**	**Area (km^2)**	**Volume (km^3)**	**Eccentricity**	**Orientation**
Avg	164	2	11	94	5.6	0.5	65
Min	79	1	6.4	32.5	2.505	0.2	9
Max	240	3	14	156	13	0.7	132
Std dev	42.7	0.5	2.3	38.4	3.0	0.1	37.0
Syria Planum Low-shields Cluster 1							
n = 11	**Height (m)**	**Slope (°)**	**Diameter (km)**	**Area (km^2)**	**Volume (km^3)**	**Eccentricity**	**Orientation**
Avg	350	4	10	96	14.8	0.5	77
Min	264	2	3.8	11.5	1.796	0.3	4
Max	476	7	19	274	47	0.8	144
Std dev	71.1	1.3	4.2	72.2	11.9	0.1	47.8

Syria Planum Low-shields Cluster 2							
n = 75	**Height (m)**	**Slope (°)**	**Diameter (km)**	**Area (km^2)**	**Volume (km^3)**	**Eccentricity**	**Orientation**
Avg	153	2	10	81	6.4	0.7	94
Min	66	1	3.1	7.4	0.486	0.5	2
Max	252	3	18	262	21	0.9	175
Std dev	51.1	0.5	3.2	52.6	4.9	0.1	36.6
Syria Planum Plain Low-shields Cluster 3							
n = 20	**Height (m)**	**Slope (°)**	**Diameter (km)**	**Area (km^2)**	**Volume (km^3)**	**Eccentricity**	**Orientation**
Avg	240	1	21	349	38.0	0.5	81
Min	134	1	15.7	192.6	16.900	0.3	15
Max	338	2	29	643	88	0.8	152
Std dev	58.2	0.3	3.5	121.5	15.9	0.2	35.8
Syria Planum Low-shields Cluster 4							
n = 25	**Height (m)**	**Slope (°)**	**Diameter (km)**	**Area (km^2)**	**Volume (km^3)**	**Eccentricity**	**Orientation**
Avg	171	1	13	135	11.4	0.4	95
Min	71	1	4.1	13.2	0.433	0.3	3
Max	259	2	19	288	26	0.5	176
Std dev	47.6	0.2	3.3	63.3	7.0	0.1	36.1
Syria Planum Low-shields Cluster 5							
n = 2	**Height (m)**	**Slope (°)**	**Diameter (km)**	**Area (km^2)**	**Volume (km^3)**	**Eccentricity**	**Orientation**
Avg	509	2	37	1083	210.9	0.6	106
Min	475	2	32.8	845.6	180.789	0.6	94
Max	542	2	41	1320	241	0.6	117
Std dev	33.5	0.1	4.1	237.3	30.1	0.0	11.5

Table 6: Principal Component Analysis

Eigenvalue	*% Vairance explained*	*Cumulative %*	*Chi²*	*DF*	*Prob > Chi²*
2.3	57	57	1579.5	5.0	<0.0001
1.1	26	84	838.3	4.5	<0.0001
0.5	13	97	415.3	1.8	<0.0001
0.1	3	100	0.0		

Eigenvectors	*PC 1**	*PC 2*	*PC 3*	*PC 4*
Height	**0.5**	0.3	-0.8	0.1
Area	**0.6**	-0.1	0.4	0.7
Volume	**0.6**	-0.1	0.3	-0.7
Slope	0.0	**0.9**	0.3	0.0

*Values greater than or equal to 0.5 are considered statistically significant

Table 7: Regression Analysis

Class*	*Diameter v Height*			*Diameter v Volume*			*Diameter v Slope*		
	m**	b	r^2	m	b	r^2	m	b	r^2
eSRP and SP	0.63	3.58	0.66	2.69	-4.56	0.97	-0.31	1.20	0.40
SRP	0.57	3.60	0.53	2.55	-4.48	0.95	-0.32	1.21	0.35
SP	0.43	4.12	0.21	2.32	-3.52	0.88	-0.32	1.25	0.16
Baptista et al. (2008)	1.32	0.23	0.46	3.77	-9.68	0.76	0.58	-2.56	0.25
LS	0.81	4.42	0.58	2.81	-3.40	0.94	-0.23	2.53	0.10
OT	1.03	2.95	0.58	3.07	-5.40	0.86	*-0.02*	*1.05*	*0.00*
PI	1.21	3.70	0.58	2.96	-4.69	0.91	*-0.03*	*1.69*	*0.00*
SI	1.19	3.63	0.52	3.19	-4.21	0.89	0.20	1.50	0.03
SS	0.40	4.07	0.16	2.41	-3.78	0.88	-0.62	2.05	0.32
SCr	0.59	5.69	0.62	2.59	-2.15	0.97	-0.42	3.58	0.47
KCa	0.56	5.07	0.24	2.57	-2.81	0.85	-0.48	3.27	0.23
AF	0.63	3.72	0.46	2.62	-4.19	0.91	-0.40	2.17	0.26
C	0.86	4.86	0.67	2.87	-2.98	0.95	-0.17	3.04	0.10
T	0.47	4.15	0.08	2.40	-3.85	0.68	-0.56	2.67	0.11
M	0.51	3.02	0.27	2.53	-6.16	0.80	-0.52	1.79	0.23
Cs	0.40	3.92	0.21	2.35	-4.11	0.85	-0.54	2.23	0.41
D	0.80	5.46	0.74	2.52	-2.78	0.97	-0.21	3.10	0.28
P	0.77	4.17	0.69	2.70	-3.85	0.96	*-0.18*	*2.59*	*0.11*
Tm	1.12	4.30	0.54	3.11	-3.52	0.90	*0.04*	*2.36*	*0.00*

Class*	*Height v Volume*			*Height v Slope*		
	m	b	r^2	m	b	r^2
eSRP and SP	3.15	-14.68	0.79	-0.11	1.20	0.03
SRP	2.80	-13.45	0.70	-0.01	0.85	0.00
SP	1.86	-7.50	0.50	0.39	-1.55	0.21
Baptista et al. (2008)	1.92	-6.36	0.74	0.51	-2.95	0.72
LS	2.42	-10.86	0.80	0.24	-0.17	0.13
OT	2.16	-10.70	0.79	0.37	-0.58	0.38
PI	1.76	-11.54	0.81			
SI	1.87	-8.91	0.83	0.54	-1.42	0.65
SS	1.79	-10.26	0.48	*0.54*	*-0.54*	*0.25*
SCr	3.08	-17.49	0.78	-0.07	2.92	0.01
KCa	1.93	-7.72	0.63	0.45	-1.40	0.27
AF	2.71	-10.87	0.74	0.23	-0.73	0.04
C	2.59	-15.60	0.85	*0.12*	*2.48*	*0.06*
T	1.45	-8.97	0.59	0.81	-1.20	0.60
M	2.49	-13.38	0.72	0.48	0.06	0.19
Cs	2.15	-14.00	0.56			
D	2.89	-17.83	0.88	*-0.04*	*3.44*	*0.01*
P	2.74	-16.42	0.85	*0.14*	*2.58*	*0.05*
Tm	1.95	-10.80	0.83	0.40	*0.11*	0.49

*See table 4 for list of class abbreviations

** power law equations are of the form $y = e^b x^m$, italicized numbers or empty cells have p-values >0.05 and are not considered to be significant correlations